Final Technical Report

A Demonstration System for Capturing Geothermal Energy from Mine Waters beneath Butte, Montana

DOE Award Number: 2010 DE-EE0002821

Grantee: Montana Tech of the University of Montana

Principal Investigator: Dr. Donald M. Blackketter

June 2015

Montana Tech
1300 West Park Street
Butte, Montana 59701

Executive Summary

An innovative 50-ton ground-source heat pump (GSHP) system was installed to provide space heating and cooling for a 56,000 square foot (5,200 square meter) building in Butte Montana, in conjunction with its heating and chiller systems. Butte is a location with winter conditions much colder than the national average. The GSHP uses flooded mine waters at 78F (25C) as the heat source and heat sink. The heat transfer performance and efficiency of the system were analyzed using data from January through July 2014. This analysis indicated that for typical winter conditions in Butte, Montana, the GSHP could deliver about 88% of the building's annual heating needs. Compared with a baseline natural-gas/electric system, the system demonstrated at least 69% site energy savings, 38% source energy savings, 39% carbon dioxide emissions reduction, and a savings of $17,000 per year (40%) in utility costs. Assuming a $10,000 per ton cost for installing a production system, the payback period at natural gas costs of $9.63/MMBtu and electricity costs of $0.08/kWh would be in the range of 40 to 50 years. At higher utility prices, or lower installation costs, the payback period would obviously be reduced.

Final Technical Report
A Demonstration System for Capturing Geothermal Energy from Mine Waters beneath Butte, Montana
DOE Award Number: 10EE0002821

A. Comparison of actual accomplishments with goals and objectives

The project's objectives were:

(1) To install a large centralized hybrid geothermal system, using off-the-shelf technology to reduce operating cost of Montana Tech's new Natural Resources Building (Figure 1).
(2) To promote commercialization of the technology by documenting system performance, publishing operational and performance information.
(3) To involve academic faculty, researchers, and engineering students in teaching, research, and training projects that utilize the system.

The project's objectives were met. The centralized hybrid geothermal system was installed, commissioned, and it has been operating, providing heating and cooling to the 5,200 square meter Natural Resources Building. The system performance has been documented and disseminated via several publications and presentations. The heat transfer performance and efficiency of the system were analyzed using data from January through July 2014 (Liu et al, in preparation). This analysis indicated that for typical winter conditions in Butte, Montana, the GSHP could deliver about 88% of the building's annual heating needs. Compared with a baseline natural-gas/electric system, the system demonstrated at least 69% site energy savings, 38% source energy savings, 39% carbon dioxide emissions reduction, and a savings of $17,000 per year (40%) in utility costs. Assuming a $10,000 per ton cost for installing a production system, the payback period at natural gas costs of $9.63/MMBtu and electricity costs of $0.08/kWh would be in the range of 40 to 50 years. At higher utility prices, the payback period would drop. In addition, it is reasonable to expect a lower installation cost now that the feasibility of such a system has been shown. Numerous academic faculty, researchers, and engineering students have been involved through course projects, senior projects, and master's projects in utilizing and studying the system. The publications are listed later in this report.

The geothermal system uses the warm waters in a flooded underground mine to provide the energy for the closed-loop heat-pump system, and it connects into the existing steam system in the building. Figure 2 is a map that shows the location of the building and the shafts of the flooded mines. The Orphan Boy shaft is the location of the heat exchangers. The surface of the water in the Orphan Boy is about 30 meters below the ground surface. The depth of the shaft is about 245 meters, and it has horizontal cross-cut drifts at 60 meters and 150 meters depth, both connecting to a large stope, filled with over 1 billion liters of water at a temperature of 24C to

26C. The heat exchanger consists of 20 pipe loops immersed in the top 100 meters of mine water. The heat pump started operation in November 2013.

Figure 1: Natural Resources Building at Montana Tech

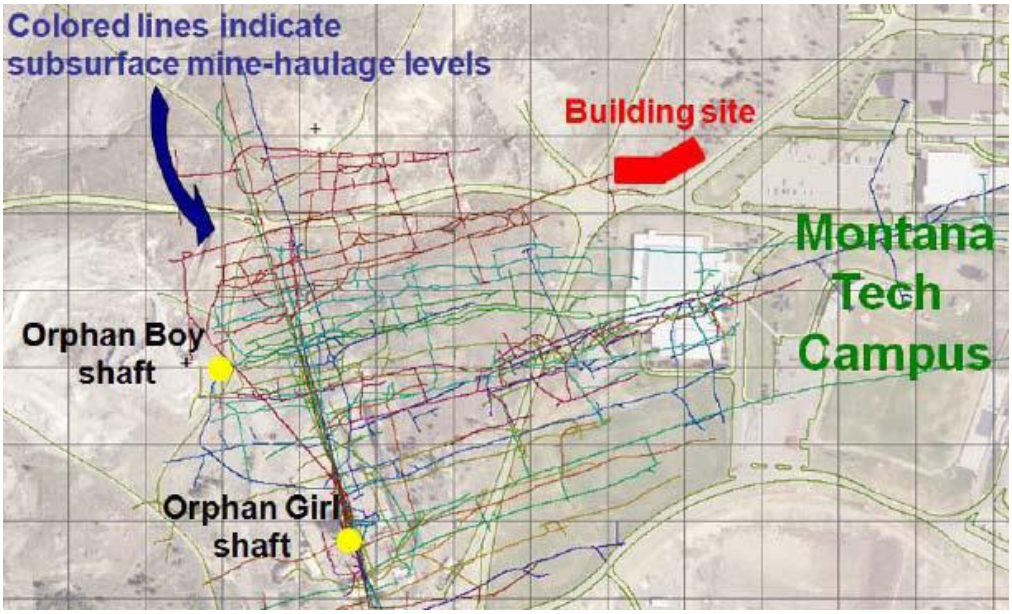

Figure 2. Map showing location of building and shafts accessing nearby flooded mines.

System description: The Ground Source Heat Pump (GSHP) system consists of one 50-ton Multistack MS050XN1H1R0AAC-R410A water-to-water heat pump (WWHP) unit. The WWHP provides either hot or chilled water for space conditioning, but not both modes simultaneously. The WWHP provides cooling when the outside temperature is ≥ 65°F, and heating when the outside temperature is ≤ 60°F. The flow in the heat pump loop is circulated by two (2) VFD controlled 10-hp TACO pumps. The HP leaving temperature will automatically reset according to the outside temperature. Figure 3 provides a simplified schematic of the system.

When ambient temperature is equal to or below 60°F, the heat pump operates in the heating mode and the valves modulate open to divert heating water to the heat pump loop. The heat pump starts when a positive flow is determined. The heat pump loop intercepts the water return to the steam converter and diverts a portion of that water according to the variable speed drive of the heat pump to vary the flow of the system. The heat pump pre-heats the building loop water and returns it to the same line before the converter. The steam converter then adds the remainder of the heat required to raise the mixed return and preheated water to the supply temperature range of 120°F to 180°F, depending on the outside temperature. The remainder of the building hot water distribution system and operation is unchanged by the addition of the GSHP unit.

The heat pump operates in the cooling mode when the temperature is equal to or above 65°F. The valves modulate to divert cooling water to the heat pump loop, and isolate the connection to the building hot water piping. When a positive flow rate is determined, the heat pump starts. The heat pump loop intercepts the chilled water at the building return piping header and diverts a portion of the flow to the heat pump. The heat pump cools the water and returns it to the same line before the building chilled water pump and chiller. The existing chiller then provides the remainder of the cooling capacity necessary to meet the required supply temperature setting of 45 to 65°F, which is reset with outdoor temperature. Similar to the heating system, the chilled water distribution piping and AHU operation is unaffected by the presence of the GSHP unit.

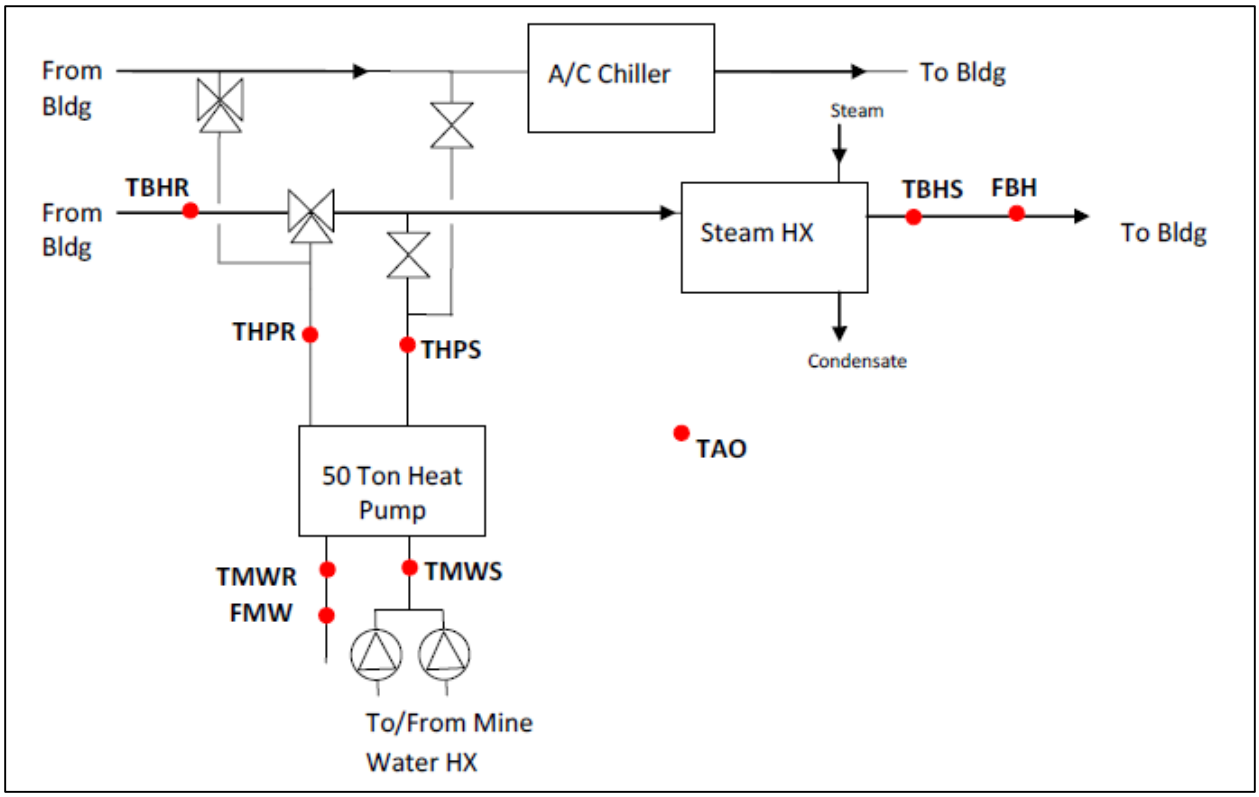

Figure 3. Simplified schematic of the Ground Source Heat Pump System.

B. Summary of project activities

The project involved designing, assessing the feasibility, and constructing a closed loop geothermal heat-pump system tapping the heat in large quantities of 25C water in abandoned mine stopes adjacent to and beneath the Montana Tech campus. Information gained from the project would be shared, to contribute to the technology base for developing and exploiting the energy in accessible geothermal reservoirs in this temperature range.

The project included several activities in three phases. Table 1 summarizes the task schedule and actual milestones. All project activities have been completed successfully.

Phase I: Feasibility Study and Engineering Design-Project Development, culminating in Go-No Go review and decision

Task 1.1 Heat Pump System Design Development

- 1.1.1 Determine the location of the interface between the heat pump and the conventional HVAC systems.
- 1.1.2 Determine the design criteria for the materials and equipment to be used in Phase 2 design.

Task 1.2 Right-Sizing of Heat Pump System

- 1.2.1 Run simulations of the building cooling and heating loads, match these loads with the mechanical systems without the heat pump system, and then match with heat pump systems of different sizes.
- 1.2.2 Estimate the relative first cost of the different-sized heat pump systems.

Task 1.3 Sequence of Operations: produce a schematic flow diagram and proposed sequence of operations to be the basis of design in Phase 2.

Task 1.4 Investigation of Mine Workings and Improved Access

- 1.4.1 Secure regulatory and environmental permits
- 1.4.2 Field investigation of stope: evaluate additional access directly to the stope via an existing raise or an inclined adit.

Phase 2. Construction

Task 2.1 Prepare Construction Bid Documents

Task 2.2 Installation and Commissioning of the Heat Pump System

Task 2.3 Installation of Additional Access to the Stope

Phase 3. Operation, Data Collection, Outreach, and Reporting

Task 3.1 Data Collection and Reporting

Task 3.2 Education and Outreach

Table 1. Summary of Activities and Schedule

Task	Brief Description of Activity	Start Date	Planned Completion Date	Actual Completion Date
Phase 1	FEASIBILITY & DESIGN			
Task 1.1	Heat pump system design/development	4/1/2010	4/1/2011	4/1/2011
1.1.1	Determine interface location	4/1/2010	4/1/2011	4/1/2011
1.1.2	Design criteria for Phase 2	4/1/2010	4/1/2011	4/1/2011
Task 1.2	Right sizing heat pump	10/1/2010	1/1/2011	1/1/2011
1.2.1	Simulations and matching	4/1/2010	1/1/2011	1/1/2011
1.2.2	Heat pump cost estimates	10/1/2010	4/1/2011	4/1/2011
Task 1.3	Sequence of operations	10/1/2010	4/1/2011	4/1/2011
Task 1.4	Investigations of mine workings/access	7/1/2010	4/1/2011	4/1/2011
1.4.1	Permits (Final DOE approval 6/8/2012)	7/1/2010	4/1/2011	4/1/2011
1.4.2	Field investigation of stope	7/1/2010	4/1/2011	4/1/2011
Phase 2	CONSTRUCTION			
Task 2.1	Construction Bid Documents	8/10/2012	10/1/2011	9/30/2013
Task 2.2	Heat Pump installation/commissioning	11/26/2012	10/2/2012	9/30/2013
Task 2.3	Additional stope access	10/1/2011	1/1/2011	9/30/2013
Phase 3	OPERATION, DATA, OUTREACH			
Task 3.1	Data collection & reporting	4/1/2011	9/30/2014	6/1/2015
Task 3.2	Education & outreach	10/1/2011	9/30/2014	5/15//2015

Some problems were encountered during the project, and plans had to be modified to cope with them. The modifications were successful. Consequently, other than schedule, there were no significant adverse impacts on the results. The significant problems are summarized here.

Problems encountered during design phase. An old ventilation fan at the site had been identified in 1988 as having historical significance. Because it was above the shaft where work would be done, it represented a safety hazard to the project. After a protracted process seeking approval to

relocate the fan, the decision was made to reduce further delays by providing underground access via a sloping tunnel ("decline") from the surface. This tunnel excavation was privately funded, costing $863 K, and resulting in a request to allow this amount of the mandatory cost share to be credited to Phase 2, rather than Phase 3, where the entire cost share had been budgeted. Without Montana Tech providing this tunnel access the project would have been unable to proceed. The tunnel access works exceptionally well, and the mine shaft through which the system piping reaches the surface was fitted with ladders to serve as an emergency egress for workers. The schedule impact was a delay of about one year.

Commissioning issues. Water leaks in the system after installation interfered with operational measurements and delayed system full operation to 2014. The leaks had to be located and fixed, in some cases necessitating excavation along the piping between the mine and the building, on other cases by replacing valves. Calibration of *in situ* temperature sensors took more time than expected. Flow needed to be closed through one of the 20 heat exchanger loops, due to problems.

System Analysis.

Extensive analysis of the system was performed by Liu *et al* (draft). Additionally, several Montana Tech students worked with the system or its data as part of their senior projects or master's degree theses. The Liu *et al.* analysis determined the heat transfer performance and overall efficiency based on data obtained from January through July 2014. Some of the figures and tables are provided here. The report is being finalized this year for publication, and the current draft is appended to this annual report. Table 2 shows the predicted annual performance, based on this analysis.

Table 2. Summary of predicted full-year performance data *(From Liu,* et al. draft*).*

	Unit	**January–April Measured**	**Full-Year Predicted (TMY3)**	**% Difference**
Building heating loads	MMBtu	1,126	3,286	-
Cumulative heat output	MMBtu	445	2,882	-
Cumulative heat pump energy use	kWh	33,025	201,335	-
Cumulative well pump energy use	kWh	4,390	28,038	-
Cumulative GSHP system energy use	kWh	37,415	229,374	-
% of building heating loads met	%	39.5%	87.7%	-
Average COP of heat pump	-	3.95	4.19	6.2%
Average COP of GSHP system	-	3.49	3.68	5.6%
Percentage of pumping energy use	%	11.7%	12.2%	4.2%

Figures 4 through 12 present some of the temperature, flow, and performance data for January through July 2014, covering about 4 months of heating season and one month of cooling. Figure 4 shows the mine water loop supply and return temperatures and outside air temperature during this period. Figure 5 shows the supply and return temperature of the building hot water loop and temperature of the load side of the heat pump. Figure 6 shows the differential temperature of the hot water loop and the flow rate, versus the outside temperature. Figure 7 presents one week of system temperatures in the cooling mode. Figure 8 shows the measured and manufacturer's reported coefficients of performance (COP) in the heating and cooling modes. Figure 9 presents the ground loop pumping power as a fraction of total power consumption and aggregated by month, showing the differences in heating and cooling modes. Figure 10 shows the heat pump and GSHP system efficiency for heating and for cooling as a function of outdoor temperature. In Figure 11 the recommended schedule for heat pump loop water temperature is presented. Figure 12 summarizes and compares the measured and predicted performance of the GSHP system in terms of energy use, ground loop power, heat pump heating COP, and GSHP system COP for heating.

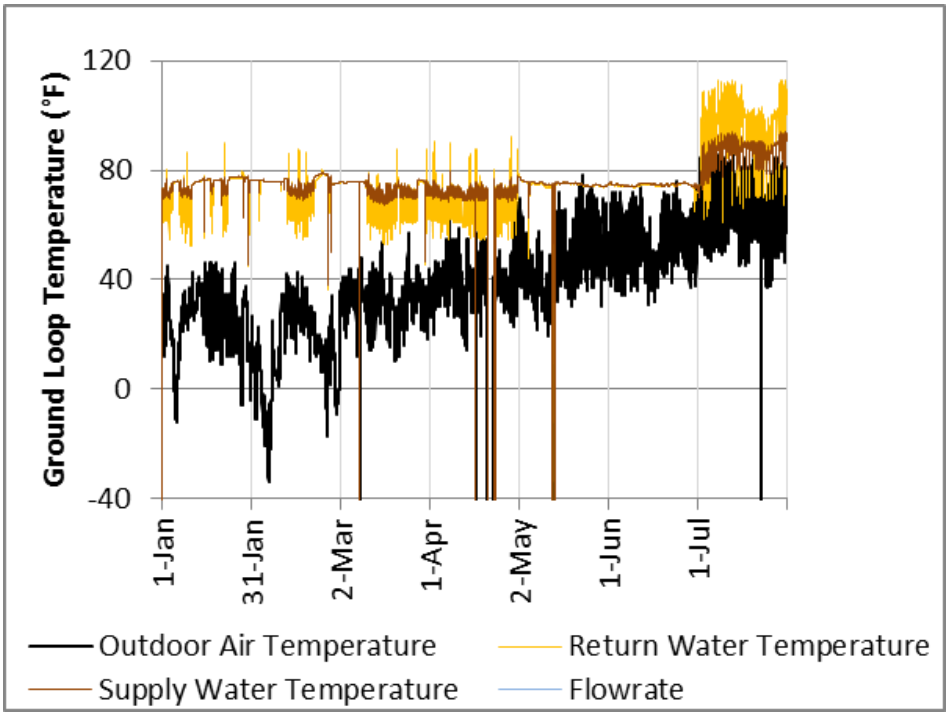

Figure 4. Mine water loop supply and return temperatures and outside air temperature during January-July 2014 (From Liu, *et al. draft*).

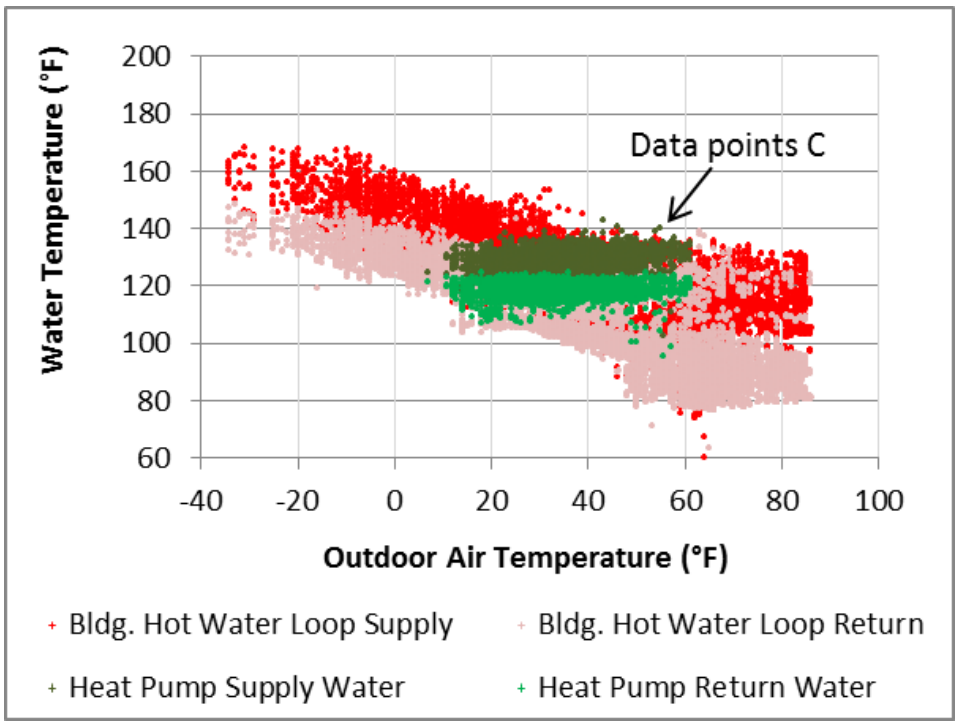

Figure 5. Measured supply and return temperature of the building hot water loop and the load side of the water-to-water heat pump (From Liu, *et al. draft*).

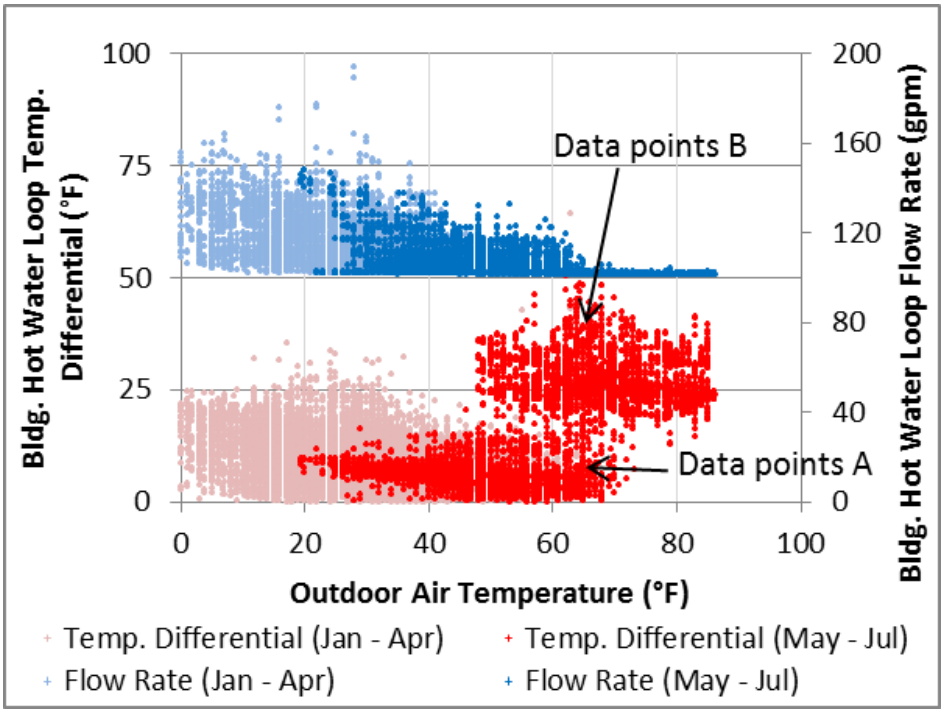

Figure 6. Building hot water loop temperature differential and flow rate versus outdoor air temperature (From Liu, *et al. draft*).

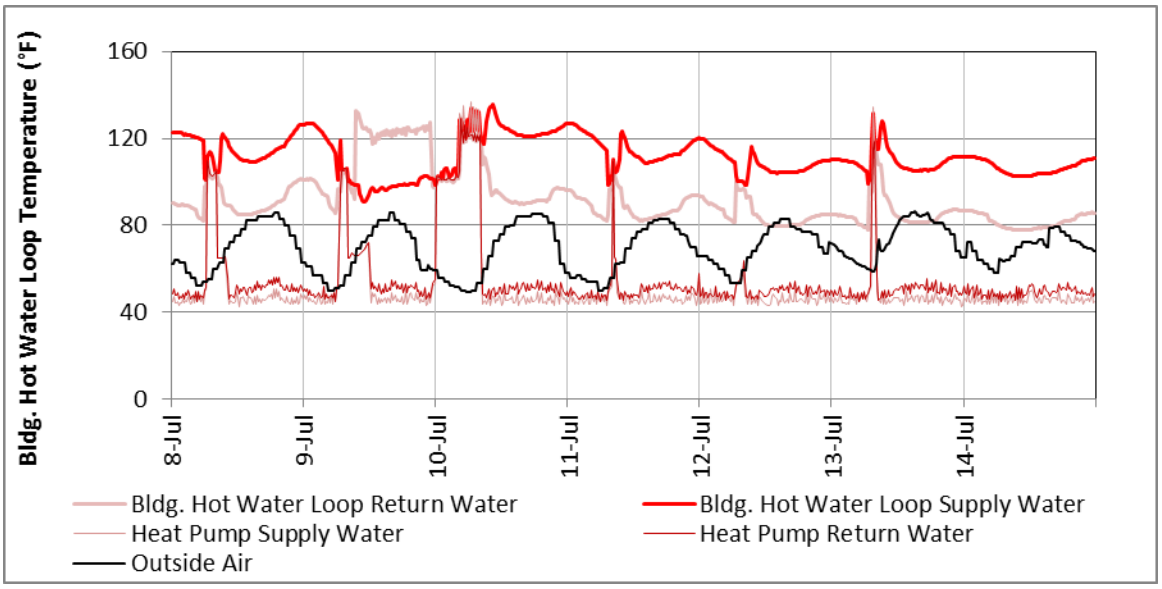

Figure 7. Building hot water loop temperature during heat pump operation in the cooling mode (July 8–15) (From Liu, *et al. draft*).

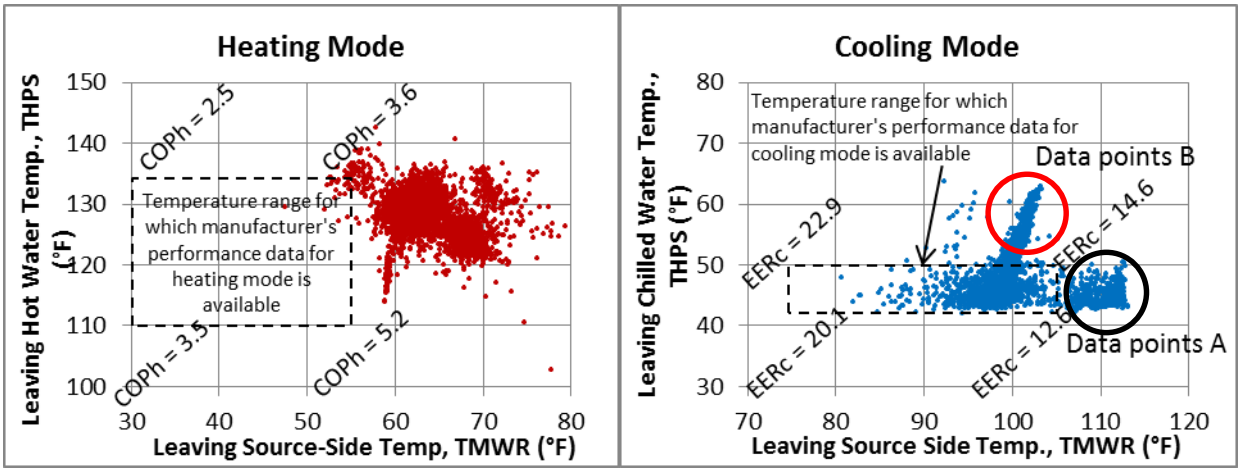

Figure 8. Range of COPs listed in manufacturer's performance data and the measured source-side and load-side leaving water temperatures of the heat pump (From Liu, *et al. draft*).

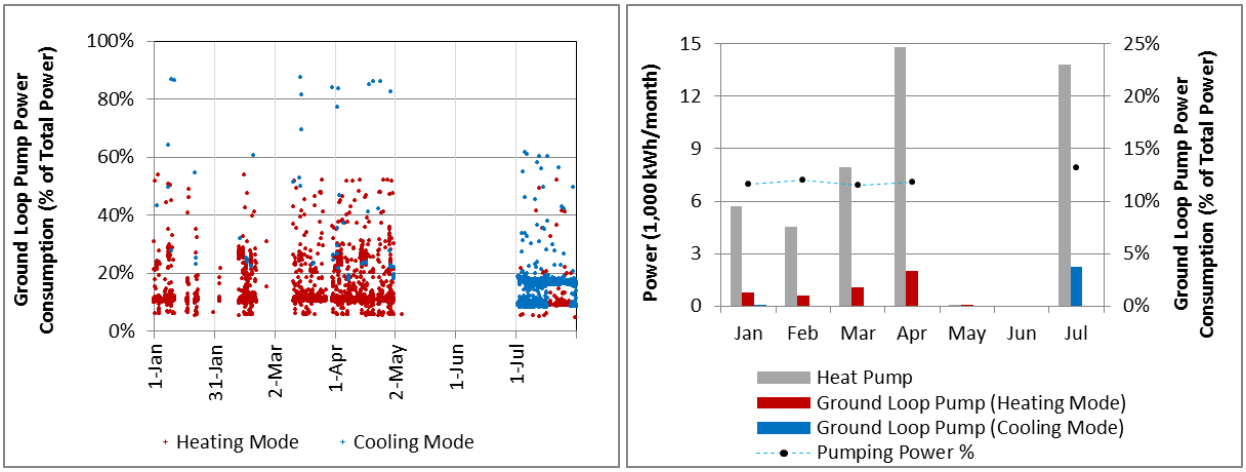

(a) (b)

Figure 9. Ground loop pumping power (a) as a fraction of total power consumption, (b) aggregated by month (From Liu, *et al. 2014*).

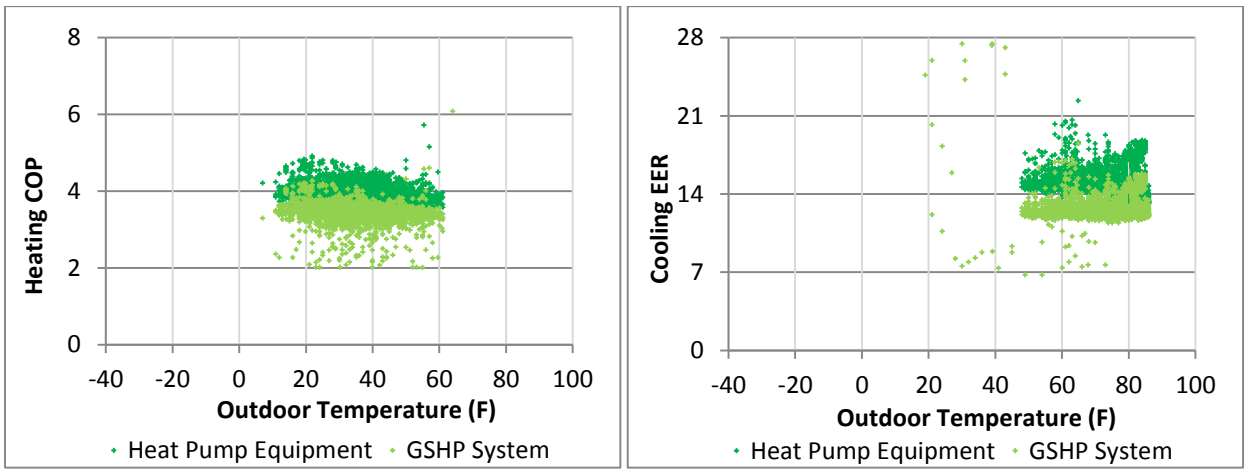

Figure 10. Ground Source Heat Pump system efficiency (From Liu, *et al. draft*).

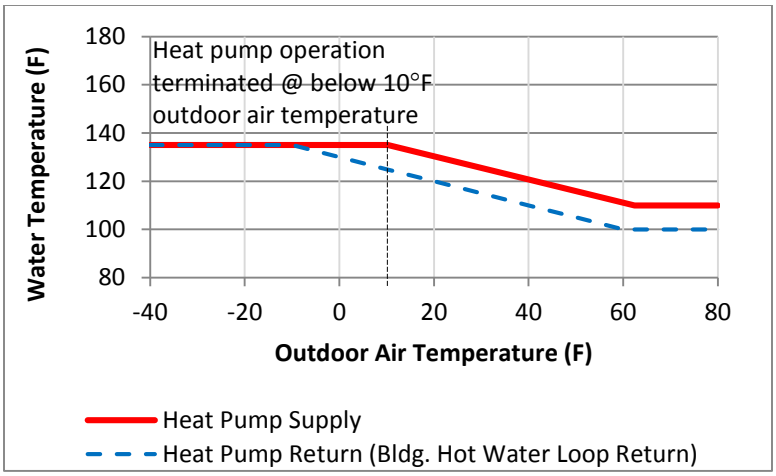

Figure 11. Recommended schedule for heat pump loop water temperature (From Liu, *et al. draft*).

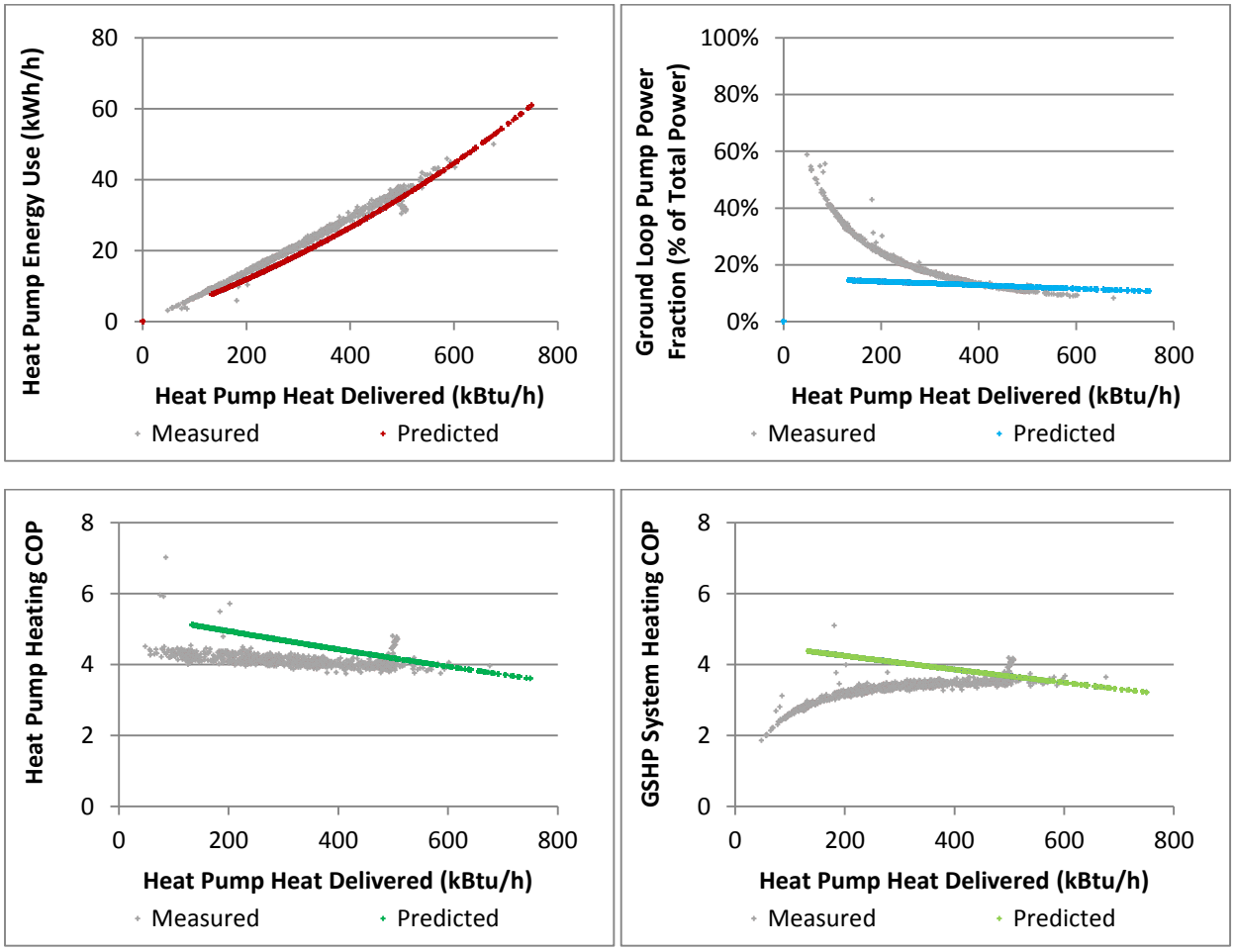

Figure 12. Comparison of measured and predicted performance of GSHP system (From Liu, *et al. draft*).

Education and Outreach highlights.

The third objective of the project was to involve faculty and students in projects about the system. Below are some of the highlights of this effort.

- Two students for their senior projects developed a program that improves the accessibility of the building system data (Jason Hamm and Chris Thrower, "Energy Analysis of a Hydronic HVAC System with a Geothermal Mine Water Heat-Pump Addition," poster presented at Montana Tech Expo, May 1, 2014).
- Rory Thornton Master's thesis was titled "Convection Mechanisms for Geothermal Heat Exchangers in a Vertical Mine Shaft" (2012). The goal of the project was to verify that water movement would result from temperature changes in the mine shaft. It was important to ascertain that water in the stope would move from the stope into shaft in order to take advantage thermal mass of the stope water. Abstract: This study evaluated the water-filled abandoned Orphan Boy mine as a heat source for an 80-ton heat pump to heat the 20,000 ft2 Natural Resources Building (NRB) at Montana Tech. The mine consists of an 800-foot vertical shaft connected to a large stope via three horizontal crosscut shafts. Total available water is 332 million gallons at 78° F with the majority held in the stope. The only practical placement of the heat exchangers is in the vertical shaft. Therefore the primary focus was to model the heat exchanger placement and configuration in the vertical shaft such that thermal currents develop between the stope and vertical shaft to access all available energy. Modeling of water flow, temperature profiles, and contribution from the walls, was done using finite difference methods and computational fluid dynamics, and then compared to empirical results. An optimum number of 11 down-hole heat exchangers (DHE) and their vertical placement was determined using the required heating load for the subject building of 810,000 BTU/hr. The results showed thermal currents developing and that water near the heat exchangers will remain above 67° F.
- Tyler Hagan's Master's project report was titled "Temperature and Pressure Sensing in Three Flooded Underground Mine Workings of Butte, Montana," (May 2015). Abstract: Temperature and pressure were measured in several flooded underground mine shafts in order to assess the potential for the development of additional mine-based geothermal heating in Butte, Montana, USA. Temperature was sensed using both optical fibers, functioning as a distributed sensor, and thermistors, functioning as point sensors; while pressure was sensed using a piezoresistive strain gauge. Upon observing good agreement between the continuous and discrete temperature sensors, we found no significant change in temperature with increasing depth within the water column. This suggests the thorough transfer of heat throughout the mine shaft via convection. Moreover, we found water temperature (T) is directly proportional to total mine shaft depth (z) via the equation: $T = 0.0225*z + 3.0194$, where T is in degrees Celsius and z is in meters – demonstrating an observed geothermal gradient of 22.5 ˚C per km.

- In the Spring 2014 semester, an advanced technical writing section performed pre-feasibility studies addressing the potential to develop a geothermal electric power plant at an abandoned mine site in Uptown Butte utilizing geothermal resources under Butte. Five teams respectively addressed (1) geological and geophysical issues with accessing these geothermal resources; (2) optimizing management practices for drilling exploration, injection, and production wells; (3) viability of using Berkeley Pit water for drilling, injection, and/or production; (4) economic feasibility; and (5) technical and economic potential for co-production of minerals through *in situ* solution mining as part of the geothermal fluid injection/recovery process.
- Through the decline tunnel built as part of the matching funds to provide construction access, many members of the public, faculty, and students have "toured" the installation, seeing the heat exchanger installation and piping systems in the Orphan Boy shaft, bringing good visibility to the project and the technology.

Products Developed

Publications

CDH Energy Corp, "Data Summary ARRA GSHP Site 10-Montana Tech," June 2014.

Hagan, Tyler D., "Temperature and Pressure Sensing in Three Flooded Underground Mine Workings of Butte, Montana, USA," May 2015, a Master's Project Report being archived in Montana Tech's Digital Commons.

Liu, Xiaobing, M. Malhotra, A. Walburger, Jack Skinner, D. Blackketter, "Performance Analysis of a Ground Source Heat Pump System Using Mine Water as Heat Sink and Source," Draft document, in preparation, expected submittal August 2015.

Liu, Xiaobing, "Performance of ARRA-Funded GSHP Demonstration Projects and Lessons Learned." Presented at the 2014 IGSHPA Annual Conference, October 15, 2014. *The Montana Tech mine-water project is among the smaller 25 projects reviewed and evaluated.*

Thornton, Rory, N. Wahl, and D.M. Blackketter, "Convection Mechanisms for Geothermal Heat Exchangers in a Vertical Mine Shaft," Society for Mining, Metallurgy, and Exploration, presented at 2013 conference, published in SME Transactions, Vol. 334, February 2014.

Thornton, Rory, "Convection Mechanisms for Geothermal Heat Exchangers in a Vertical Mine Shaft," Master's Thesis, 2012. ProQUest 1530289. http://gateway.proquest.com/openurl?url_ver=Z39.88-2004&res_dat=xri:pqdiss&rft_val_fmt=info:ofi/fmt:kev:mtx:dissertation&rft_dat=xri:pqdiss:1530289

Other products

No inventions, patent applications, or licensing agreements were developed. No software products or software manuals were developed.

Networks or collaborations: Through this project, Montana Tech and Oak Ridge National Laboratory (X. Liu) initiated a collaboration for analysis of geothermal system performance.

Appendix of Publications

Data Summary ARRA GSHP Site 19– Montana Tech

Introduction

This document describes the heat pump system configuration, and monitoring and data collection used to characterize the ground source heat pump (GSHP) system to be installed at Montana Tech's 60,000 SF Natural Resources Building (NRB) in Butte, MT. The GSHP system will operate in conjunction with an existing steam system (converted to hot water via heat exchangers) and an existing air-cooled chiller. Hot and chilled water are distributed throughout the building to various heating and cooling coils. The new GSHP unit is coupled to both the hot water piping, and chilled water piping, and will alternate between heating and cooling modes based on ambient temperature.

CWG Architects

Figure 1. Montana Tech Natural Resources Building

Data from both the conventional system and GSHP system will be used to compare the operation of the two systems for research and teaching purposes. In lieu of a well field, this GSHP system will use the warm mine waters of a flooded underground mine to provide energy for a closed-loop heat pump system that will connect into the existing steam system in the NRB. Figure 2 shows an aerial view of the building site.

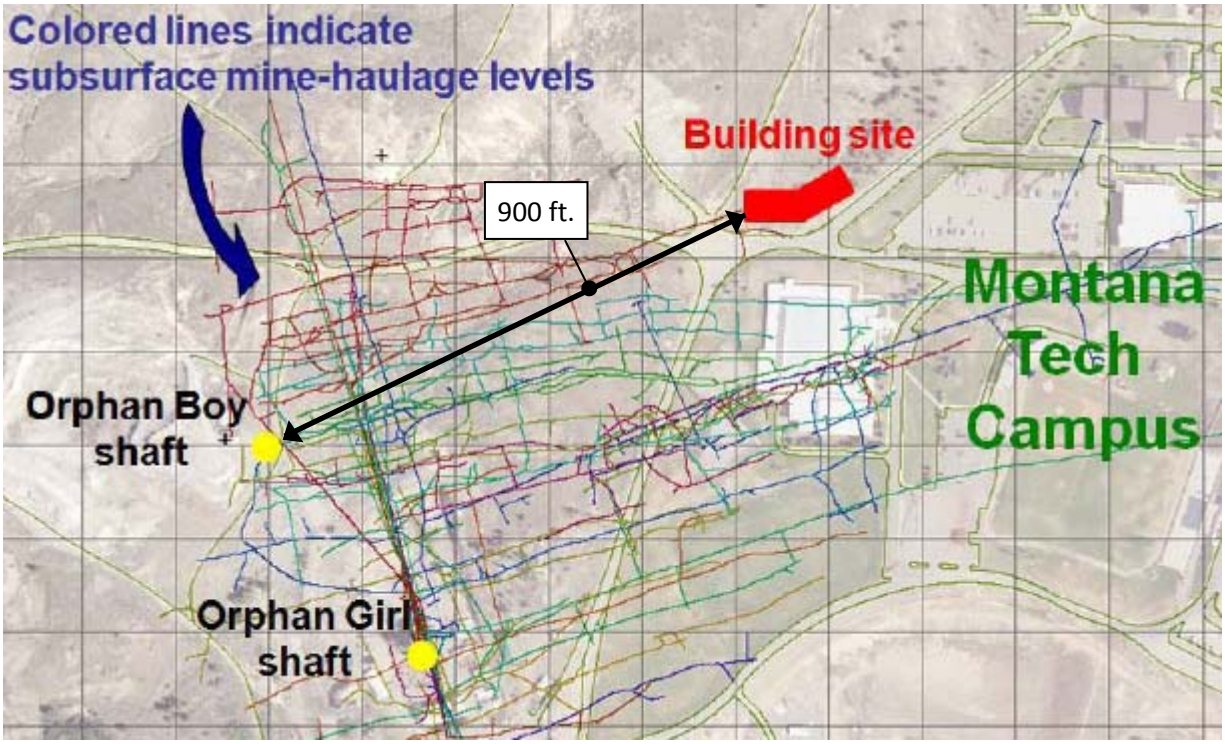

Figure 2. Aerial View of Mine Shaft and Building Location

Existing System

The building's heating/cooling system was equipped with a direct digital control (DDC) system during its construction that will provide the data point measurement output for the geothermal and conventional systems. The existing heat is supplied by a steam converter that is designed to supply up to 310 GPM of 140°F hot water. The building loop heating water pump has a VSD that varies the flow of the system. Space cooling in the existing system is supplied by a 169-ton air-cooled chiller housed outside the NBR building. The chiller supplies up to 385 GPM of chilled water with a leaving temperature of 45 – 65°F. The building chilled water pump has a VSD that varies the chilled water flow. All existing building pumps have both primary and standby pumps that are alternated by a schedule in the control room.

GSHP System Description

The GSHP system at this facility consists of one 50-ton Multistack MS050XN1H1R0AAC-R410Awater-to-water heat pump (WWHP) unit. The WWHP will provide either hot or chilled water for space conditioning, but not both modes simultaneously. The WWHP will provide cooling when the outside temperature is ≥ 65˚F, and heating when the outside temperature is ≤ 60˚F. The flow in the heat pump loop is circulated by two (2) VFD controlled 10-hp TACO pumps. The HP leaving temperature will automatically reset according to the outside temperature.

When ambient temperature is equal to or below 60˚F, the heat pump operates in the heating mode and the valves will modulate open to divert heating water to the heat pump loop. The heat pump will start when a positive flow is determined. The heat pump loop will intercept the water return to the steam converter and will divert a portion of that water according to the variable speed drive of the heat pump to vary the flow of the system. The heat pump will pre-heat the building loop water and return it to the same line before the converter. The steam converter will then add the remainder of the heat required to raise the mixed return and preheated water to the supply temperature set point of 140°F. The remainder of the building hot water distribution system and operation is unchanged by the addition of the GSHP unit.

The heat pump will operate in the cooling mode when the temperature is equal to or above 65˚F. The valves will modulate to divert cooling water to the heat pump loop, and isolate the connection to the building hot water piping. When a positive flow rate is determined, the heat pump will start. The heat pump loop will intercept the chilled water at the building return piping header and divert a portion of the flow to the heat pump. The heat pump will cool the water and return it to the same line before the building chilled water pump and chiller. The existing chiller will then provide the remainder of the cooling capacity necessary to meet the required supply temperature setting of 45 to 65°F, which is reset with outdoor temperature. Similar to the heating system, the chilled water distribution piping and AHU operation is unaffected by the presence of the GSHP unit. Appendix A lists the AHUs and ERUs in operation at the facility.

All of the new pumps associated with the installation of the heat pump system have primary and standby pumps alternated by a schedule in the control system.

Mine Water System

The WWHP uses a closed loop system in the warm mine waters of the flooded underground Orphan Boy Mine that is connected at depth with the nearby Orphan Girl Mine. Together they are considered as a single underground reservoir. The water level in the mines is 110 to 120 ft. The Orphan Boy Mine is located approximately 1100 feet from the Natural Resources Building. The distance from the mine entrance to the water is 200 feet. There exists a set of 6-inch supply and return pipes from the building to the exterior of the building. The pipe was extended to the 100-foot level using 3-inch HDPE pipe. Twenty ¾-inch HDPE parallel loops, each 600 feet long, that was lowered into the existing mine shaft and into the mine waters.

The heat sink for the new heat pump is the Orphan Boy mine, a flooded mine with water that remains at a steady state temperature of 78˚F. The flow in the ground loop (which exchanges heat with the mine water) is circulated by two redundant 7.5-hp constant speed TACO pumps that are housed on the second floor of the Natural Resources Building. The ground loop pumps operate in conjunction with the existing pumps on the building side of the heat pump unit. The instrumentation and trending for the ground loop is an extension of the existing control system. Sensors are used to measure the heat sink water temperature to document ground loop heat transfer.

Figure 3 displays a basic schematic of the GSHP system, along with the location of the data points to be monitored for ongoing performance monitoring. Only the data points currently available are shown. The performance data so far describes heating performance only.

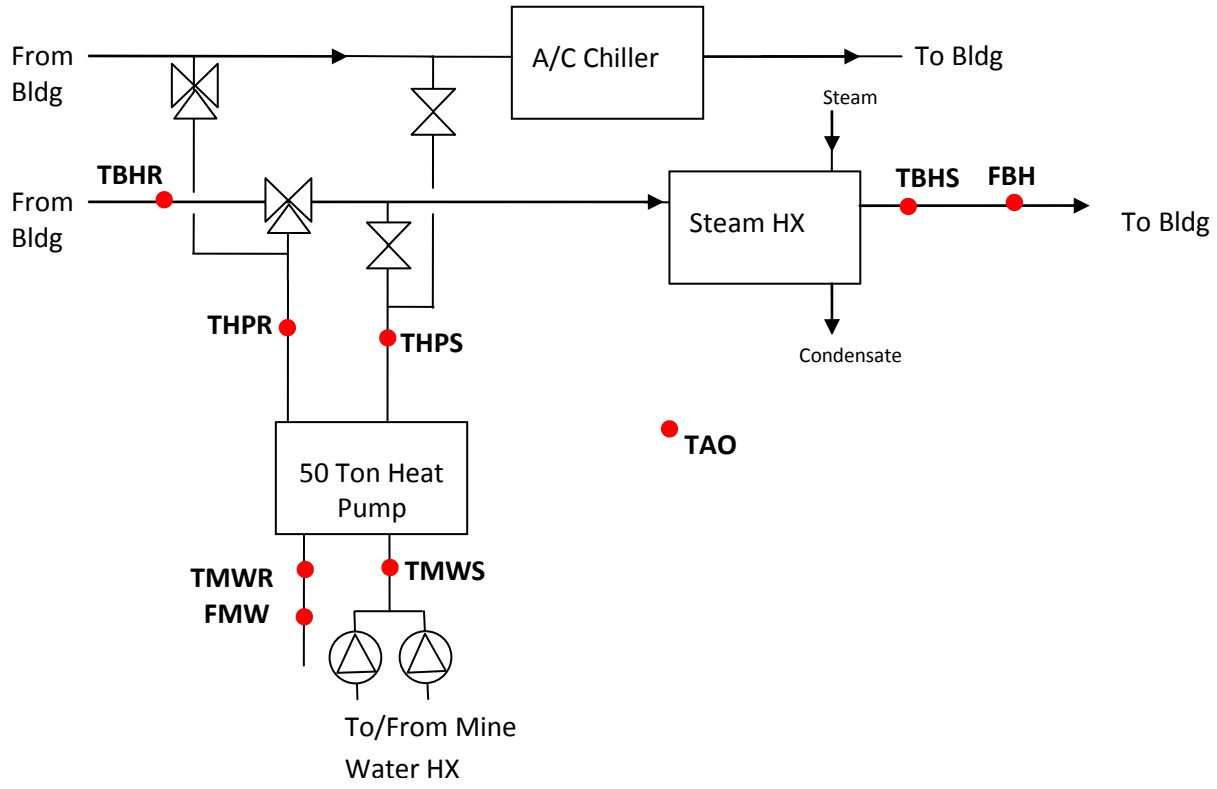

Figure 3. GSHP Simplified System Schematic

Data Collection

Performance monitoring and data collection for the WWHPs system will be provided by Montana Tech using the on-site Niagara^{AX} system. The Niagara^{AX} system will poll the sensors once per second and provide 15-minute totals or averages of each sensor depending on the sensor type. The data records will be recorded in a column oriented, comma delimited file (CSV format) along with a corresponding date/time stamp for the data record.

Table 1. Montana Tech Monitored GSHP Data Points – Currently Available

No.	Data Point	Description	Units
Ground Loop (coupled to Mine Water)			
1	TMWS	Mine Water Loop Supply Temperature	deg F
2	TMWR	Mine Water Loop Return Temperature	deg F
3	FMW	Mine Water Loop Flow	GPM
Heat Pump Building Loop			
4	THPS	HP Loop Supply Temperature	deg F
5	THPR	HP Loop Return Temperature	deg F
Building Heating Loop			
6	TBHS	Building Heating Loop Supply Temperature (After Steam HX)	deg F
7	TBHR	Building Heating Loop Return Temperature	deg F
8	FBH	Building Heating Loop Flow	GPM
Ambient Conditions			
9	TAO	Ambient Temperature	deg F
Total Facility			
10	WT	Total Building Power	kW/kWh

Ground Loop (Mine Water) Trends

Figure 4 displays the variation in the supply and return temperatures from the ground loop (mine water) observed during the monitoring period spanning from January 1, 2014 to April 31, 2014. The ground loop temperature supplied from the ground loop ranged from 64.7°F – 79.8°F, with an average temperature of 73.3°F. Supply temperature decreases slightly during HP operation to an average of 72.4°F.

During HP operation, the ground loop return temperature ranged from 52.0°F – 84.9°F, with an average temperature of 67.8°F. The average temperature differences during heat extraction and heat rejection are observed to be 4.1°F and 1.1°F respectively. The ground loop flow rate for the monitoring period averaged at 63.5 GPM with flow reaching up to 90.4 GPM during heat pump operation.

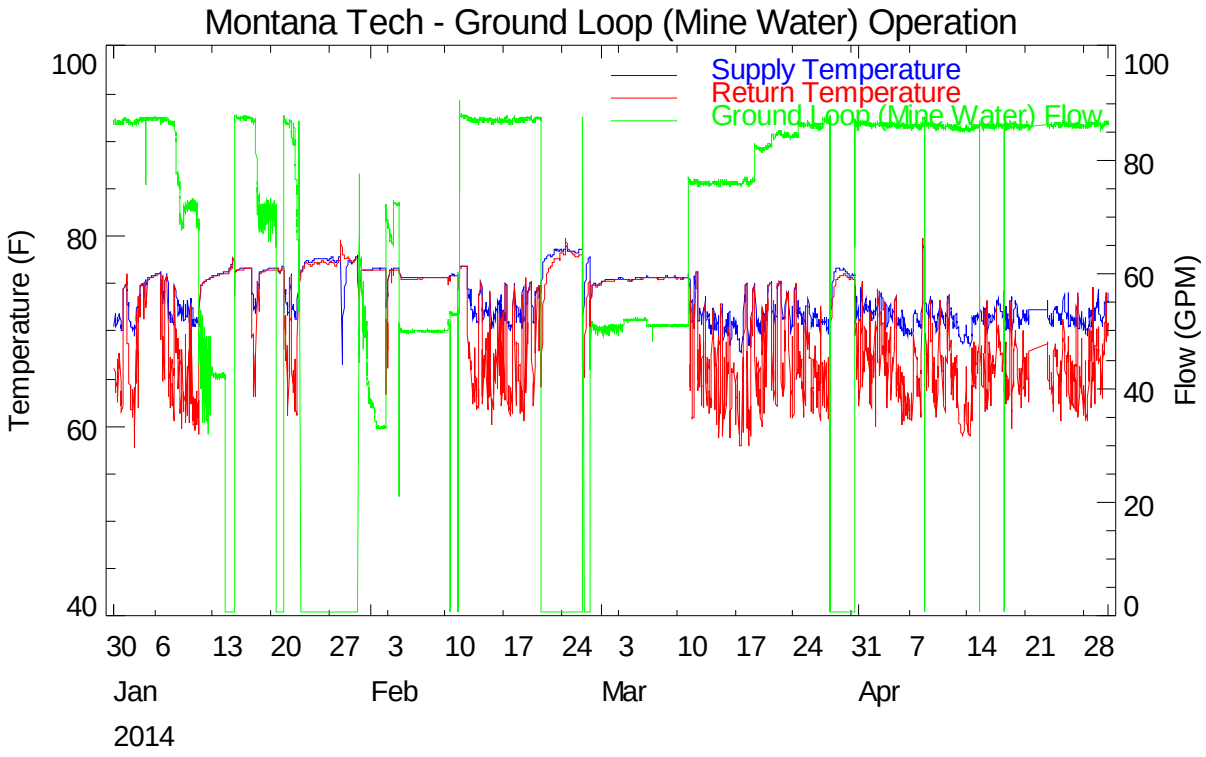

Figure 4. Ground Loop (Mine Water) Temperature and Flow Trend

Temperatures are also monitored on the building side of the heat pump. Heat pump operation was observed by a deviation of the supply and return temperatures during heating operation. No cooling operation was observed so far. In Figure 5 the building side supply temperature of the heat pump ranged from 118°F - 138°F, with an average temperature of 128°F. The building side return temperature of the heat pump ranged from 111°F – 122°F, with an average of 118°F resulting in a temperature difference of 10°F across the building loop during heat pump operation.

High temperature excursions with low temperature difference occur when the heat pump is not operating, and the building is operating under steam heat on the building loop.

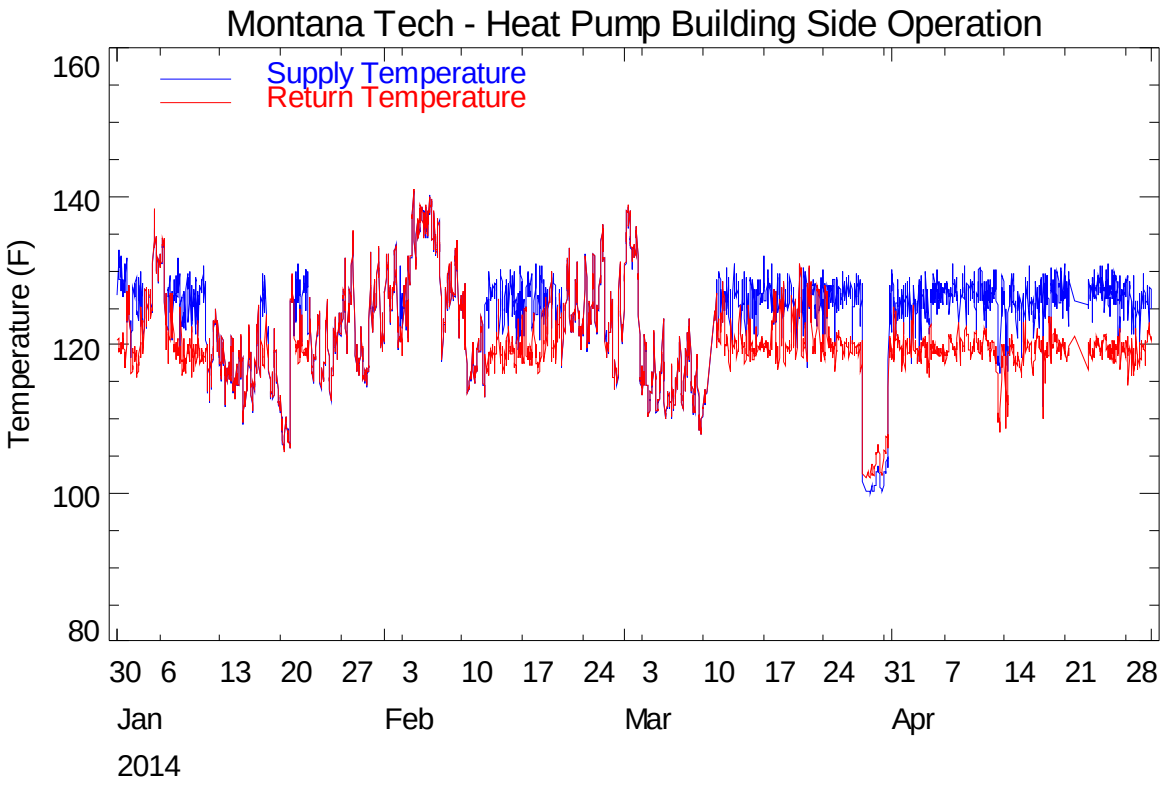

Figure 5. Heat Pump Building Side Temperature Trend

Heat Transfer on the Ground Loop (Mine Water)

Heat transfer through the ground loop was calculated using the ground loop flow rate and the temperature difference between the ground loop supply and return temperatures. The equation used to calculate heat transfer in MBtu/h is below. In this equation, k is a factor that incorporates conversion factors and the specific gravity of the fluid, which is estimated to be 480 Btu/h-gpm-°F for 20% ethanol at 60°F.

$$Q_{GL} = K \times FMW \times (TMWS-TMWR) /1000$$

Where:

Q_{GL}	=	Heat transfer to mine water (MBtu/h) (extraction >0, rejection <0)
FMW	=	Mine water loop flow rate (GPM)
TMWS	=	Mine water supply temperature to heat pump (°F)
TMWR	=	Mine water return temperature to heat pump (°F)

Figure 6 shows the heat transfer rate over the monitored period with heat extraction during heating operation shown as positive while heat rejection during cooling operation is shown as negative. No considerable heat rejection was observed in the ground loop, because the building is in the heating mode during the period examined. The brief areas of heat rejection are transients at startup and shutdown of a heat pump cycle.

The heat extraction through the ground loop averaged 367 MBtu/h during heat pump operation, with brief periods reaching a maximum of 697 MBtu/h. Over the 120 day monitoring period, the ground loop was observed to extract 340,973 MBtu from the mine water.

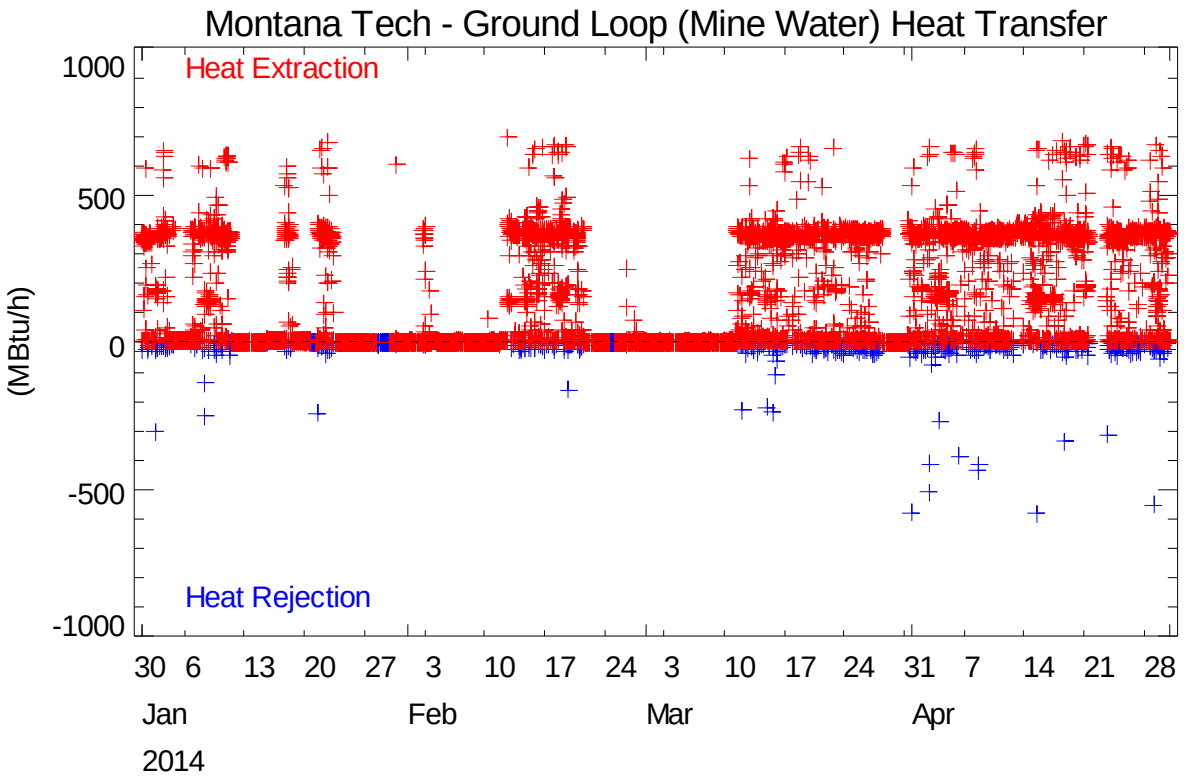

Figure 6. Heat Transfer over Monitored Period

The shade plots of heat transfer displayed in Figure 7 show the operating patterns for heat extraction operation in the ground loop. On the shade plot, the day of the year is shown on the x-axis and the hour of the day is shown on the y-axis. Each day is represented by a vertical stripe of 96 15-minute data records. Heat transfer in each period is represented by varying shades of gray. Intervals with higher heat transfer are represented by darker shades of gray, and intervals of lower heat transfer are represented by light shades of gray. Heat extraction (and HP heating operation) are highly scattered throughout the monitored period, with periods of HP operation spanning from a few days in early winter, to several weeks of runtime in early spring.

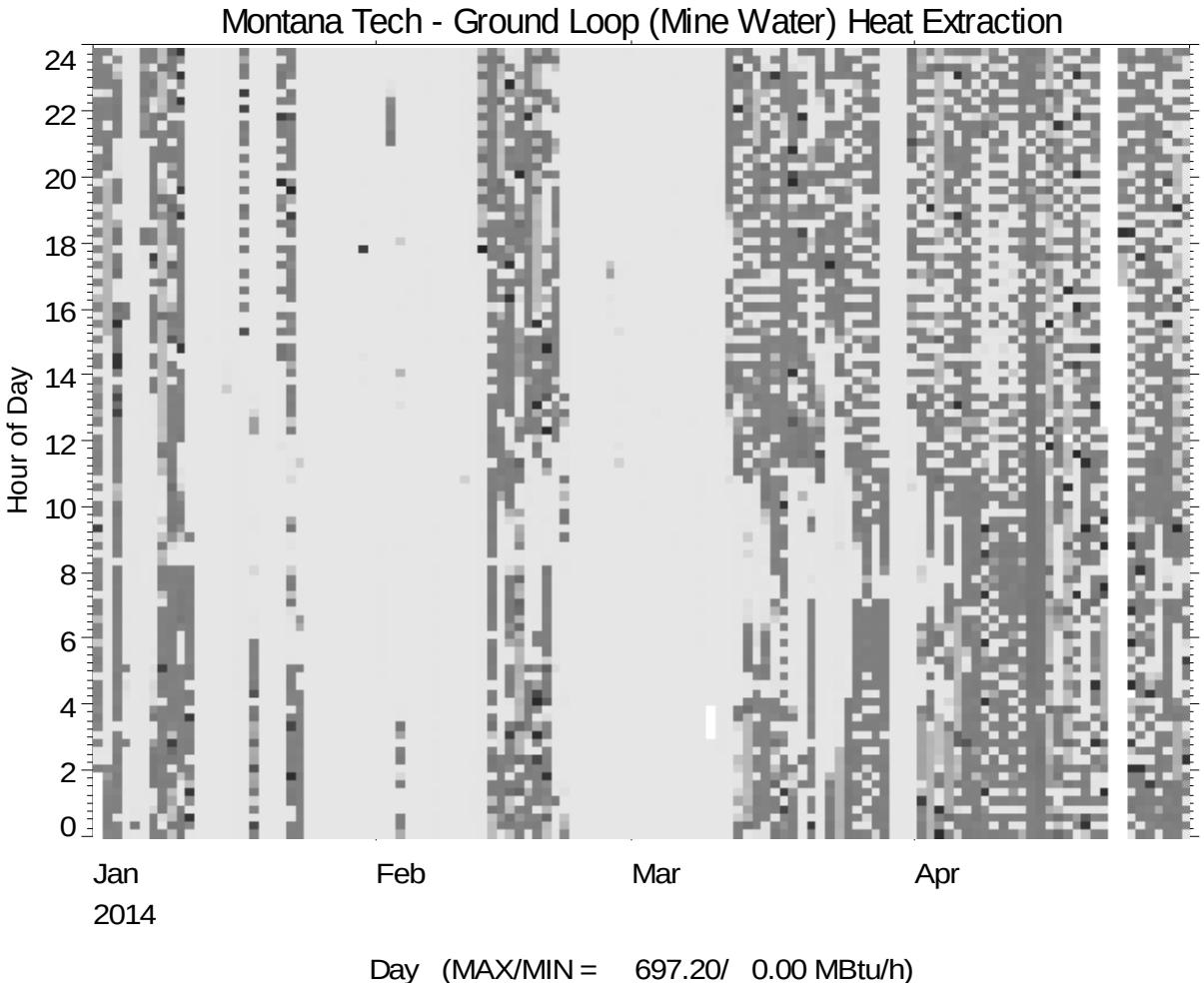

Figure 7. Ground Loop Heat Extraction (Heating Operation) Patterns

Figure 8 shows variation of daily heat transfer through the ground loop with changes in ambient temperature. The heat pump can only operate to meet the entire heating load of the building at mild ambient temperatures at and above 40°F, where the daily heat extraction trend becomes linear. Other heat extraction data is scattered due to intermittent operation of the heat pump. On the peak day of April 13, 2014, the HP unit extracted a total of 8,657 MBtu from the ground loop and mine water.

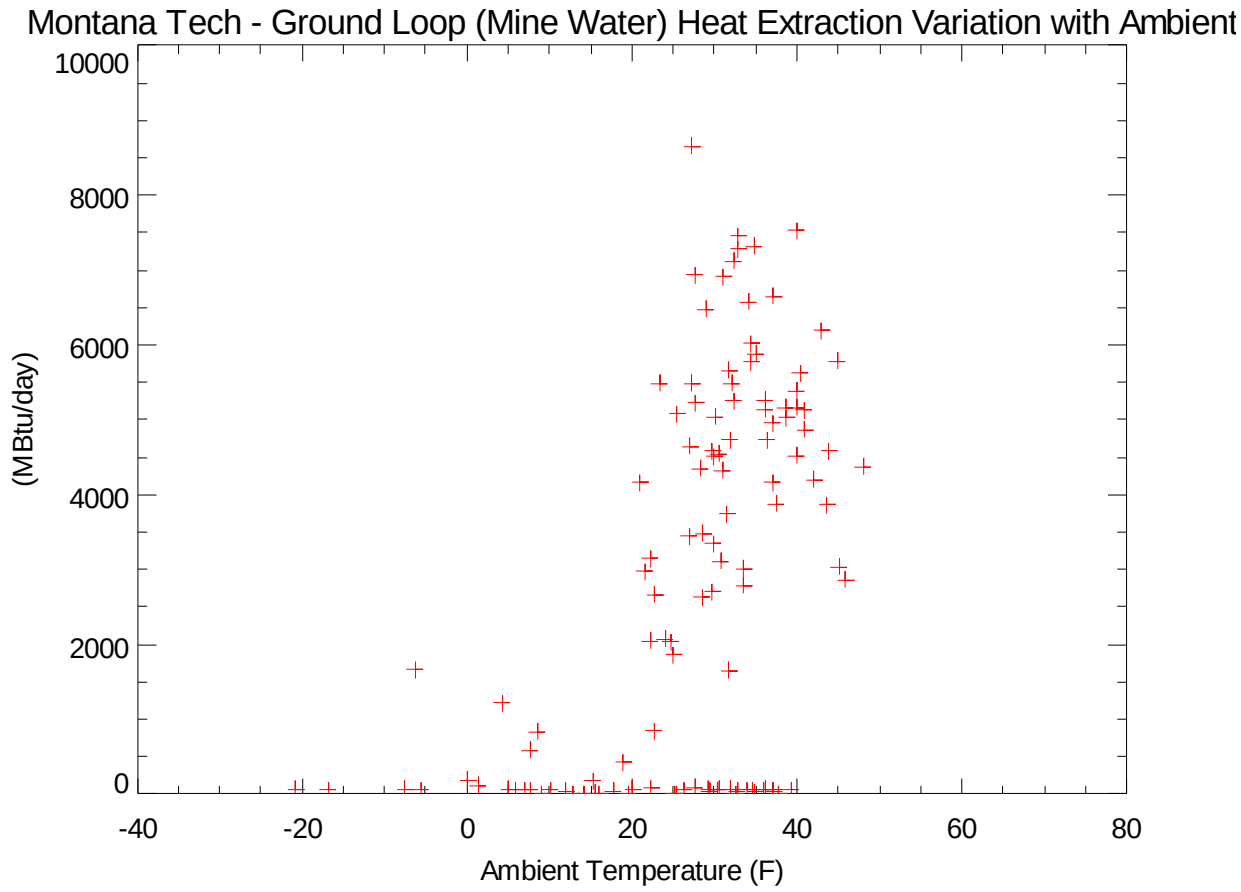

Figure 8. Daily Heat Pump Energy Variation vs. Ambient Temperature

Heat Pump Performance

Heat pump performance will be determined using a curve fit of the manufacturer's performance data relating heating COPh and cooling EERc to entering source water and leaving water conditions.

$$COPh = f(TSW, TLW)$$

$$EERc = f(TSW, TLW)$$

Where:

TSW = Source Water Temperature (F) (TMWS)
TLW = Leaving Water Temperature (F) (THPS)

The curve fit relating COP to TSW and TLW is a second order polynomial with a cross product of the form:

$$C_0 + C_1 \times TSW + C_2 \times TLW + C_3 \times TSW^2 + C_2 \times TSW \times TLW + C_5 \times TLW^2$$

Coef.	COPh	EERc
C_0	8.240000	24.940000
C_1	0.118200	-0.292400
C_2	-0.083030	0.454500
C_3	0.000543	0.000981
C_4	-0.000897	-0.003214
C_5	0.000279	0.001488

LEAVING CHILLED WATER

MS050XN	42°F			44°F			46°F			48°F			50°F		
Leaving Source Water °F	Power (kW)	Cool (Tons)	Cool (EER)	Power (kW)	Cool (Tons)	Cool (EER)	Power (kW)	Cool (Tons)	Cool (EER)	Power (kW)	Cool (Tons)	Cool (EER)	Power (kW)	Cool (Tons)	Cool (EER)
75°F	32.6	54.6	20.1	32.8	56.8	20.8	33.0	59.0	21.5	33.2	61.3	22.2	33.4	63.7	22.9
80°F	34.1	53.3	18.8	34.3	55.4	19.4	34.4	57.6	20.1	34.6	59.8	20.7	34.8	62.1	21.4
85°F	35.7	51.9	17.4	35.9	54.0	18.0	36.1	56.1	18.7	36.2	58.3	19.3	36.4	60.6	20.0
90°F	37.5	50.5	16.1	37.7	52.5	16.7	37.8	54.6	17.3	38.0	56.7	17.9	38.1	58.9	18.6
95°F	39.5	49.1	14.9	39.6	51.0	15.5	39.7	53.1	16.0	39.9	55.1	16.6	40.0	57.3	17.2
105°F	43.8	46.0	12.6	43.9	47.9	13.1	44.1	49.8	13.6	44.2	51.8	14.1	44.3	53.8	14.6

LEAVING HOT WATER

MS050XN	110°F			120°F			125°F			130°F			135°F		
Leaving Source Water °F	Power (kW)	Heat (MBH)	Heat COP	Power (kW)	Heat (MBH)	Heat COP	Power (kW)	Heat (MBH)	Heat COP	Power (kW)	Heat (MBH)	Heat COP	Power (kW)	Heat (MBH)	Heat COP
30°F	46.1	558.1	3.6	51.4	544.6	3.1	54.3	538.3	2.9	57.4	532.2	2.7	60.6	526.6	2.5
35°F	46.3	605.5	3.8	51.7	588.6	3.3	54.7	580.7	3.1	57.8	572.8	2.9	61.0	565.5	2.7
40°F	46.6	656.7	4.1	52.0	636.4	3.6	55.0	626.5	3.3	58.1	617.1	3.1	61.4	607.8	2.9
45°F	46.9	712.5	4.5	52.3	688.5	3.9	55.2	676.7	3.6	58.4	665.2	3.3	61.7	653.9	3.1
50°F	47.2	773.4	4.8	52.6	745.1	4.2	55.5	731.2	3.9	58.7	717.6	3.6	62.0	704.0	3.3
55°F	47.5	839.4	5.2	52.8	806.4	4.5	55.8	790.3	4.2	58.9	774.6	3.9	62.3	758.7	3.6

Note: COPc = EERc / 3.413

Figure 9. Multistack MS050XN Performance Data

Heat pump energy is then calculated from the measured ground loop heat extraction or rejection for each mode using:

$$WHPc = QGL / (EERc/3.413 + 1) \qquad (QGL < 0 \text{ only})$$

$$WHPh = QGL / (COPh - 1) \qquad (QGL > 0 \text{ only})$$

Figure 10 shows the calculated heat pump heating power using the measured heat extraction and performance curves. Heat pump power during typical operation averaged 27 kW, with a peak power of 55 kW. During the monitoring period, the heat pump consumed a calculated 23,294 kWh.

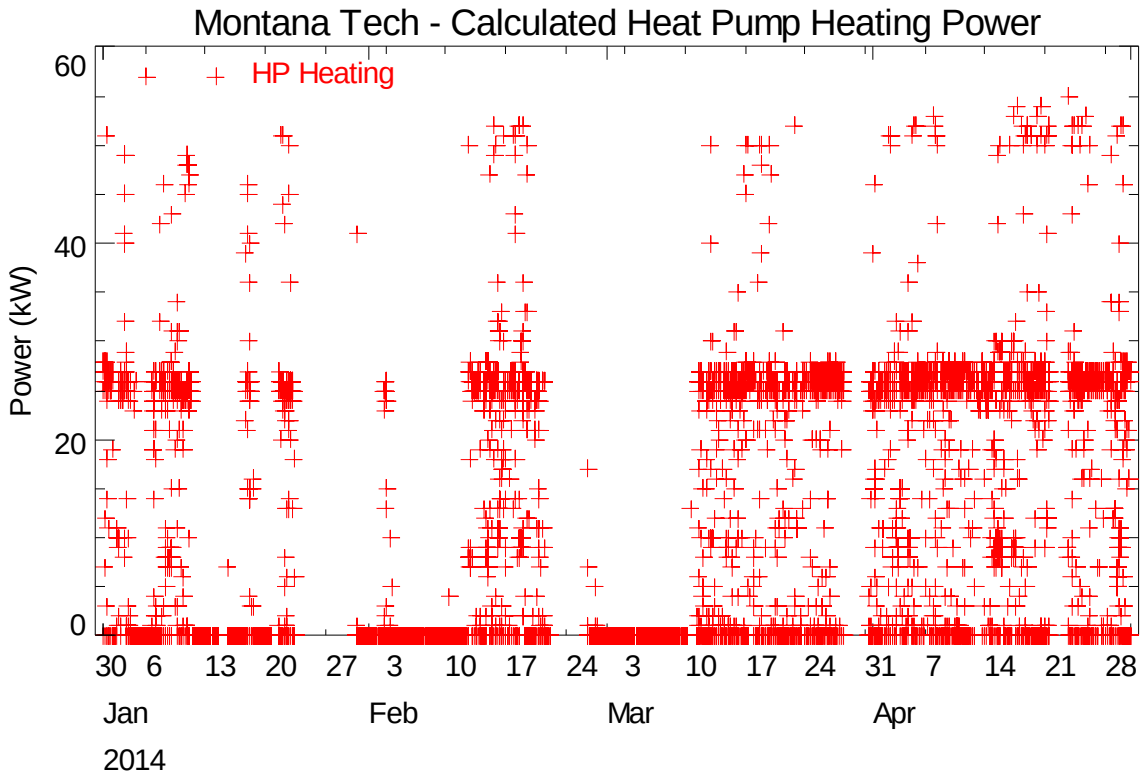

Figure 10. Heat Pump Heating and Cooling Power Calculated by Ground Loop Heat Transfer and COP/EER

Figure 11 shows variation of heat pump energy with ambient temperature, which has a similar pattern to the daily heat extraction trends shown in Figure 11. The daily heat pump energy consumption reaches a maximum 540 kWh/day.

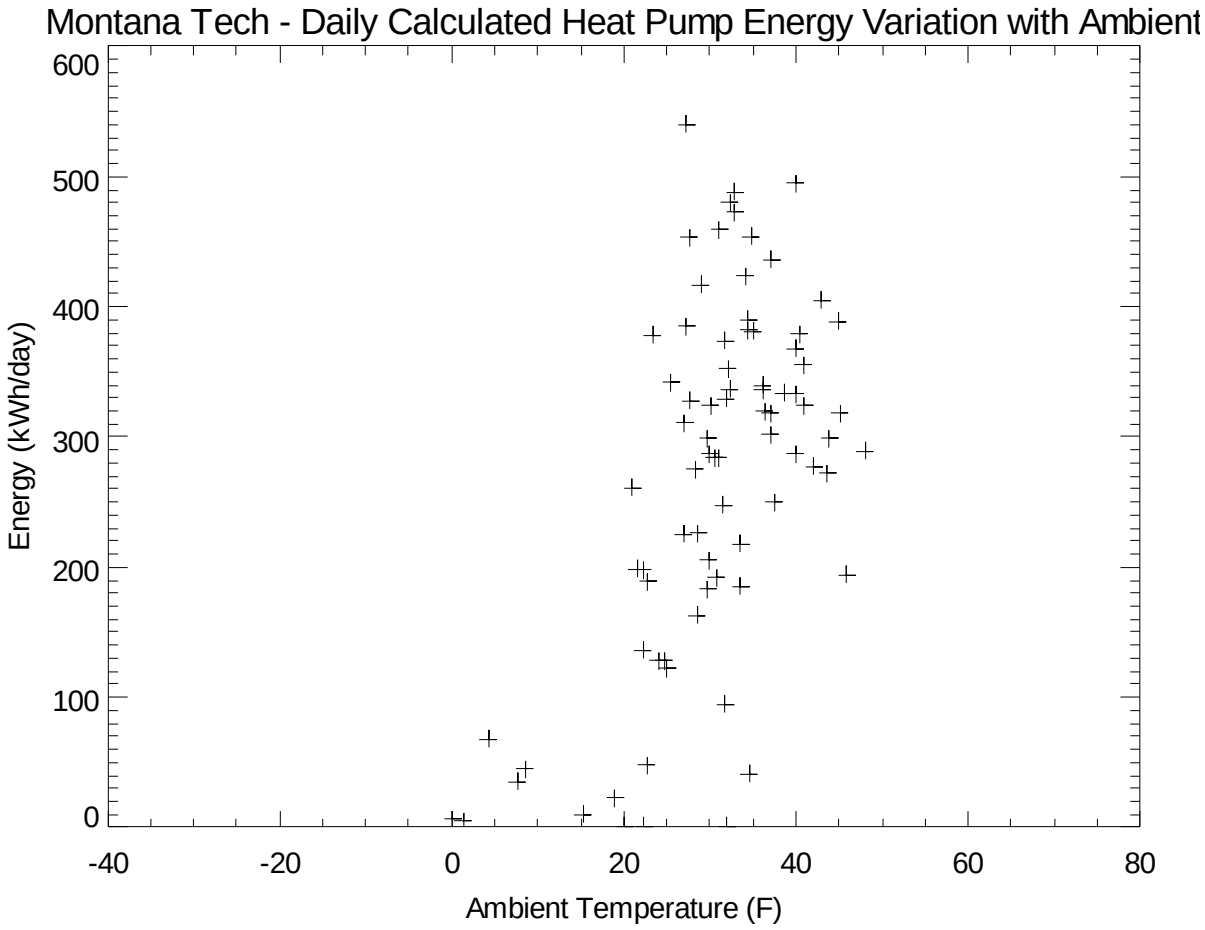

Figure 11. Heat Pump Daily Energy Variation with Ambient Temperature

Mine water pump energy is not measured. The energy consumption for pumping mine water to the heat pump unit was calculated using a fixed power of 4.47 kW (7.5 HP × 0.746 kW/HP × 80% loading) for each 15-minute interval where mine water flow was observed. The mine water pump was estimated to consume 12,643 kWh over the monitored period.

Heat Pump Operation and Loading

The flow on the building side of the heat pump is not measured, but a flow-setting valve is in place to limit the flow through the heat pump to 80.9 GPM. Using this stipulated flow and the measured temperature difference the heat delivered by the heat pump unit was calculated.

The heat pump cooling and heating load is determined using the calculated heat pump power and ground loop heat transfer

$$\mathrm{QHPH} = \mathrm{QGL} + \mathrm{WHPH} \times 3.413$$

Where:

QHPH = Heat Pump Heating Load (MBtu/h)
QGL = Ground Loop Heat Transfer (MBtu/h)
WHPH = Heat Pump Cooling Power (kW)

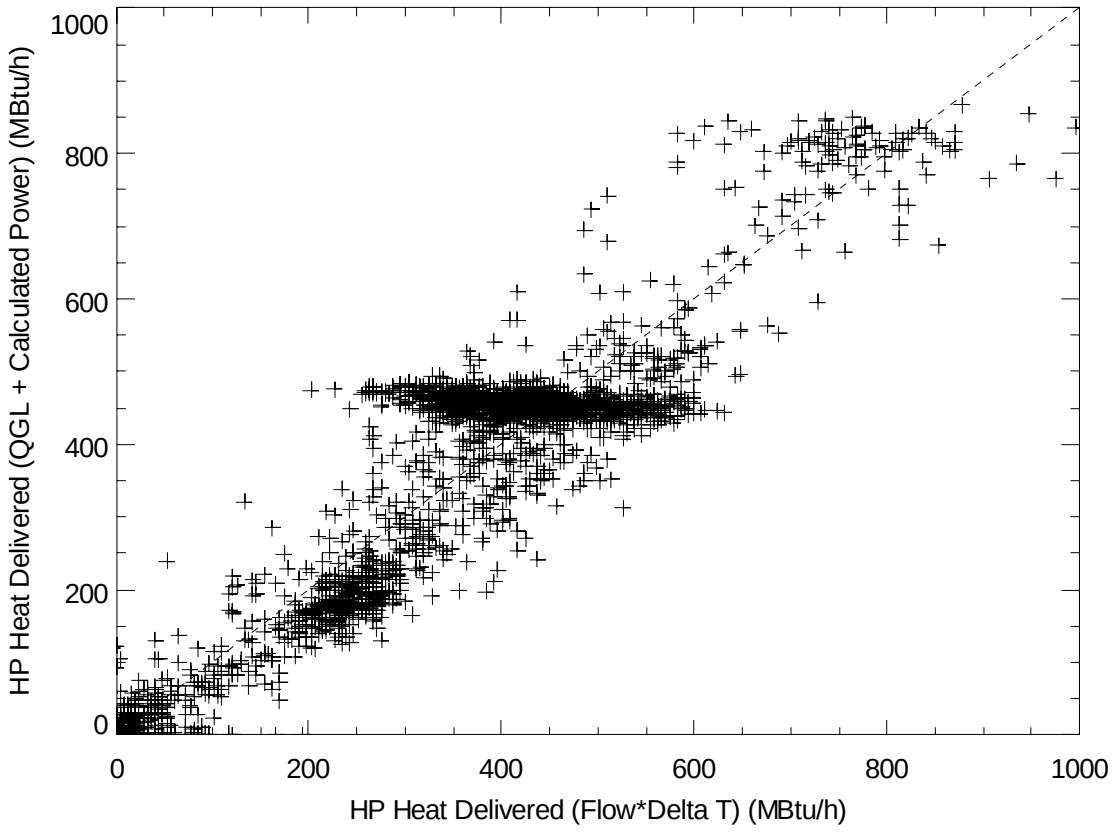

Figure 12. Heat Pump Daily Energy Variation with Ambient Temperature

The heat pump heating capacity calculated using both methods are in agreement. The heat pump unit provides up to 865 MBtu/h to the building heating loop. During the monitored period, the heat pump provided 398,216 MBtu of heat to the building.

Building Heating Loop Trends

The heat pump interfaces with the building heating loop via a series of three-way valves that direct a portion of the building loop flow through the heat pump unit for pre-heating prior to entering a steam to hot water heat exchanger. When the heat pump is down, all the building heat is provided by the steam heat exchanger. The installed instrumentation allows calculation of the total building heating load, and determining the amount of heat supplied by the heat pump unit.

Figure 13 displays the variation in the supply and return temperatures from the building heating loop. The supply temperature of the building heating loop ranged from 106°F – 168.2°F with an average temperature of 129.8°F. The building heating loop return temperature ranged from 101°F – 153.5°F, with an average temperature of 120.4°F. The average temperature difference on the building heating loop was 9.4°F. Flow on the building heating loop displayed substantial variation, ranging from 100 GPM to 177 GPM, with an average of 113 GPM.

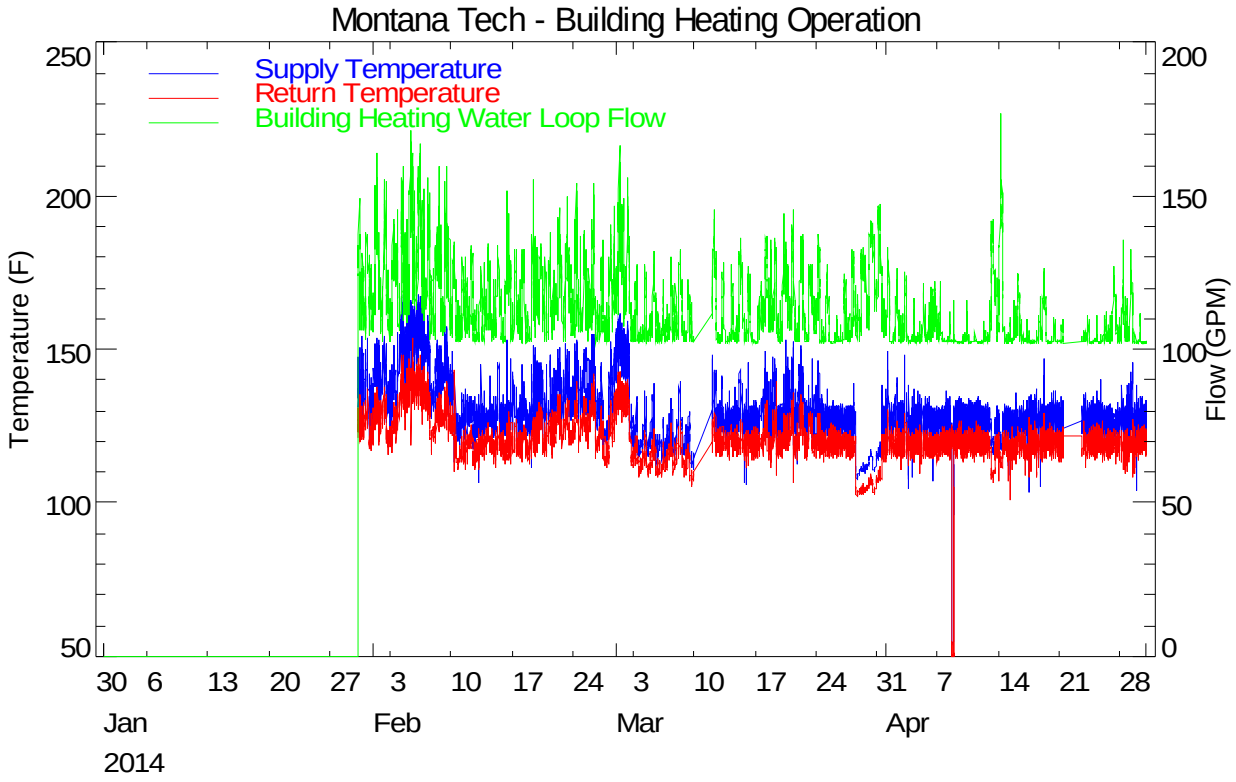

Figure 13. Building Heating Loop Temperature and Flow Trend

Total Building Heating Load

The total building heating load can be calculated from flow rate and the temperature difference between the supply and return temperature of the building heating loop.

$$QH = K \times FBH \times (TBHS-TBHR) /1000$$

Where:

QH	=	Building heating load (MBtu/h) (heating >0)
FBH	=	Building heating water loop flow rate (GPM)
TBHS	=	Building heating loop supply temperature (°F)
TBHR	=	Building heating loop return temperature (°F)
K	=	500 for water, or the appropriate value for glycol

Figure 14 shows the heating load on the building heat loop over the monitored period, with heat supplied from all sources (steam and heat pump). The peak building heat load in early February was near 2,000 MBtu/h, but a more typical value for building heat load during winter periods was 1,500 MBtu/h.

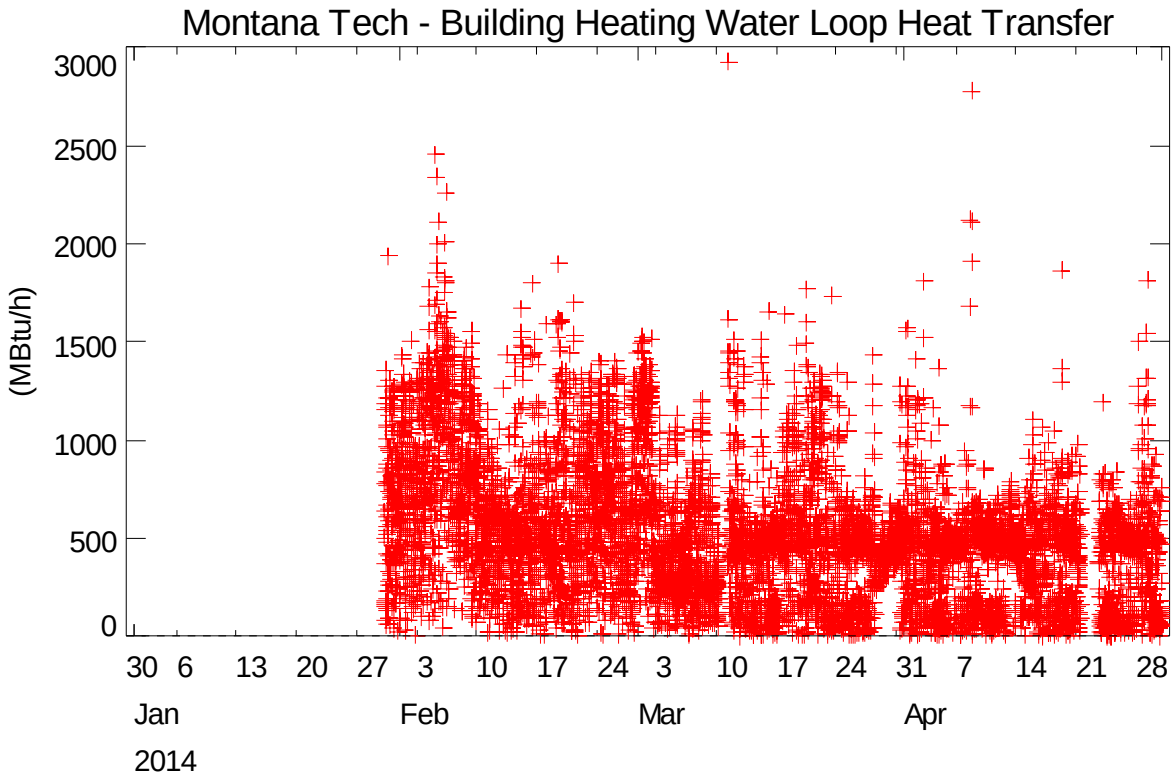

Figure 14. Building Heating Water Loop Heat Transfer

The shade plot in Figure 15 shows no distinct changes in the heating pattern at the building, other than the generally decreasing trend with the change of seasons. Heating is required in the building throughout the day, and no thermostat setback or scheduling is observed.

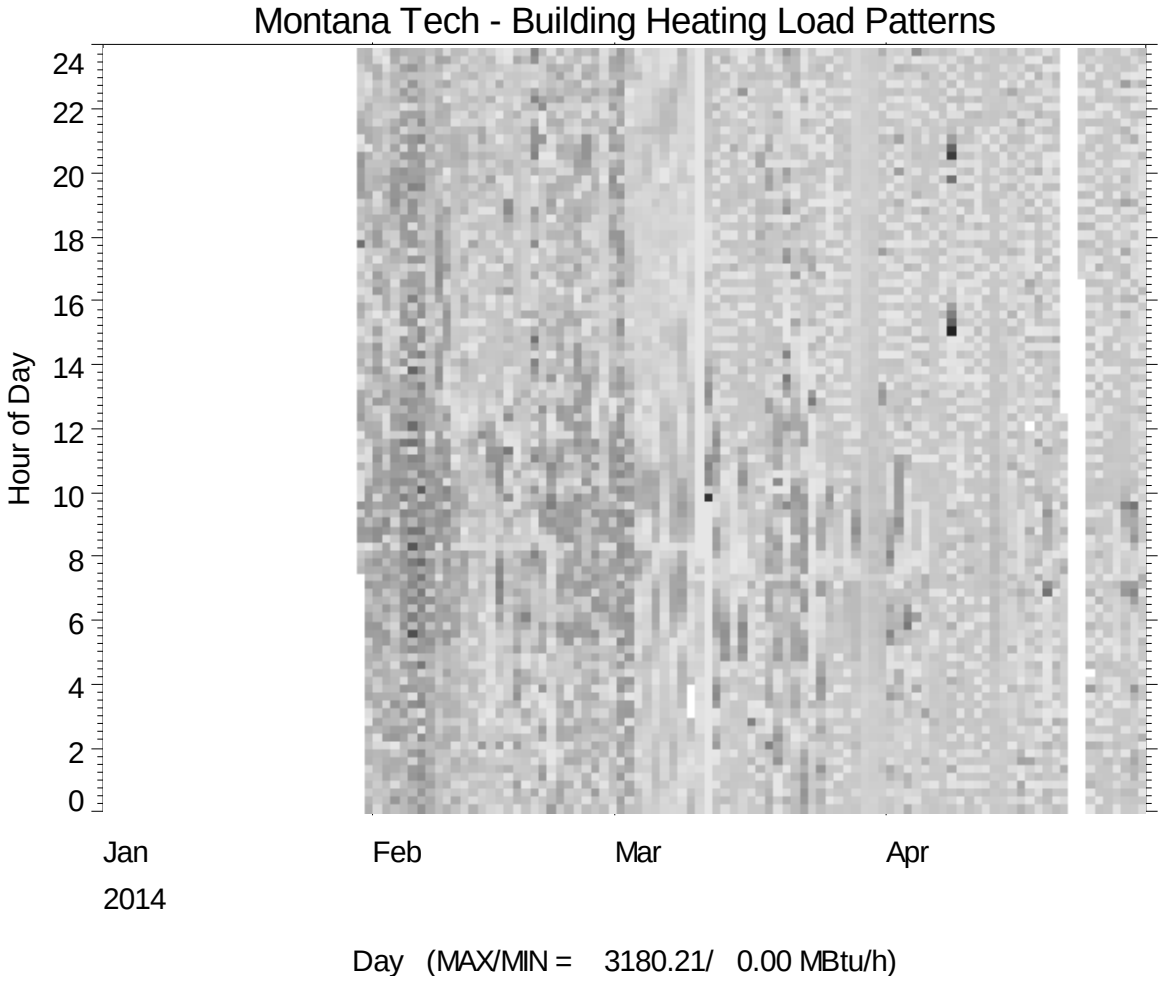

Figure 15. Heat Rejection to the Building from Building Heating Loop

Figure 16 shows variation of the building heating load with ambient temperature. The figure indicates that the total building heating load follows a linear trend with ambient temperature. A maximum heating load of around 25 MMBtu/day was observed around 0°F. The heat pump is observed to contribute a considerable heating when the ambient temperature is between 20°F and 40°F. During the period examined, the building load totaled 1,055 MMBtu, and the heat pump supplied 331 MMBtu (31%) of the total heating load.

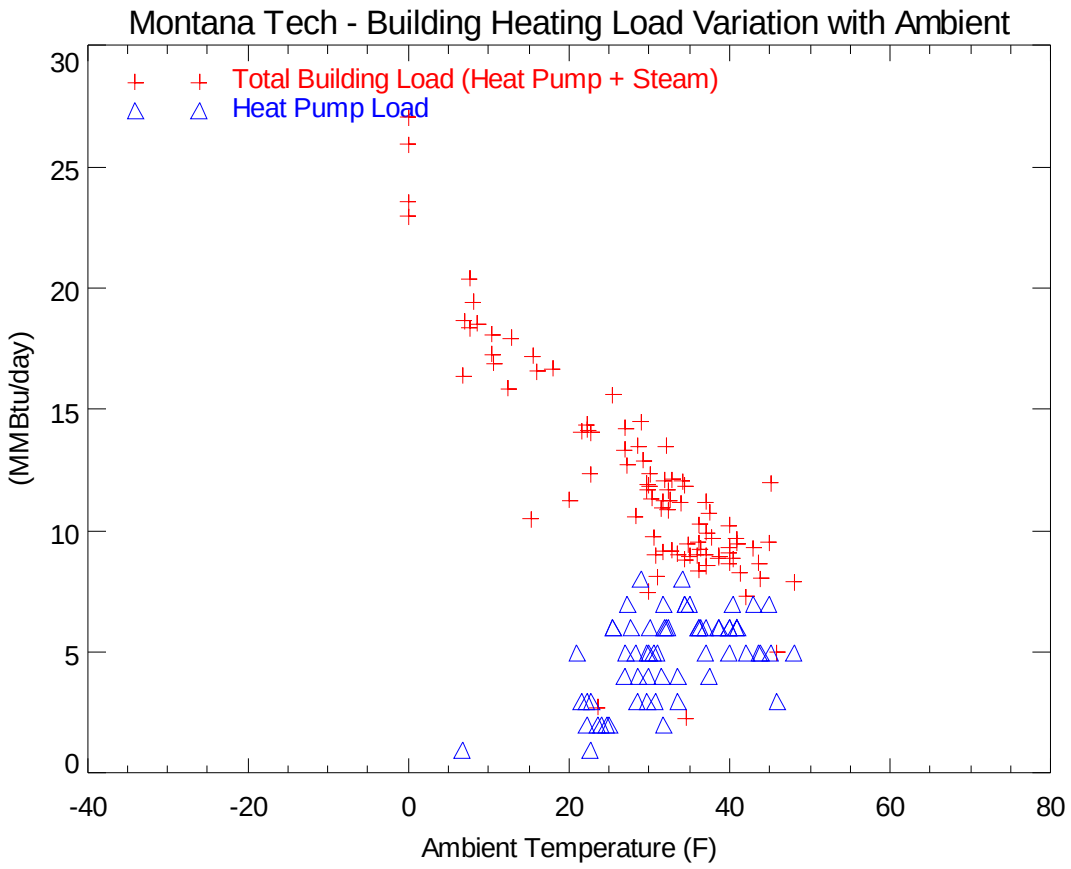

Figure 16. Variation of Building Heating Load with Ambient Temperature

Total Building Energy

Figure 17 displays the total building power data collected. Building power is typically near 55 kW when the heat pump is not in operation. Peak power when the heat pump operates in heating reaches 130 kW. Also displayed on the plot is the calculated heat pump power for comparison. Over the monitored period, the heat pump unit consumed 23,294 kWh (12%) of the 193,960 kWh building energy consumption.

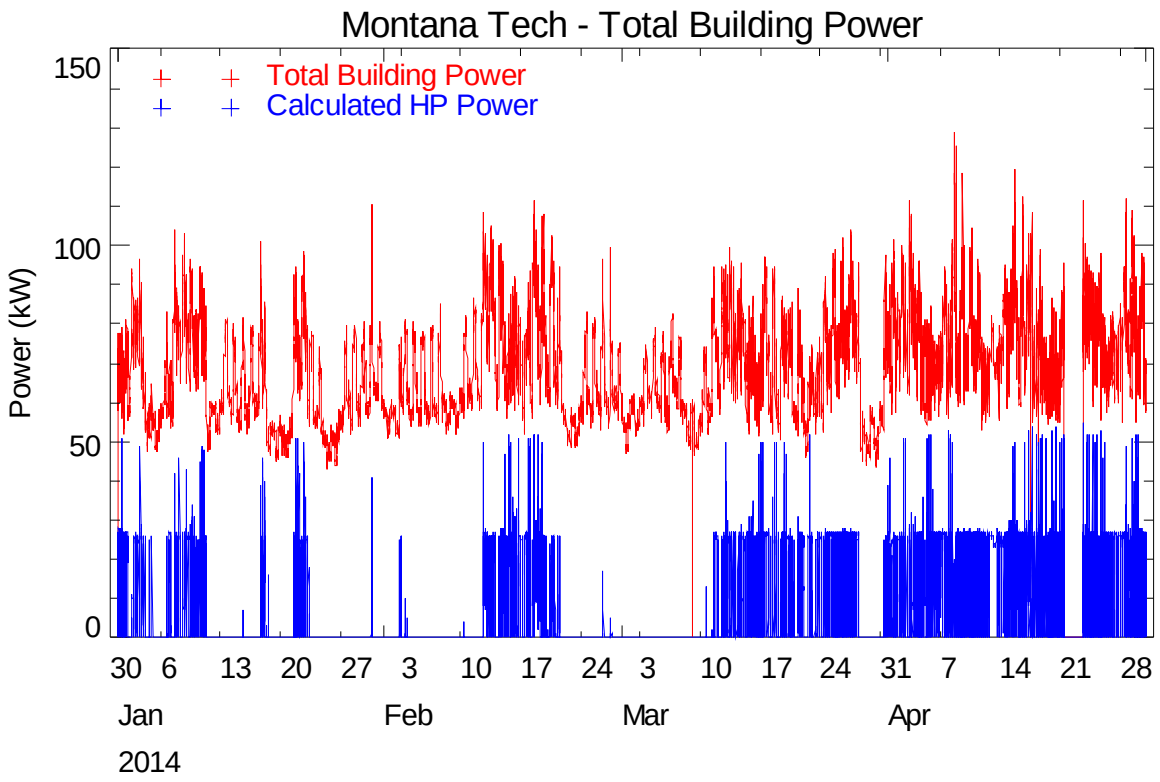

Figure 17. Total Building Power Trend

The trend of total facility energy with ambient temperature is shown in Figure 18. Because of the limitation of the data available, the plot displays no meaningful correlation of the building energy to ambient temperature. During the heating months with low ambient temperature, the building energy is typically 1,500 kWh/day and increases by up to 600 kWh/day when the heat pump operates.

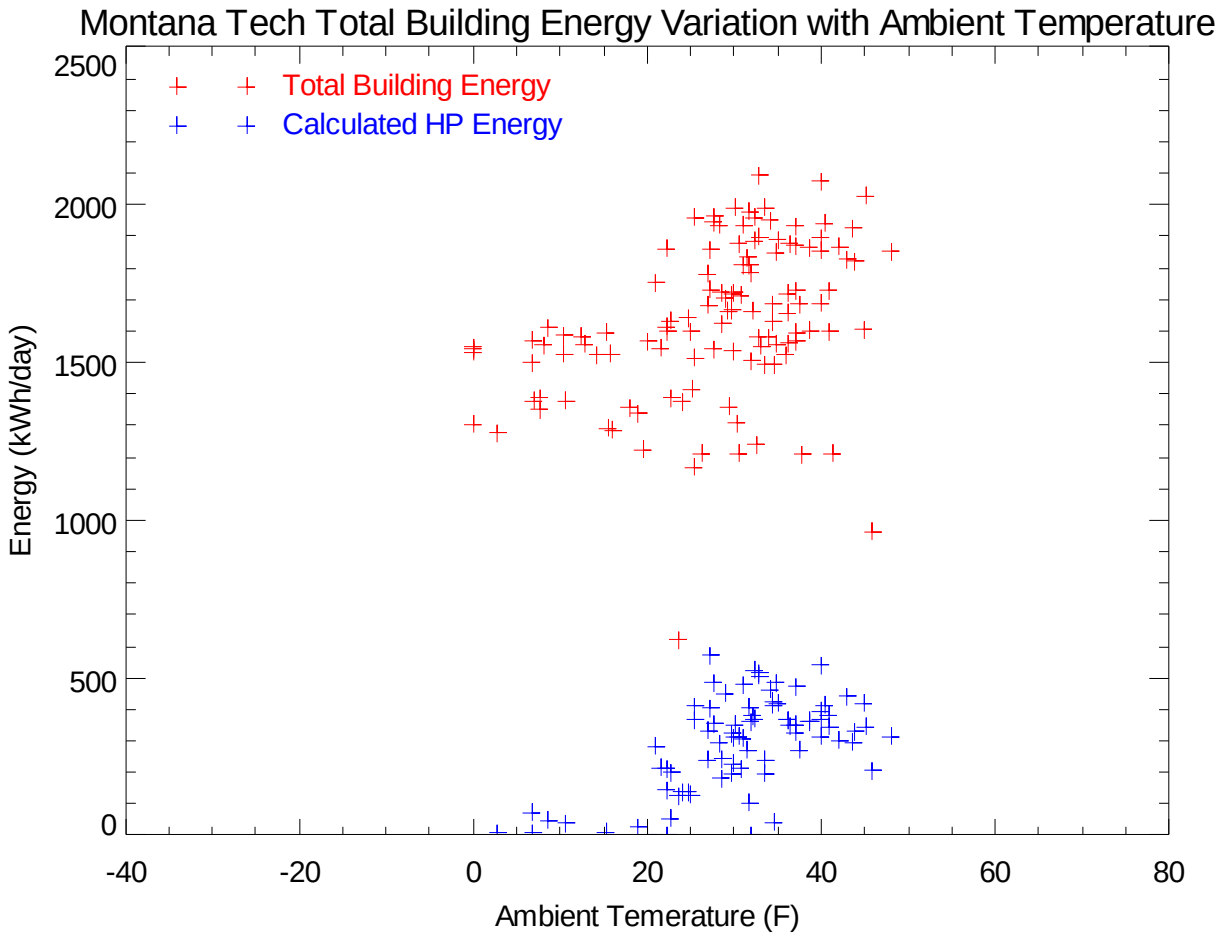

Figure 18. Building and Heat Pump Daily Energy Variation with Ambient

The shade plot in Figure 19 shows variation of total building power for the monitoring period. Periods of heat pump operation are observed as slightly darker, vertical, speckled bands on the shade plot. Weekend/weekday power use patterns are also apparent, as well as astronomical clock control on exterior lighting systems.

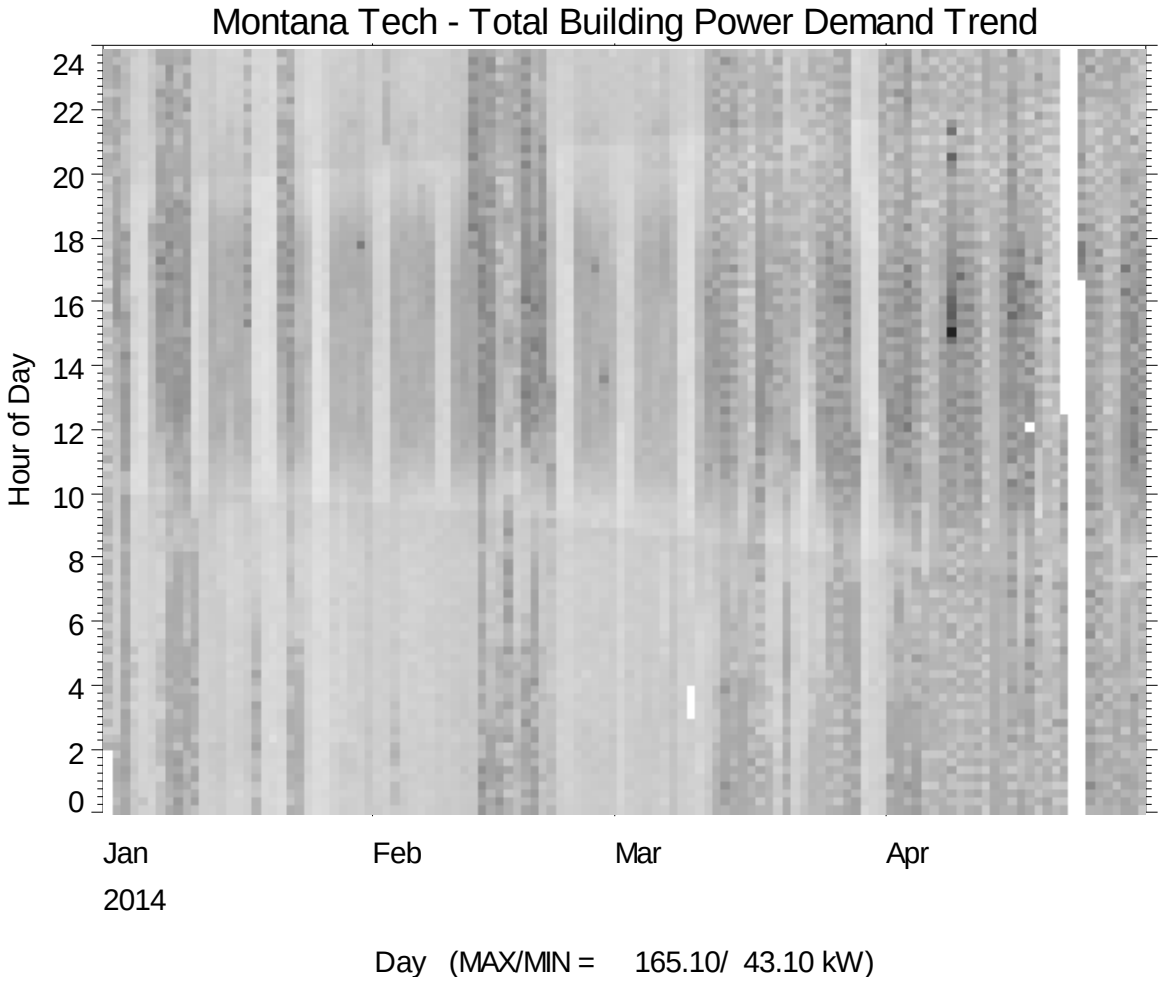

Figure 19. Total Building Power Patterns

Monthly Ground Loop Data and Building Energy Consumption

The ground loop heat transfer and building energy data collected from January 2014 through April 2014 are summarized in Table 2 through Table 4.

Table 2. Monthly Heat Pump Heat Transfer, Energy, and Efficiency

	Ambient Temp. (F)	Mine Water Temp. (F)	Mine Water Loop Flow (GPM)	Heat Pump Heat Extraction (MBtu)	Heat Pump Heat Delivered (MBtu)	Compressor Energy (kWh)	Mine Water Pump Energy (kWh)	COP (-)
Jan 2014	24.1	75.9	48.2	58,562.1	67,005.4	3,962.8	3,321.2	2.7
Feb 2014	15.0	75.2	51.5	47,373.9	54,130.2	3,160.3	3,007.9	2.6
Mar 2014	30.6	72.4	80.4	84,646.8	92,156.2	5,678.3	3,325.7	3.0
Apr 2014	37.5	68.8	81.7	150,390.1	184,924.3	10,492.8	2,987.7	4.0
Total				***340,973***	***398,216***	***23,294***	***12,643***	***3.2***

Table 3. Monthly Building Heating Load

	Ambient Temp. (F)	Heat Pump Heat Delivered (MBtu)	Steam Heat Delivered (MBtu)	Building Heat Load (MBtu)	Fraction of Heat From HP (%)
Jan 2014	Incomplete Month				
Feb 2014	15.0	54,130	404,671	458,801	11.8%
Mar 2014	30.6	92,156	236,229	328,385	28.1%
Apr 2014	37.5	184,924	82,800	267,724	69.1%
Total		***331,211***	***723,700***	***1,054,910***	***31%***

Table 4. Monthly GHP and Building Energy

	Ambient Temp. (F)	GHP System Energy (HP & Mine Pump) (kWh)	Total Building Energy (kWh)	HP Fraction of Building Energy (%)
Jan 2014	24.1	7,284	48,000	15.2%
Feb 2014	15.0	6,168	45,366	13.6%
Mar 2014	30.6	9,004	49,571	18.2%
Apr 2014	37.5	13,481	51,023	26.4%
Total		***35,937***	***193,960***	***19%***

Assessment of Data

- Direct measurement of heat pump power is not provided. Calculation of heat pump operation in both heating and cooling mode using loop temperatures, ground loop heat transfer, and performance curves provides a reasonable calculation for heat pump power.

- Pumping systems for the ground loop are not monitored. Pump energy is stipulated using a nominal pump power and ground loop flow to indicate operation. Pump system is constant speed.

- Building power data appears to be off by a factor of 4.0 (corrected in this report).

- Performance monitoring has been adequate to assess impact on heating operation. No cooling data collected yet. Full scope of cooling data collection yet to be determined.

Temperature and Pressure Sensing in Three Flooded Underground Mine Workings of Butte, Montana, USA

TYLER D. HAGAN

Department of Geological Engineering, Montana Tech of the University of Montana, 1300 W. Park Street, Butte, Montana 59701

Abstract

Temperature and pressure were measured in several flooded underground mine shafts in order to assess the potential for the development of additional mine-based geothermal heating in Butte, Montana, USA. Temperature was sensed using both optical fibers, functioning as a distributed sensor, and thermistors, functioning as point sensors; while pressure was sensed using a piezoresistive strain gauge. Upon observing good agreement between the continuous and discrete temperature sensors, we found no significant change in temperature with increasing depth within the water column. This suggests the thorough transfer of heat throughout the mine shaft via convection. Moreover, we found water temperature (T) is directly proportional to total mine shaft depth (z) via the equation: $T = 0.0225*z + 3.0194$, where T is in degrees Celsius and z is in meters – demonstrating an observed geothermal gradient of 22.5 ˚C per km.

Introduction

Geothermal heating is the direct use of geothermal energy for heating applications. As of 2007, 28 GW of geothermal heating power are installed around the world, satisfying approximately 0.07% of our primary energy consumption (Fridleifsson et al., 2008). The extraction of this heat from the Earth is accomplished with ground source heat pumps (also known as geothermal heat pumps). Thermal energy can be extracted from any source at any temperature; although, higher temperature sources permit higher efficiencies.

In recent years, flooded underground mine shafts and horizontal workings have been developed as heat sources to accommodate heat pumps (Kranz and Dillenardt, 2010). Using water, refrigerant, and/or antifreeze, as the working fluid(s) in the heating, ventilation, and air-conditioning (HVAC) cycle, coefficients of performance (COP) ranging between 3.0 and 5.0 are practical. One example of such an installation exists in the Orphan Boy mine shaft, located in the outer mining camp of Butte, Montana (Thornton et al., 2013). See figures 1 and 2 on the next page. In winter, warm water (25 ˚C) in the mine shaft is used as the heat source, and the floors of Montana Tech's Natural Resources Building are the heat sink. Placing a closed loop geothermal heat pump between the heat source and sink increases the temperature of the working fluid from 25 ˚C to upwards of 50 ˚C. In the summer, when cooling is needed: the heating cycle is reversed, mine water becomes the heat sink, and the system becomes a refrigeration cycle. Figure 3 displays a schematic of the closed loop heat pump employed in the Orphan Boy mine. In this case, a closed-loop heat pump is advantageous to an open loop heat pump because it is undesirable to use mine water as the working fluid in the system (Watzlaf and Ackman, 2006).

In order to convert abandoned, flooded mine shafts into heat sources for geothermal heating, it is important to evaluate the temperatures and pressures in the mine workings so thermal efficiency can be maximized (Toth and Bobok, 2007). Additionally, the cost of materials needed to install a mine-based heat pump must be weighed against the maximum temperature in the mine shaft as a means to build the most economic heating application.

The remainder of this paper describes two methods used to measure temperature and pressure, provides depth vs. temperature profiles for three flooded mine shafts, and supplies a discussion proposing sensor precision, mine shaft water convection, seasonal temperature variation, and an observed geothermal gradient for Butte, Montana, USA.

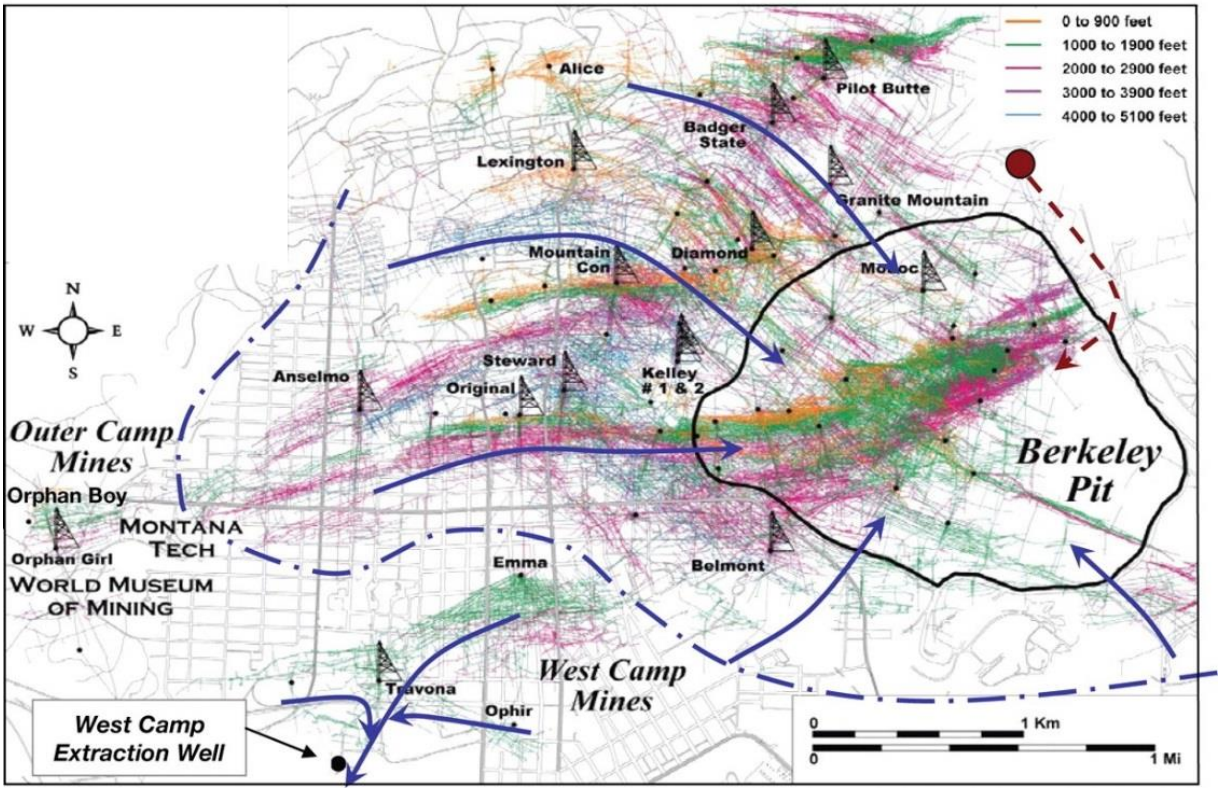

Figure 1. A plan view map shows mine shafts (head frames) and horizontal workings (colored lines) at depths between 0 and 5000 ft below the ground surface (Duaime et al. 2004 and revised by Gammons et al. 2009). The Kelley mine is located near the center of the figure and the Orphan mines are located on the left-most side of the figure.

Figure 2. Pictured is the closed-loop heat pump as it sits above the Orphan Boy mine shaft in Butte, Montana, USA. The 2011 installation of this mine-based heat pump was funded by the American Recovery and Reinvestment Act of 2009.

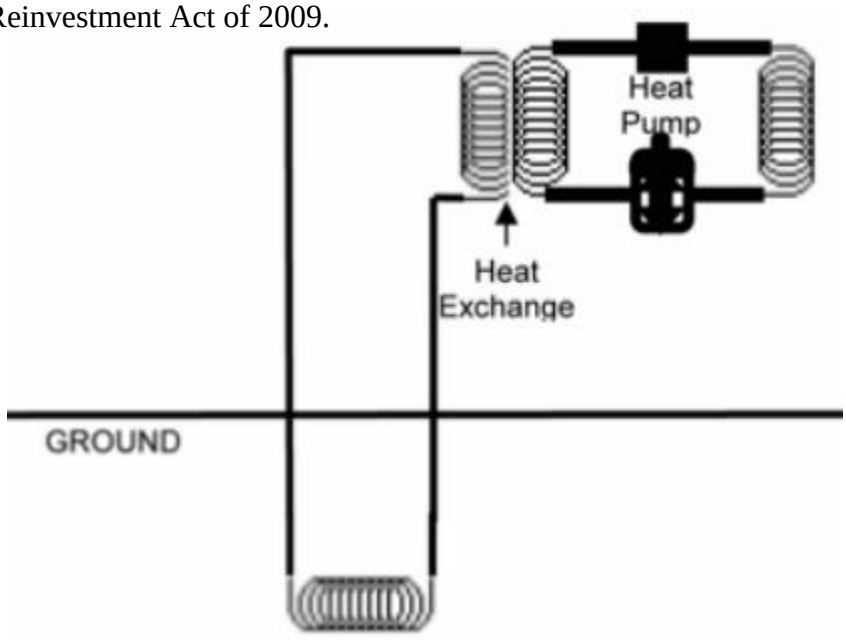

Figure 3. From Watzlaf and Ackman (2006), a closed-loop geothermal heat pump system is utilized to avoid using mine water as the working fluid. Instead, the heat pump loop (right) contains refrigerant, and the ground loop contains an antifreeze solution.

Methods

Temperature and pressure were measured in the Orphan Boy, Orphan Girl, and Kelley mine shafts (see figure 1 for locations). The two, connected, Orphan mines are located in Butte's outer mining camp on the west side of Montana Tech; these mine shafts and their respective horizontal workings constitute the underground mine education center (UMEC). The Kelley mine (located on the western margin of the Berkeley Pit) was the last of the operating mine shafts in Butte, halting operations in 1983; it was considered technologically advanced for its time, boasting a concrete-lined shaft and a cage that could hold 50 miners. A summary of the characteristics of each of the three mine shafts is outlined in the table below.

Table 1. The measured dimensions and attributes of the Orphan Boy, Orphan Girl, and Kelley mine shafts are outlined (Montana Bureau of Mines and Geology, unpublished records). Effective depth refers to the maximum depth at which temperature was sensed in this study. All three shafts have three compartments: one for miners, one for waste and ore, and one for ventilation and utilities.

	Orphan Boy	Orphan Girl	Kelley
Depth (m)	100	1000	1600
Width (m)	4	4	4
Length (m)	4	4	4
Effective depth (m)	100	400	450
# of compartments	3	3	3
Concrete lining?	No	No	Yes
Average temperature (˚C)	27	27	36

Two methods were utilized to measure temperature in the three aforementioned flooded mine shafts: distributed and point temperature sensing. Distributed (also known as continuous) temperature sensing was accomplished in the Orphan Boy mine shaft with an Omnisens DITEST STA-R™ and approximately 600 feet of fiber optic cable (see Figure 4). These instruments, in unison, record Brillouin frequency shifts of laser light along the length of the cable; the frequency shift is caused by a change in density of the glass fibers; and, the change in density is caused by thermally or mechanically induced strain (MacLaughlin and Wang, 2013). The fiber optic cable is installed in a loop so that the light source/detector measures strain on the way down and on the way up. This sensing technique is employed on a semi-permanent basis, and can be used to measure the seasonal variation in mine water temperature (Aminossadati et al., 2010).

Point (also known as discrete) temperature sensing was accomplished in all three mining shafts with two Hobo Tidbit thermistors/loggers, one Seastar combination thermistor-piezoresistive strain gauge, and approximately 650 meters of nylon rope (see Figure 5). All three point sensors were fastened to the rope with duct tape. A 10 kg slug was used to overcome the buoyant force of the rope; it also proved useful for dodging obstructions in the mine shafts. Point temperature sensing was implemented for three reasons: firstly, as a means to verify temperatures measured by the distributed temperature sensor, secondly, to gather temperature data in mine shafts where temperature-sensitive fiber optic cable is not installed (e.g. in the Orphan Girl and Kelley mine shafts), and thirdly, to measure temperature at greater depths.

Equipped with a piezeoresistive strain gauge, the Seastar temperature logger also provided a means to measure pressure in the static water columns. This proved to be an invaluable asset while discretely measuring temperatures. Pressure was calibrated to atmospheric pressure at Butte, Montana's ground surface elevation of 1690 m. Depth within the water column, z, was calculated by dividing the measured pressure, P, by the density of water, ρ, and Earth's gravitational acceleration, g (i.e. the specific weight of water):

$$z = \frac{P}{\rho g} = \frac{P}{\gamma}$$

where, the density of water was calculated (based on temperature and conductivity measurements) to be 996.5 kg/m^3 and the gravitational acceleration constant is approximately 9.81 m/s^2. The maximum depth to which temperature and pressure were measured was 100, 380, and 425 m in the Orphan Boy, Orphan Girl, and Kelley mine shafts, respectively. Obstructions in the Orphan Girl mine shaft and a lack of cable in the Kelley mine shaft prevented the discrete samplers from being lowered below these depths. Temperature and pressure were logged while lowering and also while raising the slug and sensors; this enabled us to retrieve two temperature profiles per each sensing session.

The Seastar logger also contains a built-in electrical conductivity (also known as specific conductance) meter. Specific conductance was measured both in the middle and left compartments of the Orphan Girl mine shaft. This enabled us to: determine if a chemical stratification within the mine shaft's water column is present, and calculate a more accurate value for the mine water's density.

As a means to check the accuracy of our primary sensors, a Hydrolab multiparameter water quality instrument was used to measure temperature, pH, EC, and Eh in the top 140 m of the Orphan Girl mine shaft.

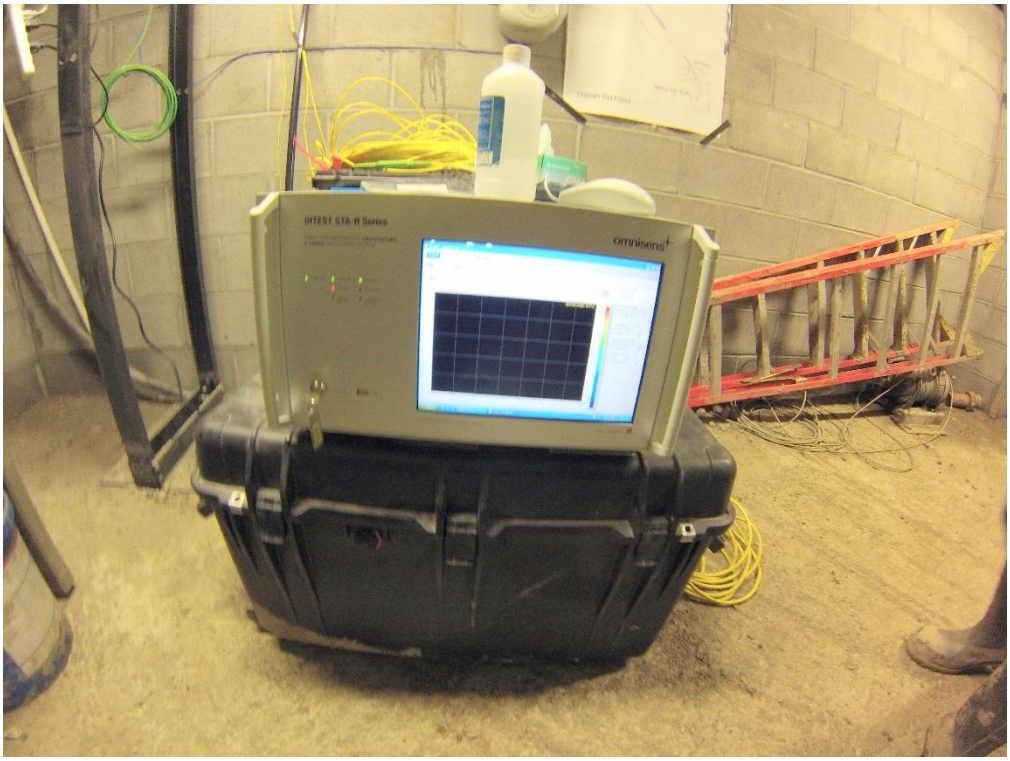

Figure 4. Pictured above is an Omnisens DITEST STA-R™ high-performance Brillouin-based fiber optic distributed temperature and strain analyzer collecting temperature data in the Orphan Boy mine shaft.

Figure 5. Pictured here (from left to right) is: one 20 kg slug, one Hobo Tidbit temperature logger, one Star-Oddi Seastar DST CTD miniature salinity/temperature/depth logger, another Hobo Tidbit, and 2000 feet of 3/8" nylon rope.

Results

Point sensing was applied to measure temperature in all three mining shafts: the Orphan Boy, Orphan Girl, and Kelley mines while distributed sensing was applied to measure temperature in only the Orphan Boy mining shaft. The following four pages of figures display temperature (in degrees Celsius) on the x-axis and depth (in meters of water column) on the y-axis. These are henceforth referred to as temperature profiles. The following table outlines these figures.

Table 2. This list describes the figures displayed on the following four pages.

Figure #	Description
6	Seasonal variation in the Orphan Boy mine using the distributed sensor
7	Comparison of distributed and point sensing in the Orphan Boy mine
8	Variation in temperature between compartments in the Orphan Girl mine
9	Temperature variation among Hobos, Hydrolab, and Seastar in Orphan Girl
10	Point sensing in the Kelley mine
11	Variation in temperature between the Orphan Girl and Kelley mines
12	Seastar vs. Hydrolab specific conductance values in the Orphan Girl mine
13	Hydrolab temperature, pH, conductance, and Eh profiles

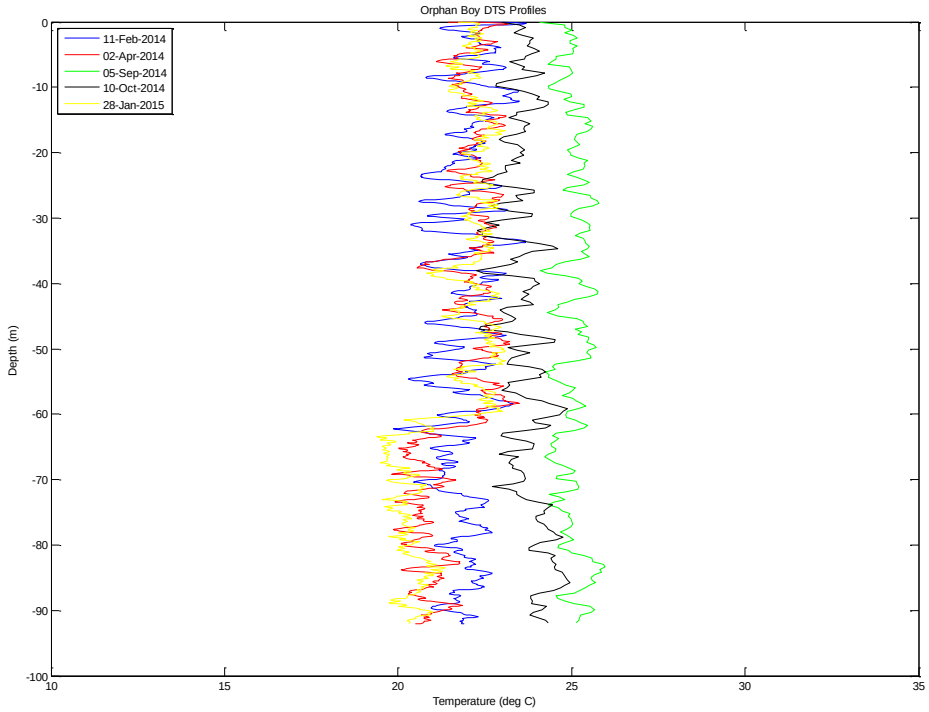

Figure 6. Distributed temperature scans, using the distributed temperature sensing setup, are shown from February 2014 to January 2015 in the Orphan Boy mine shaft.

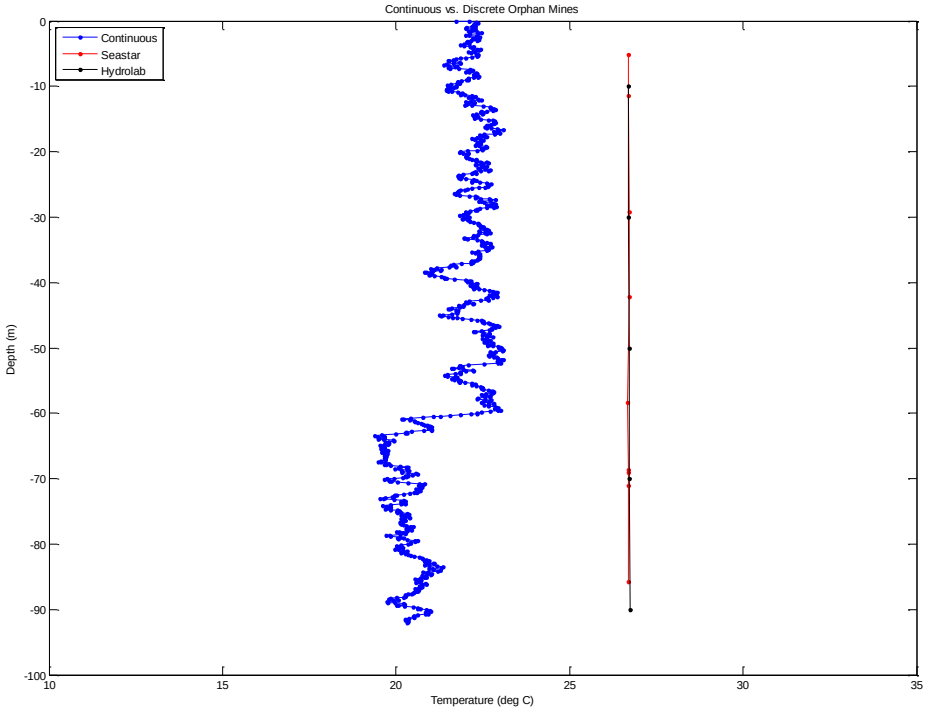

Figure 7. A comparative plot of distributed (blue) and point (red and black) temperature sensing as a function of water column depth in the Orphan Boy mine shaft shows fair agreement between the three measuring techniques. The distributed temperature profile shows the February 2015 scan. The discrete profiles recorded temperatures in the top 90 m of the Orphan Girl shaft as the sensor was being raised to the surface in February 2015.

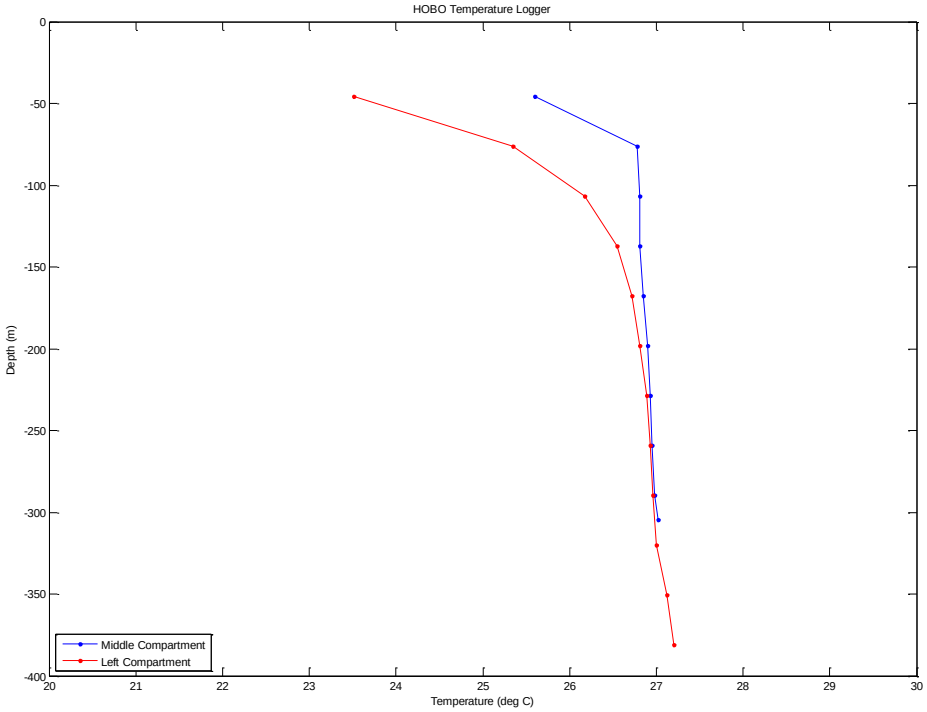

Figure 8. Temperature profiles, as measured by the Hobo loggers, in the Orphan Girl mine shaft do not vary between the middle (blue) and left (red) compartments. Temperatures shown are an average of two Hobo temperature loggers as the sensors went down.

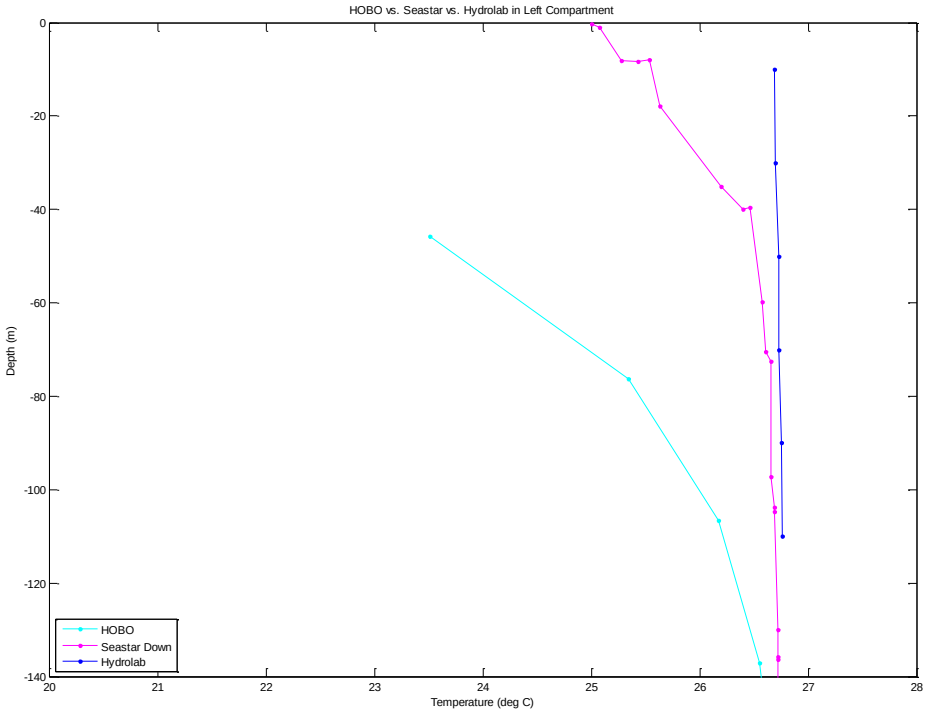

Figure 9. A comparison of the three point temperature sensors shows the Hobo Tidbit sensor is the slowest to equilibrate to the elevated temperature in the Orphan Girl mine shaft as the sensors are going down.

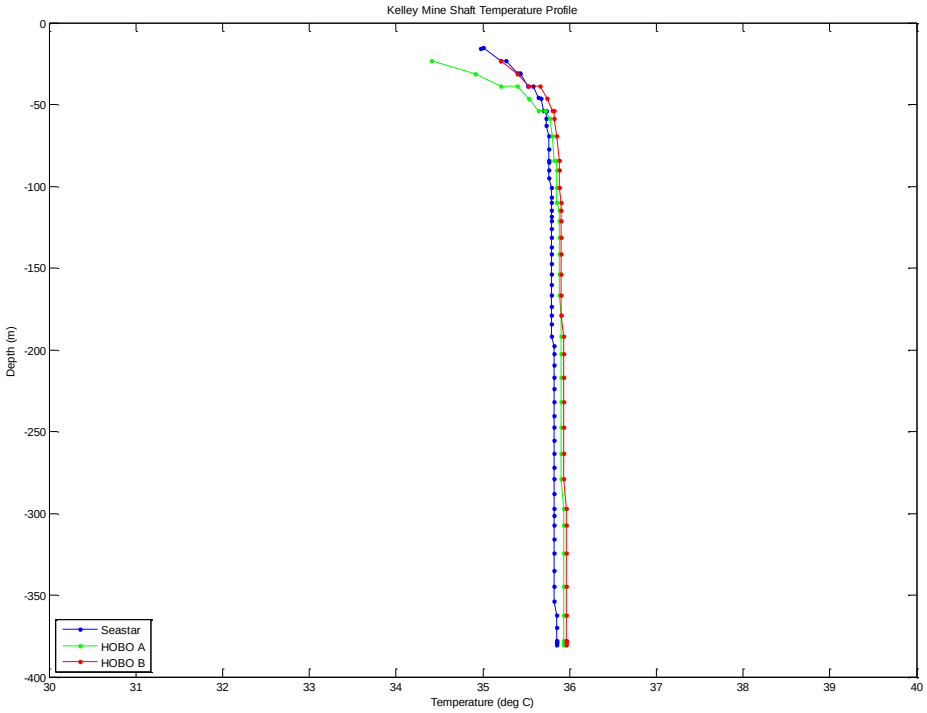

Figure 10. A plot of water depth vs. water temperature in the Kelley mine shaft shows a slight, but systematic, discrepancy between the three point temperature instruments as they sensed temperature on their way down the mine shaft.

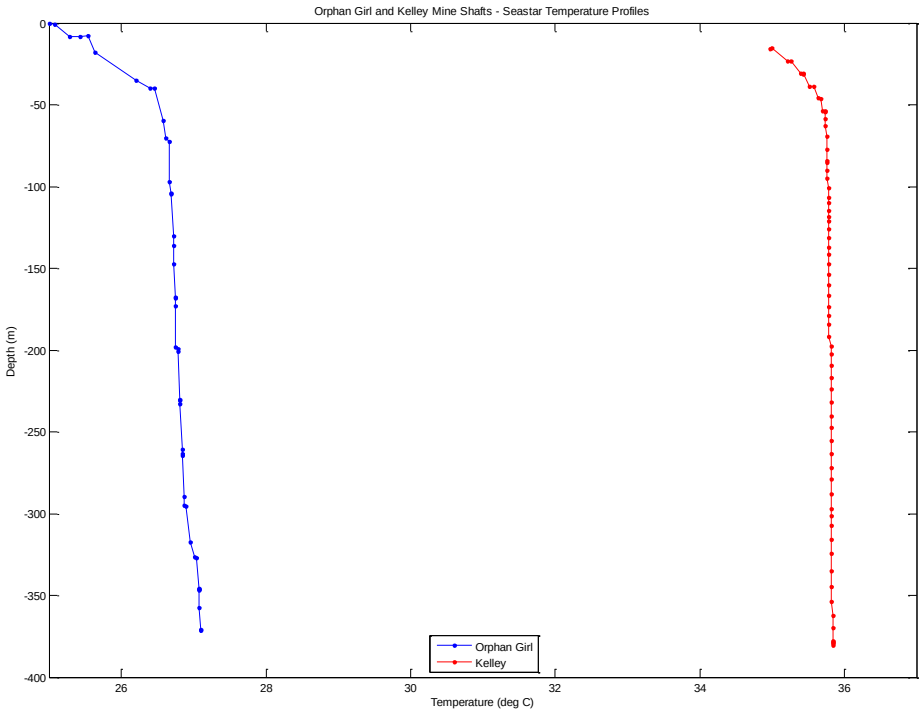

Figure 11. Orphan Girl (blue) and Kelley (red) mine shaft depth vs. temperature profiles are plotted together to show the ~9 ˚C temperature increase.

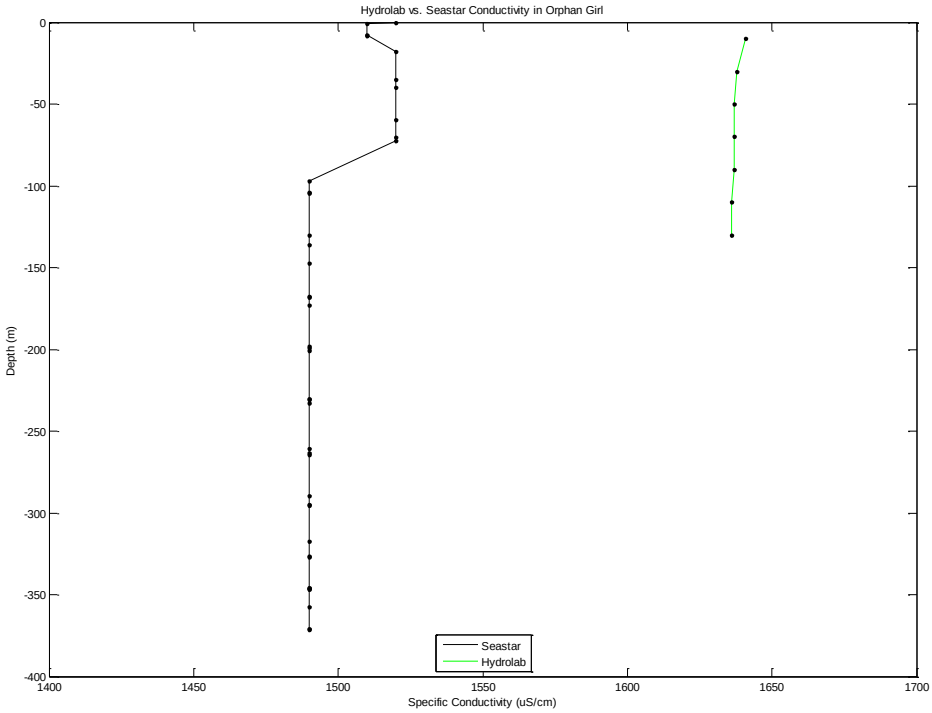

Figure 12. A comparison of the specific conductivity profiles, as measured by the Seastar (black) and Hydrolab (green) instruments, shows systematic error between the two sensing devices in the Orphan Girl mine shaft.

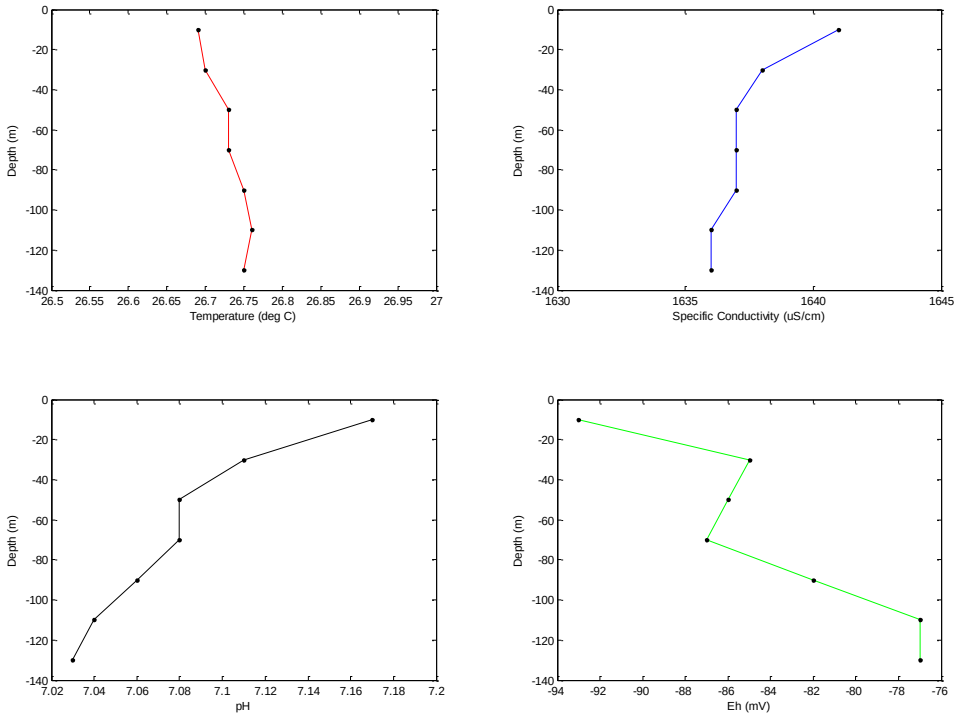

Figure 13. Temperature, SC, pH, and Eh were measured with the Hydrolab multiparameter water quality instrument in the middle compartment of the Orphan Girl mine shaft on 20 February 2015.

Discussion

The results show, first and foremost, fair agreement between point and distributed temperature sensing in the Orphan mine shafts. The distributed temperature data is more scattered due to errors that are an artifact of the fiber optic cable deformations. The agreement between the point sensors, however, is spectacular. It should be noted that none of the temperature sensors were calibrated properly. Calibration is especially important for the fiber optic setup because the particular cable used in this study was not manufactured to measure temperature with good accuracy. The Hobo and Seastar thermistors/temperature loggers, on the other hand, should hold their factory calibration well.

Secondly, it is obvious there is little to no increase in temperature with increasing depth within the water column, suggesting the thorough transfer of heat throughout the flooded mine shafts via convection. This suggestion is also supported by a lack of change in chemistry within the mine waters (Gammons et al., 2009). Additionally, Reichart et al. (2011) and Wolkersdorfer et al. (2007) have proposed convection takes place in flooded mines in Lorraine, France and Freiberg, Germany. Thus, it is rational to claim the waters in Butte's flooded underground mine shafts are undergoing convection and these waters are chemically and thermally well-mixed.

Thirdly, Figure 6 shows water temperature in the Orphan Boy mine shaft varies seasonally: increasing in the summer and decreasing in the winter. Temperature variation of this sort implies the influence of meteoric water into the mine shafts, either directly, or via a connection with the local groundwater table.

Fourthly, Figure 9 signals the effect of total mine shaft depth on water temperature; namely, temperature increases with mine shaft depth. This trend does not occur between the Orphan Boy and Orphan Girl mine shafts because these two mine shafts are connected by a horizontal working; that is, the water is the same in both shafts. By plotting average temperature vs. total mine shaft for the Orphan Girl and Kelley mine shafts, an observed geothermal gradient beneath Butte, Montana can be determined (see Figure 10 on the next page).

Lastly, an applied comparison of the different temperature sensing technologies is outlined in Table 2 below. The fiber optic temperature sensing setup is the most robust because it can be installed semi-permanently without much physical effort; however, the initial cost of this system is substantial compared to the point temperature sensors. But, this cost can be justified if your application requires frequent sensing over long periods of time because its ease of use will save countless hours of work.

Table 2. A practical comparison of the three methods used to measure temperature in the flooded mine shafts shows each sensor's primary functions, cost, setup time, ease of use, and durability.

	Omnisens DITEST STA-R™ + Fiber Optic Cable	Star-Oddi Seastar CTD logger	HOBO Tidbit Temp. Logger
Primary functions	temperature and strain	conductivity, temperature, and pressure	temperature
Cost	$$$$	$$$	$
Setup time	days to weeks	minutes	minutes
East of use	install and forget	tedious to repeat	tedious to repeat
Durability	very durable	very durable	very durable

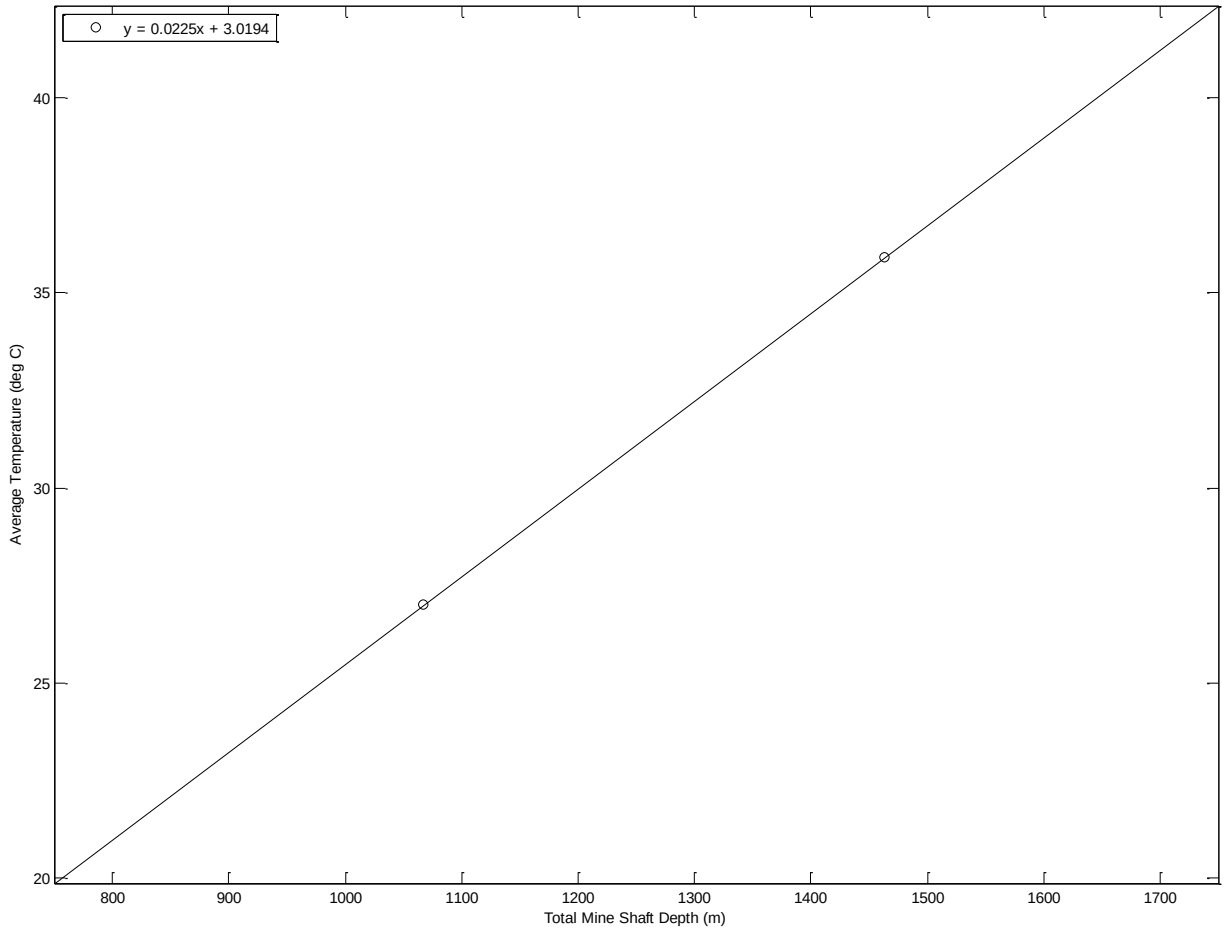

Figure 14. Average water temperature and total mine shaft depth are plotted for the Orphan Girl and Kelley mine shafts to determine the approximate geothermal gradient beneath Butte, Montana.

The equation of this line is:

$$T = 0.0225\left(\frac{^{\circ}\mathrm{C}}{m}\right) * z(m) + 3.0194(^{\circ}\mathrm{C})$$

where, T is the temperature in degrees Celsius and z is the depth below the ground surface in meters. Therefore, based on the slope in the equation above, the observed geothermal gradient is 22.5 ˚C per kilometer. According to Fridleifsson et al. (2008), the average geothermal gradient of continental crust (away from tectonic plate boundaries) is approximately 25.0 ˚C per kilometer. Therefore, the percent difference between the observed value and this average value is 11.1%. Additionally, the computed y-intercept of 3.0194 ˚C closely matches Butte's annual mean air temperature of 3.9 ˚C.

It should be noted that the Orphan Girl and Kelley mine shafts contain anomalously high-temperature water, as compared to the other flooded underground mine shafts in Butte, Montana. In fact, Figure 16 in Gammons et al. (2009) shows the Anselmo, Belmont, Emma, Lexington, Ophir, Pilot Butte, Steward, and Travona mine shafts all fall on thermal gradients between 10 °C and 20 °C per kilometer.

Water in the Kelley mine shaft may be much hotter than the other shafts because it is lined with concrete: a feature no other mine shaft possesses. A concrete-lined mine shaft prevents water from entering along the length of the shaft. Therefore, if the concrete is still relatively intact, water can only infiltrate from the bottom or via horizontal workings (stopes and adits). Since block caving was used in the Kelley mine, most (if not all) of the horizontal openings must have been sealed, and consequently, water may only enter at the bottom of the mine shaft. If this is the case, heat would strictly transfer from bottom to top, and the influence of meteoric or ground water would be negligible.

Water in the Orphan Girl mine shaft may be hotter than the other shafts (with the exception of Kelley) because it is completely hydraulically separated from the rest of Butte's underground mine workings (refer to Figure 1). As a result of its location on the boundary of a small drainage basin, the Orphan Girl mine shaft receives very little rain and ground water input. As shown in the hydrographs in Figure 15 below, the water table elevation in the outer mining camp has decreased from 2012 to 2014; this differs significantly from the main zone and west mining camps.

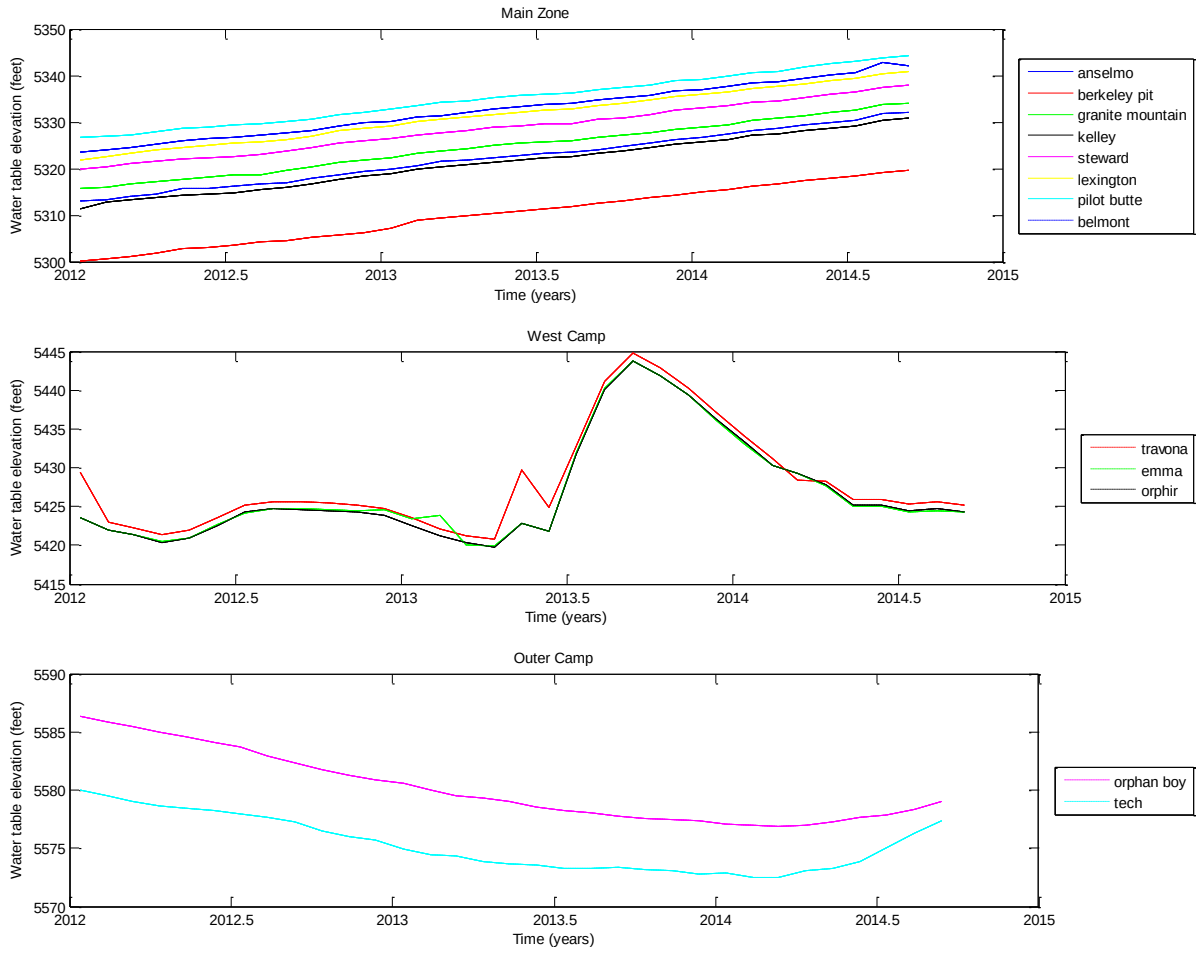

Figure 15. Plots of water table elevations vs. time (hydrographs) for the main zone, west, and outer mining camps show dramatically different flooding scenarios. Data sourced from monthly, open-file monitoring reports by Contract No. 400022-TO-35, Butte Mine Flooding-September 2014. These reports are available at pitwatch.org.

Conclusions

This paper described two methods used to measure temperature and pressure, provided depth vs. temperature profiles for three flooded mine shafts, supplied a discussion proposing sensor precision, mine shaft water convection, seasonal temperature variation, and an observed geothermal gradient for Butte, Montana, USA. The findings show first, for this application, point temperature sensing, using thermistors, is more accurate and precise than distributed temperature sensing using fiber optic cable. Secondly, it was found that water in the three studied mine shafts is both thermally and chemically well-mixed. Thirdly, water temperatures in the Orphan Boy mine shaft vary seasonally. Fourthly, it has been shown that there is a hydraulic disconnect between the mine shafts in the main zone and the mine shafts in the outer and west mining camp; although, a complete water balance for Orphan mine system has not been realized. Finally, measuring temperature and pressure in Butte's flooded underground mine shafts provide a means to determine the observed geothermal gradient of 22.5 °C per kilometer beneath southwestern Montana.

Recommendations for Further Work

My first recommendation for further work is to complete a rigorous temperature calibration for the fiber optic setup and/or perform a side-by-side comparison of point vs. distributed temperature sensing in the Orphan Boy mine shaft. This could be accomplished by fastening the Hobo temperature sensors at systematic intervals along the fiber optic cable and logging temperature, with both devices, over a period of a few months. Unfortunately, this strategy could not be implemented in this study because there is currently limited access to the Orphan Boy mine shaft.

My second recommendation for further work is to use the fiber optics and/or discrete temperature sensors to monitor long-term changes in water temperature when Montana Tech's mine-based heat pump system is active and inactive. Information gathered, as a result of this recommendation, is important for the prediction of the heat pump's expected lifetime and efficiency during extended periods of continuous heating and cooling operations.

My final recommendation for further work is to use the aforementioned methods to measure temperature in other flooded mine shafts in the Butte Montana's main zone and west mining camps. Gammons et al. (2009) looked at eight different mine shafts, but they did not have a piezoresistive strain gauge to measure depth and did not attempt to lower their temperature loggers below the top 300 m of the mine shafts' water columns.

References

Fridleifsson, I. B., Bertani, R., Huenges, E., Lund, J. W., Ragnarsson, A., Rybach, L., O. Hohmeyer and T. Trittin, ed. (2008). "The possible role and contribution of geothermal energy to the mitigation of climate change." Luebeck, Germany. pp. 59–80, PDF.

Kranz, K. and Dillenardt, J. (2010). "Mine water utilization for geothermal purposed in Freiberg, Germany: Determination of hydrogeological and thermophysical rock parameters." Mine Water Environ. v. 29, pp. 68-76. PDF.

Thornton, R., Wahl, N., and Blackketter, D.M. (2013). "Convection mechanisms for geothermal heat exchangers in vertical mine shaft." Transaction of the Society of Mining, Metallurgy, and Exploration, v. 332, pp. 2-5. PDF

Watzlaf, G. R. and Ackman, T.E. (2006). "Underground mine water for heating and cooling using geothermal heat pump systems." Mine Water and the Environment, v. 25, Issue 1, pp. 1-14. PDF.

Toth, A. and Bobok, E. (2007). "A prospect geothermal potential of an abandoned copper mine." Proceedings, Thirty-Second Workshop on Geothermal Reservoir Engineering. Standford University, Standford, California, Januarry 22-24, 2007. SGP-TR-183. PDF.

Duaime, T.E., Kennelly, P.J., Thale, P.R. (2004). "Butte, Montana: Richest hill on Earth, 100 years of underground mining: Montana Bureau of Mines and Geology." Misc. Contribution, v. 19. Poster.

Gammons et al. (2009). "Geochemistry and stable isotopes of the flooded underground mine workings of Butte, Montana." Economic Geology. v. 104, pp. 1213-1234. PDF.

MacLaughlin M. M., and Wang, H. (2013). "Demonstration of the ability of distributed fiber optic sensing technologies to enhance mine safety through distributed monitoring of ground deformation, temperature, & dynamic events." Proposal submitted to the Alpha Foundation for Mine Safety and Health. PDF.

Aminossadati, S.M., Nayeemuddin, M.M., Shemshad, J. (2010). "Distributed temperature measurements using optical fibre technology in an underground mine environment." Tunneling and Underground Space Technology. v. 25, pp. 220-229. PDF.

Reichart, G., Vaute, L., Collon-Drouaillet, P., Bues, M.A. (2011). "Modelling heat and salinity related convective processes in deep mining flooded wells." Mine Water – Managing the Challenges. IMWA Symposium 2011. Aachen, Germany.

Folkersdorfer, C., Neumann, C., Hasche-Berger, A. (2007). "Hydrodynamics of the flooded Freiberg/Saxony underground mine." Water in Mining Environments. IMWA Symposium 2007. Cagliari, Italy.

Convection mechanisms for geothermal heat exchangers in a vertical mine shaft

R. Thornton, N. Wahl and D.M. Blackketter
M.S. graduate student, professor (emeritus), and chancellor and professor, respectively,
General Engineering, Montana Tech, Butte, MT

Abstract

This paper evaluated using a water-filled abandoned mine (Orphan Boy) as a heat source for a 240-kW closed-loop heat pump with the goal of heating a 2,000-m^2 building. The mine has a 245-m vertical shaft connected to a large stope by three horizontal cross-cut shafts. There is 1,250 x 10^6 L of water at a consistent temperature of 24-26° C that is available mostly in the stope. The only heat exchanger placement option is in the vertical shaft. Therefore, the focus was to model heat exchanger placement in the vertical shaft to determine the extent to which the systems will induce thermal currents between the stope and vertical shaft. Modeling of thermal currents, temperature profiles and heat contribution from the ground was done using finite difference and computational fluid dynamics. An optimal configuration was determined showing sufficient water movement and heat transfer will occur with a low water temperature in the shaft above 20° C. This project supports a U.S. Department of Energy (DOE) grant that will implement the full-scale system.

Key words: Geothermal energy, Geothermal installation, Abandoned mines, Mine shaft, Heat transfer technology

2013 *Transactions of the Society for Mining, Metallurgy, and Exploration*, Vol. 332, 4 pp.

Introduction

Montana Tech is located in the historic mining town of Butte, MT and is adjacent to the Orphan Boy Mine. This abandoned underground mine will be the heat source for a down-hole heat exchanger (DHE)/heat pump system. The mine was abandoned in the 1950s and has since filled with water to within approximately 30 m of the surface. The shaft is composed of a 245-m vertical shaft connected with horizontal crosscut drifts at 60 m and 150 m below the water level, as depicted in Fig. 1. The drifts connect to a large stope with approximately 1,250 x 10^6 L of water at a consistent 24-26° C. The intent is to build this heating system to augment or fully heat a newly built 2,000-m^2 building on the Montana Tech campus.

As designed, the system uses "off-the-shelf" parts, making the basic configuration straightforward, with the exception of the DHEs, which need to be placed into the vertical shaft. Because there are few or no examples of placing heat exchangers in a vertical shaft, the primary focus of this work was to model the heat exchanger placement and configuration in the vertical shaft to determine the extent to which thermal currents develop between the stope and vertical shaft via the horizontal crosscut drifts. The movement of water is necessary to be able to provide the required energy. Without inducing thermal currents to exchange the shaft water with water from the stope, there is insufficient energy for the heat pump system to work at the desired level. This study includes the modeling of water flow, temperature profiles and the heat contribution from the surrounding rock walls.

Background

Geothermal heating and cooling is an established method of heating commercial and residential buildings. For example, Ball State University in Indiana is building an $80-million system with 3,600 vertical boreholes 120-160 m deep, tied to more than 1,600 km of piping (Fickes, 2012). This system is designed to heat and cool 47 buildings and is expected to be cost effective. The use of coal-produced electricity for the heat pumps is a subject for another time, but it does point to the practicality of using geothermal heat pumps to service large buildings or complexes.

Mine water use for geothermal systems is a concept that is being considered worldwide. Conventional underground mining has been practiced for centuries, and there are many mines that have been abandoned and subsequently flooded. The authors refer the readers to an article by Watzlaf and Ackman (2006), which provides an excellent summary of the status of the use of geothermal systems in abandoned mines in the United States and Canada. Other examples include the flooded lead mines in Park Hills, MO, which serve to heat and cool a 750-m^2 municipal building. The water is only 110 m deep and is at a temperature of 14° C. In Springhill, Nova Scotia, the water in abandoned coal mines is used to heat and cool 14,000 m^2, with the supply water held between 13-20° C during the year. While there have been a number of other examples and reports on using heat pumps in abandoned water-filled mine formations (Culver and Lund, 1999), no example was found in which heat exchangers were placed in a vertical

Paper number TP-12-068. Original manuscript submitted November 2012. Revised manuscript accepted for publication July 2013. Discussion of this peer-reviewed and approved paper is invited and must be submitted to SME Publications Dept. prior to Sept. 30, 2014.

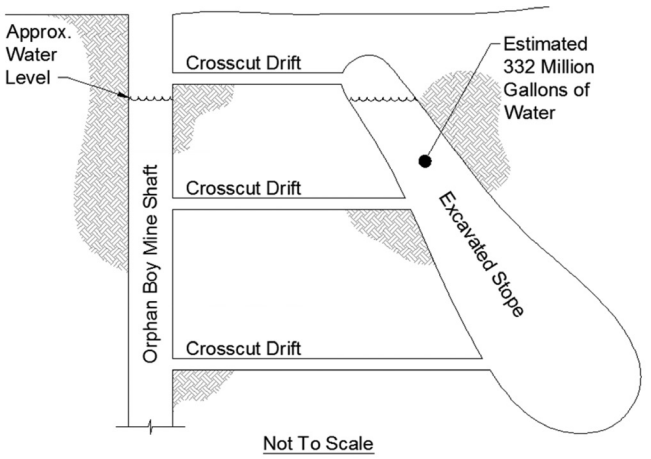

Figure 1 — Basic illustration of Orphan Boy Mine shaft and stope.

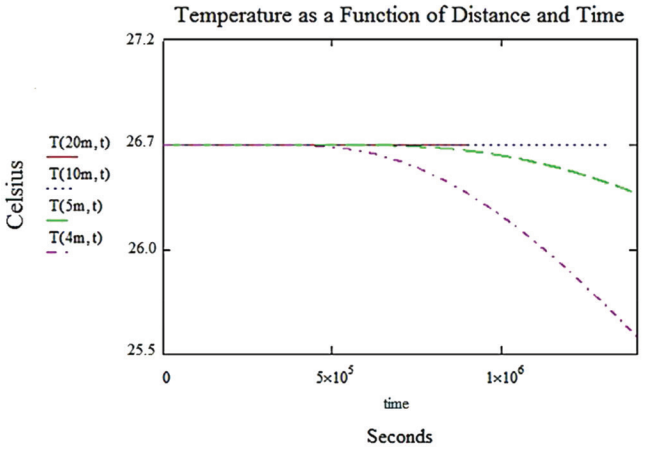

Figure 2 — Transient temperature for a semi-infinite solid with surface convection over time.

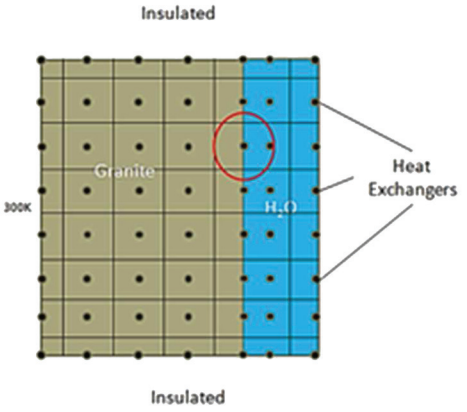

Figure 3 — Nodal grid of mine shaft with formation and energy balance of each node.

mine shaft with the intent to induce thermal currents in order to move water from abandoned workings to the DHEs. In this context, a series of models were constructed to simulate the DHE configuration to determine the extent to which the design would induce thermal currents.

Modeling approach

The overall modeling approach was to first use a simpler 2-D model to inform more complex 3-D models. The 2-D model used a finite difference approach to quantify the heat transfer within the mine shaft from the surrounding walls and to determine the stability of the model when the DHEs were included. The 3-D model of the shaft, including the surrounding rock and stope interaction, was built to simulate the heat transfer and fluid dynamics.

Before the 2-D convection model could be created, the effective distance of the surrounding rock was required. The effective distance is the point at which the far distant rock material temperature is unaffected by the heat extraction. To determine this, it was assumed that the convection in the shaft behaved as a vertical plate, allowing the authors to calculate the distance within the model where the temperature could be assumed to be constant (Eq. (1)) (Fausett, 1999). It was also assumed that the heat extraction was 240 kW, and that the far wall was held at 26° C.

$$\theta(x,t) = erfc\left(\frac{x}{2\cdot\sqrt{\alpha\cdot t}}\right) - \left(\exp\left(\frac{h\cdot x}{k} + \frac{h^2\cdot\alpha\cdot t}{k^2}\right)\right)\cdot \left(erfc\left(\frac{x}{2\cdot\sqrt{\alpha\cdot t}} + \frac{h\cdot\sqrt{\alpha\cdot t}}{k}\right)\right) \quad (1)$$

For Eq. (1) to be valid, it was assumed that natural convection would be the primary means of heat transfer. This would imply little to no forced flow rate within the mine shaft (no leaking in or out). To confirm this, a camera was lowered into the mine shaft with a 30-m tube attached to the line so that visible ink could be injected and any movement of water confirmed. The results showed the water to be essentially stagnated.

The rock surrounding the mine shaft and stope supplies the heat to the water and the assumption is that the rock will hold a constant temperature when energy is extracted at some certain distance within the formation. By knowing this distance, boundary conditions could be set for both the 2-D finite difference model and the 3-D SolidWorks model. Also needed was an average convection coefficient from the surface of the rock and the water. To determine this, a Nusselt number for a flat plate of 21,100 was calculated using a Grashof number of 1.32×10^{17}, a Prandtl number of 0.146 and a Rayleigh number of 1.92×10^{16} (Hellums and Churchill, 1962). An average convection coefficient could be determined from the Nusselt number, along with the characteristic length and the thermal conductivity of the water (Hellums and Churchill, 1962). This value was found to be $48 W/m^2 \times K$. More detail is provided in the Thornton thesis (2012). Using these values and assumptions, the temperature within the surrounding rock formation around the shaft reached a constant at a distance of approximately 20 m from the shaft as shown in Fig. 2 (along with other distances and times).

The 2-D finite difference model was created assuming symmetry throughout the formation and mine shaft. To include the heat exchangers, the finite difference model was set up on a 2-D grid, as seen in Fig. 3. The partial distance for the *X* and *Y* direction were set equal to each other at 3 m. Each node represents a steady state temperature for that section.

Standard finite difference methods were used, where for each section of the grid, the energy entering and leaving the section were summed in keeping with the first law of thermodynamics. Conservation of energy within the granite was represented by Fourier's Law, meaning that only conduction occurs in the granite, while convection was assumed from the surface of the granite to the water, which was represented by

Newton's law of cooling (NCEES, 2010). The steady-state heat transfer that occurred within the water itself was calculated by Fourier's Law (NCEES, 2010). The 2-D model provides representative parameters of heat transfer within the system. Once the equations were set, the equation for a 42-by-42 matrix was input into MATLAB (Fausett, 1999). The results showed that with the DHE, the temperature profile of the surrounding rock reached a constant temperature at 20 m.

With boundary conditions quantified by the 2-D model, the 3-D model was built using SolidWorks for input into the computational fluid dynamics software FloEFD (2011). However, there were some modeling problems to resolve. First, a cylinder representing the rock surrounding the actual shaft was built in SolidWorks. The cylinder was set to a length of 240 m, a radius of 18.3 m and a square shaft voided in the middle and having a cross-sectional area of 10 m^2 that represented the vertical shaft. However, it was found that by having the rock around the shaft modeled as a cylinder and the shaft modeled as a square section, numerical instabilities were induced at the corners and caused lengthy calculation times. This was resolved by modeling the rock and the shaft as cylinders, with the scaled volume of material for the rock and 10 m^2 for the shaft, as in Fig. 3a. The material assigned to the cylinder representing the surrounding rock was granite. Thermal material properties were defined in this section, including conductivity, specific heat and a thermal expansion coefficient.

The other obstacle to resolve was the required computation time. The time the simulation took to complete its calculation was significant, due to the number of elements of the shaft compared to the surrounding rock. With the focus of the study to determine whether natural convection can be induced within the mine, more elements were needed for the shaft (water) portions. However, with this particular model, there is much more rock than water, and the computer resources available were insufficient. Two steps were taken to reduce model size and computation time. First, the properties of the rock were scaled by a factor of 10. Second, the model was broken into three sections and run separately.

To scale the properties of the rock, the thermal conductivity was changed from 2.79 W/m x K to 0.279 W/m x K, and the heat capacity was changed from 775 J/kg x K to 7,750 J/kg x K. In doing this, the "thickness" of the rock portion of the model could be reduced by a factor of 10 and reduced the number of elements required by a factor of approximately seven times.

Second, the complete model of the Orphan Boy shaft was divided into three sections and modeled in SolidWorks as 61-m-long pieces with a diameter of 4 m, as shown in Fig 4. The cross-sectional area of the shaft was maintained at 10 m^2. The horizontal crosscut drifts that connect the shaft to the stope were included in the model. Boundary conditions were set for each section such that they matched between their respective adjacent sections. Specifically, the hydrostatic pressure was set at each section in respect to its depth, each section was forced to match continuity and the temperature was set equal at boundaries. The specifics of matching boundary conditions between sections can be found in Thornton (2012). By scaling the material properties, dividing the model into three sections, and modeling the shaft as a circular cross-section, the computational time was significantly reduced. The models allowed the visualization of the currents and temperature gradients as will be shown.

The method of heat exchange in the system is via a closed loop plastic pipe system that will be lowered into the shaft. Currently, the design calls for 4,000 m of 2.54-cm-(1-in.-) diameter pipe that is in 200-400-m sections. In this case, each section is referred to as a DHE. Each DHE, or approximately each 200-400-m loop, will have water circulated from the heat pump via a manifold system that can have varying flow rates for each loop. Therefore, each loop was considered as its own heat exchanger and modeled as such. Consequently, the number and location of the DHEs are important in how the thermal currents are developed relative to the crosscut drifts.

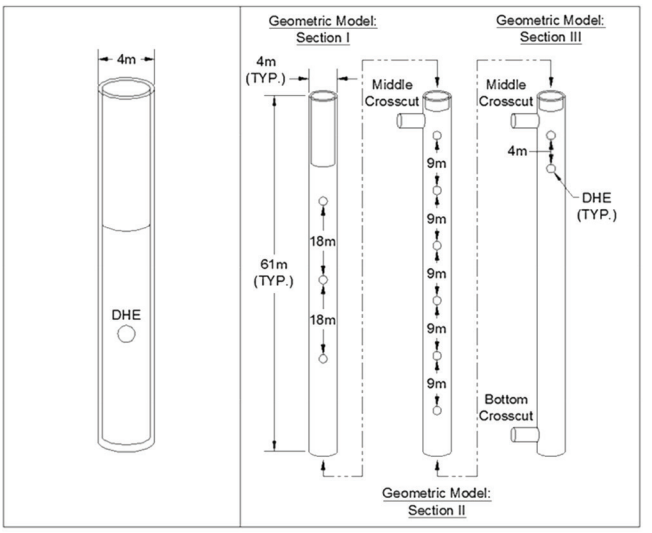

Figure 4 — Geometric models a) initial model with surrounding rock formation (left) and b) model with scaled rock properties and spherically shaped heat exchangers, Section I, Section II and Section III (right).

To determine the number of heat exchangers and their locations relative to the crosscut drifts, a number of variations of the model were run to determine what was optimum. The goal of these runs was to determine the basic location and configuration. These variations focused on the placement of heat exchangers within the shaft and relative to the horizontal connector shafts to the stope. The authors have designed the DHEs such that they can be moved up or down in the shaft in order to optimize the system. The DHE will be instrumented and data collected and reported. While several configurations were modeled, only what we determined was the best of several different models will be presented. In this context, generally, it was found that placing 11 DHEs near the top of the shaft was best. Specifically, three heat exchangers were placed in Section I at 18 m apart. Six were placed in Section II with the beginning DHE placed in close proximity to the crosscut, then descending at 9 m apart, and two were placed in Section III in close proximity to the 150-m level crosscut at 4 m apart. This is where the water was believed to be the coolest due to the slight density difference in the water.

The total maximum building load expected is 240 kW and was used as the input value into the model. With the 11-DHE design, there was an energy extraction gradient in each section, with 20% of the required 240 kW being extracted from the Section I section, 70% being extracted from Section II and 10% being extracted from Section III. Section I had a descending extraction gradient, with the beginning heat exchanger being set at 33 kW, the second being set at 9.5 kW and the third being set at 5 kW. Section II also had a descending energy extraction gradient, with first heat exchanger being set at 66 kW, higher because of its location being so close to the inlet flow of the crosscut. The second carried a load of 42 kW, the third set at 25 kW, the fourth set at 17 kW and the deepest two were set at 8

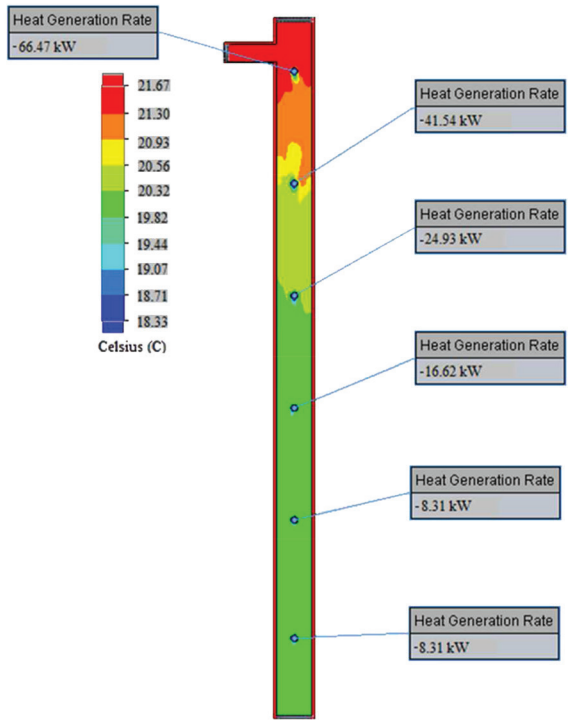

Figure 5 — Section II temperature profile for the case considering the 11-DHE design.

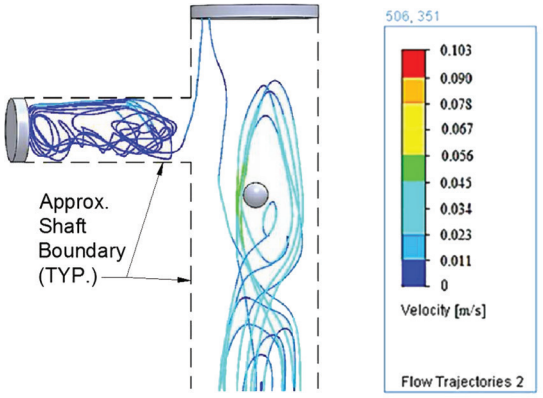

Figure 6 — Flow trajectories around the DHE located at the 100-m level of the shaft.

kW. Section III's two heat exchangers were both set at 12 kW.

Results and discussion

Overall, the simulation indicated the system would experience a steady-state temperature in a range of 20-26° C. The largest temperature difference was measured at the bottom of Section II, as shown in Fig. 5. This occurred even though this is the section in which the largest amount of energy is being extracted. This substantiates the prediction that thermal currents were induced and water would be moved from the stope to the vertical shaft. The low temperature of 20° C was measured at the bottom of the middle section.

Looking at specific sections, Section I consisted of the three heat exchangers that carried 20% of the 240 kW load and reflected only a 1° change (23-24° C, Fig. 5). The velocities that were simulated reached a maximum of 0.092 m/s and the flow patterns were consistent with natural convection.

Section II had the most heat exchangers placed in the entire model, consisting of six DHEs placed 9 m apart. The water velocities reached a maximum of 0.1 m/s around the heat exchanger located at the 100-m level near the crosscut. A low temperature of 20° C was calculated at approximately the 150-m level. The flow trajectories did not reflect ideal flow patterns, but some consistency could be seen near the heat exchanger located near the crosscut. The flow pattern around the 100-m heat exchanger and the temperature profile of Section II can be seen in Fig. 6.

Section III is not shown, but had a nearly constant temperature and low flow rates. For more details, see Thornton (2012).

One of the most important results was that the model indicated that natural convection is the primary mechanism of heat transfer from the water and can be induced. Since the temperature reached a steady state, it was concluded that the surrounding formation rock was sufficient in providing the required heat to the water and with the water movement there is sufficient energy within the system to more than heat the building.

Eleven heat exchangers appeared to be the optimum number to place in the three sections of the model. However, additional experimental work is needed to fully optimize the DHE locations. The lowest temperature surrounding a heat exchanger was modeled to be 20° C. Section II, where six of the 11 DHE were located, had the most water movement. The authors determined that the majority of heat exchangers should be placed in Section II to induce thermal currents.

What is clear is that the relative location of the heat exchangers is critical relative to the location of the crosscuts that connect to the stope. This is critical to having "access" to the stope water. The simple model has shown that using heat pumps in vertical mine shafts is feasible. Installation of the system will occur in late 2012 and early 2013 and implementation results will be reported.

Acknowledgments

Work for this project was supported in part by Grant DE-EE0002821 from DOE EERE-PMC. The authors acknowledge and are grateful for technical and editing assistance by Susan Barth of the Montana Bureau of Mines and Geology and by Jason Hamm, currently a General Engineering student at Montana Tech.

References

Culver, G. and Lund, J.W., 1999, "Downhole heat exchangers," *Geo-Heat Center Bulletin*, September, pp. 1-11.

Fausett, L.V., 1999, *Applied Numerical Analysis Using MATLAB*, pp. 29-35, London, UK, Pearson.

Fickes, M., 2012, "Below the surface," *College Planning & Management*, April, pp. 40-44.

FloEFD, 2011, *FloEFD 11 for SolidWorks*, Wilsonville, OR: Mentor Graphics Software.

Hellums, J.D., Churchill, S.W., 1962, "Transient and steady state, free and natural convection, numerical solutions: part i: the isothermal vertical plate," *American Institute of Chemical Engineers*, November, pp. 690-692.

Incropera, F.P., Dewitt, D.P., Bergman, T.L., and Lavine, A.S., 2007, "Physical origins and rate equations," *Introduction to Heat Transfer*, pp. 4-10.

NCEES, 2010, *Fundamentals of Engineering*, Supplied Reference Handbook, 8th edition, 2nd revision.

Thornton, R., 2012, Convection Mechanisms for Geothermal Heat Exchangers in a Vertical Mine Shaft, MS thesis, Montana Tech Library, Butte, MT.

Watzlaf, G.R. and Ackman, T.E., 2006, "Underground mine water for heating and cooling using geothermal heat pump systems," *Mine Water and the Environment*, March, pp. 1-14.

CONVECTION MECHANISMS FOR GEOTHERMAL HEAT EXCHANGERS IN A VERTICAL MINE SHAFT

by

Rory Thornton

A thesis submitted in partial fulfillment of the requirements for the degree of

Master of Science in General Engineering

Montana Tech of The University of Montana

2012

Abstract

This study evaluated the water-filled abandoned Orphan Boy mine as a heat source for an 80-ton heat pump to heat the 20,000 ft^2 Natural Resources Building (NRB) at Montana Tech. The mine consists of an 800-foot vertical shaft connected to a large stope via three horizontal crosscut shafts. Total available water is 332 million gallons at 78° F with the majority held in the stope. The only practical placement of the heat exchangers is in the vertical shaft. Therefore the primary focus was to model the heat exchanger placement and configuration in the vertical shaft such that thermal currents develop between the stope and vertical shaft to access all available energy. Modeling of water flow, temperature profiles, and contribution from the walls, was done using finite difference methods and computational fluid dynamics, and then compared to empirical results. An optimum number of 11 down-hole heat exchangers (DHE) and their vertical placement was determined using the required heating load for the subject building of 810,000 BTU/hr. The results showed thermal currents developing and that water near the heat exchangers will remain above 67° F.

Key Words: Geothermal, Mine Shaft, Convection, Heat Exchanger

Dedication

I wish to dedicate this paper to my son, Aidan, for all his patience, love and understanding. Time during this study was sometimes unfairly taken from him. Hopefully, he has gained an appreciation for science and engineering.

Acknowledgements

I would like to thank Dr. Neil Wahl for his support, patience, and wisdom during the study of this thesis as well as the rest of my graduate studies. I would also like to thank Chancellor Don Blackketter for giving me the opportunity to conduct this study and for his guidance in writing this paper. I would like to thank Dr. David Bunnell for his help in all my computer simulations. I would also like to thank Gloria Carter for helping me format this paper. Finally, I would like to thank my classmates for their camaraderie and support.

Table of contents

List of Figures

Glossary of Terms

Term	Description
Crosscut	A passageway in a mine shaft that cuts across the geologic formation
Stope	Void space in a geologic formation that comes from mining ore in a steep or vertical mine shaft
θ	normalized temperature at specific position and time
erfc	complementary error function operator
x	position of calculation
α	thermal diffusivity
t	time
k	thermal conductivity
h	convective heat transfer coefficient between the surface of an object and a particular fluid
g	acceleration due to Earth's gravity
β	coefficient of thermal expansion
υ	kinematic viscosity
T_s	temperature of a surface
T_∞	steady-state temperature of the fluid
k_f	thermal conductivity of a certain fluid
Cp	heat capacity of a certain material or fluid
ρ	density of a material or fluid
h_{avg}	average convective heat transfer coefficient between the surface of an object and a particular fluid

1. Executive Summary

The Orphan Boy mine shaft has access to 332 million gallons of water that holds a temperature range of 75°-78° F year round. A down-hole heat exchanger (DHE) system to heat the 20,000-ft^2 Natural Resource Building (NRB) at Montana Tech has been designed based on the building's heating requirements and the energy available in the mine shaft. The building was initially designed to use the mine water and a heat pump either as the primary source or to augment the heating and cooling needs. The energy within the water, if lowered to freezing, was calculated to be 124 billion BTU. It was assumed that heat transfer within the mine system would be by natural convection. The goal of the work was to model the convective mechanisms, the flow of the water due to thermal currents, and heat transfer of the exchangers.

Initially, a 2-D finite difference model was used to quantify the heat transfer within the mine shaft and the stability of the model with the added DHE. The 2-D model helped eliminate configurations that would have hindered the 3-D fluid dynamic model. The 3-D physical model of the shaft and formation was built with the CAD software SolidWorks. Simulation software complementary to SolidWorks, FloEFD, was used to simulate the heat transfer and fluid dynamics involved in the shaft. Models were compared to calculations that gave a value of the total heat transfer available within the system.

An isothermal plot of the 2-D finite difference model showed a temperature drop beginning approximately 60 feet into the granite formation to the center of the shaft where the heat exchangers would be placed. The original design involved 15 heat exchangers, which was determined to be feasible through simulation. The question remained if 15 heat exchangers were necessary. The placement of the heat exchangers within the system was also a factor because the mine shaft was connected to the main reservoir via crosscut shafts. With seepage flow rates

varying between 25 and 58 gallons/minute, it was determined that natural convection, rather than water replacement, would be the mechanism that caused water movement. A cut-plot of the 3-D model was made for various configurations simulating the system and the temperature change to meet the heating requirement. It was found that 11 heat exchangers sustained the system. The 11 heat exchangers were strategically placed throughout the shaft to optimize heat transfer. The required load of 810,000 BTU/hr for the NRB was distributed to each DHE, but not equally. The bulk of the load was set at the middle section of the shaft (Section II). This section was the most likely place where natural convection would occur.

Although 11 heat exchangers showed that sufficient heat transfer could occur within the system while sustaining the mine water temperature above 67° F, 15 heat exchangers would require a heat transfer rate of 54 kBTU/hr per coil. 15 heat exchangers gave a better temperature profile such that the temperature did not fall below 65° F around the heat exchangers. It was shown that the Orphan Boy could be a primary or supplementary means of heating the NRB.

2. Introduction

Geothermal heating and cooling is not only an economical way to heat commercial and residential buildings; it is an extremely efficient way of heating a building. Ball State University in Indiana has a plan to build an $80 million system that includes 3,600 vertical boreholes, between 400 feet and 500 feet deep, tied together with over 1000 miles of piping [1]. Expensive as it sounds, this system was created to heat 47 buildings and to keep the university from burning over 36,000 tons of coal per year. This will prevent 85,000 tons of CO2 emissions from entering the atmosphere.

Mine water used for geothermal systems is a concept that is being considered worldwide. Since conventional underground mining has been practiced for centuries, the world is full of

mines that have been abandoned and flooded. These abandoned mines are no longer productive, but exist, nonetheless. Watzlaf and Ackman provide an excellent summary of the status of the use of geothermal systems in abandoned mines in the U.S. and Canada [2]. The flooded lead mines in Park Hills, Missouri serve to heat and cool an 8,100-ft^2 municipal building. The water is only 360 feet deep and holds a temperature of 57° F. In Springhill, Nova Scotia the water in abandoned coal mines is used to heat and cool 151,000-ft^2 with the supply water held between 55° F and 68° F during the year. While there have been a number of other examples and reports on using heat pumps in abandoned water-filled mine formations, there was not a found example in which heat exchangers were placed in a vertical mine shaft with the intent to use thermal currents to access a large stope.

Montana Tech, located in the historic mining town of Butte, owns the Orphan Boy mine. The mine shaft is located west of the campus and is a candidate for a geothermal down-hole heat exchanger (DHE). The section of interest is an 800-ft vertical shaft that provides accessibility to approximately 332 million gallons of water via three crosscuts that connect to the Orphan Girl mine shaft. The water, which holds a constant 78° F, fills a stope that was excavated in the early 20^{th} century. The water seeps to the surface through the Green Springs seep located west of the mine. The seep has a volumetric flow rate that is measured monthly and ranges from 18-58 gallons/minute. This flow rate is considered to occur within the mine shaft and was used in the simulations.

This configuration is unique because the layout of the heat exchangers is in a shaft and not in the stope, so additional modeling and calculations were needed to determine if this arrangement was feasible. This work was funded through the Department of Energy (DOE) and the Energy Efficiency and Renewable Energy (EERE) grant where Phase I is the design of the

system, and Phase II is the installation of the actual complete system to heat a 20,000-ft^2 building. This paper is part of Phase I focusing on optimizing heat exchangers in a shaft to get water movement and heat exchange. A feasibility study was conducted to determine the amount of energy within the water if it were lowered to 32° F and was calculated to be 124 billion BTU. Initially, it was assumed that natural convection is the driving force for heat transfer within the system.

The surrounding formation (mine shaft and stope) is made up mostly of quartz monzonite. The United States Geological Survey considers quartz monzonite to have the same properties as granite [3]. Therefore, thermal calculations used granite properties for the conductivity, heat capacity, and density. These calculations were vital in finding the feasibility of energy extraction from the Orphan Boy.

It was assumed that convection would be the driving force for heat transfer. It was also assumed that the formation itself was transferring heat to the water inside the stope which circulated water through the Orphan Girl and Orphan Boy mine shafts. There is also seepage from the mine that may contribute to water movement. This study included determining the contribution from each mechanism that would impact the heat transfer. Even though convection was assumed to be occurring within the shaft, it was unknown whether it was forced convection or natural convection. Due to interference inside the Orphan Boy, the Orphan Girl's water velocities were measure via a submersible camera. Through the use of the submersible camera, it was later determined to be natural convection occurring because of the low velocity of 0.1 ft/sec inside the Orphan Girl.

Originally, 15 coils, 700 feet long with 1-inch diameters, were planned to be installed inside the Orphan Boy [4]. The feasibility of this would be later compared to an alternative

design that had the bulk of the heat exchangers placed where it was believed to have the most potential for natural convection. This location was believed to be the middle section of the shaft. Convection coefficients that apply to Newton's Law of Cooling [5] were also calculated for each heat exchanger on both designs.

The best method for a feasibility study was the use of computational fluid dynamics software. With the software it was possible to visualize flow trajectories and view temperature profiles in a 3-D model of the shaft that was built in CAD software.

3. Literature Review

Natural convection is a poorly understood phenomenon, especially when water is the working fluid. The magnitude of convective heat transfer, in part, is based on the velocity of the fluid. However, in natural convection the density difference in the fluid promotes movement. The governing equations that can be used to determine the parameters of the fluid (e.g., pressure, temperature, velocity, and density) are the laws of conservation of energy, momentum, and continuity. The reduced form to these equations is called the Navier-Stokes equations [13]. Different numerical solutions are used to give simultaneous solutions to these equations. The paragraphs that follow present the most relevant published work on heat exchangers.

In 1999, research was conducted on the actual installation of a DHE in Klamath Falls, OR. Klamath Falls is considered a geothermal "hot-spot" as opposed to Butte where the heat exchange is mostly dependent on the local mine water. The Klamath Falls DHE used a consistent pattern of "hair-pin" loops. These tubes were made of a cross-linked polyethylene (PEX) that had a thermal conductivity of approximately 200 times less than that of iron. A promoter pipe made of iron was used to enhance water circulation [6]. This study looked at a DHE in a well as

opposed to an open shaft, but it did have a closed loop DHE in warm water. The information supplied within this paper provides some idea on how to design a closed loop DHE system.

In 1962, J.D. Hellums and S.W. Churchill explained the numerical methods used in modeling the parameters of an isothermal vertical plate. This paper included normalizing the parameters and used finite difference methods in building a temperature profile [9]. This paper was useful in determining the feasibility of the shaft and the heat pump supplying heat for a 20,000-ft^2 building. Their study used a 2-D finite difference model to visualize a temperature profile and heat migration. Also, the CFD software uses complex mathematical series requiring long computational times whereas the finite difference code shortened the computational time while still achieving accurate, but general results.

Although the designs of the heat exchangers themselves are not discussed in this paper, a practical use for non-corrosive mine water that is held at 78° F needs to be visualized. Everything from the fluid inside the tubes to the geometry of the tubes themselves is a factor in the total heat transfer. In this paper, it is stated that coiled 1-inch diameter tubes make up the heat exchangers. S.A. Guerrieri discusses natural convection and the use of glycols versus water inside heat exchangers and the geometry of these tubes affecting the heat transfer coefficients on the surface of the tubes. This validated that the geometric design is essential in optimizing heat transfer [11].

The Navier-Stokes equations used in the finite difference equations as well as the simulations on the CFD software can be put in many different forms (e.g., shear stress, stagnated pressure, temperature, density, velocity, etc.). For the 2-D finite difference model, a version that included only temperature, velocity, and density fit best for the shaft and the water supply. The

section in Engineering Fluid Mechanics by C.T. Crowe and J.A. Robertson gave several versions of the continuity (1) [13], energy (2) [13], and momentum (3) [13] equations.

$$\frac{\partial U}{\partial \tau} + U\frac{\partial U}{\partial X} + V\frac{\partial U}{\partial Y} = T + \frac{\partial^2 U}{\partial Y^2} \tag{1}$$

$$\frac{\partial T}{\partial \tau} + U\frac{\partial U}{\partial X} + V\frac{\partial T}{\partial Y} = \frac{1}{Pr}\frac{\partial^2 T}{\partial Y^2} \tag{2}$$

$$\frac{\partial U}{\partial X} + \frac{\partial V}{\partial Y} = 0 \tag{3}$$

Within the granite section of the formation in the 2-D finite difference model, only the use-of-the-energy equation was required. Interactions of thermal properties are much different for fluids as opposed to solids, so momentum and continuity must be considered for the fluid section. This gave an idea of the complexity of convection itself. In other words, the means of heat transfer as it migrates from the surface of the rock to the water will change significantly because of the movement of the water. Simultaneous solution of these equations is extremely tedious and difficult, but it was accomplished with the use of computer software and the application of the right boundary conditions.

Once a temperature profile could be visualized and values for those temperatures were apparent, methods to find heat transfer coefficients needed to be researched. Dimensionless variables including Rayleigh (Ra), Grashof (Gr), Prandtl (Pr), and Nusselt (Nu) numbers were used to calculate natural convective heat-transfer coefficients. There are specific equations for different geometric models (i.e., horizontal and vertical plates). Hilbert van Nydeck Schenck

summarizes empirical solutions in using dimensionless parameters in determining convective coefficients [7].

4. Methods

To size the design and quantify the stability of the mathematical model, a 2-D finite difference model was built. To simplify calculations, symmetry was assumed to occur throughout the formation and mine shaft. With this in mind, a mathematical equation could be used to calculate the distance within the formation where the temperature could be assumed to be constant (4) [14]. Since the system is a vertical shaft filled with water, an equation specified for surface convection off a vertical plate can be used.

$$\theta(x,t) := \operatorname{erfc}\left(\frac{x}{2\cdot\sqrt{\alpha\cdot t}}\right) - \left(\exp\left(\frac{h\cdot x}{k} + \frac{h^2\cdot\alpha\cdot t}{k^2}\right)\right)\cdot\left(\operatorname{erfc}\left(\frac{x}{2\cdot\sqrt{\alpha\cdot t}} + \frac{h\cdot\sqrt{\alpha\cdot t}}{k}\right)\right) \quad 4)$$

Originally, it was assumed that natural convection would be the primary means of heat transfer. For this to be true there had to be very little to no flow rate within the mine shaft. To confirm this, a camera was lowered into the Orphan Girl mine shaft with a 100-ft tube attached to the line. Visible ink was injected into the water and it confirmed the existence of little to no flow. The make-up of the camera along with the measuring system can be seen in Figure 1.

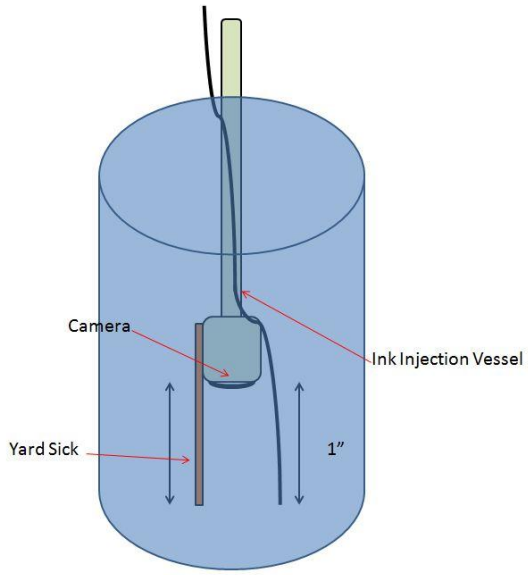

Figure 1: Submersible camera with make-shaft measuring device.

The rock surrounding the mine shaft and stope is believed to supply the heat to the water inside. If this is true, heat is migrating towards the surface of the rock. This means that the rock would hold a constant temperature a certain distance within the formation. With this distance, boundary conditions could be set for both a 2-D finite difference model and a 3-D simulation. An average convection coefficient from the surface of the rock and the water needed to be calculated before this distance could be found. To find the distance, dimensionless parameters needed to be found. A Nusselt number for a flat plate of 21,100 (8) [9] was calculated using a Grashof number of $1.32*10^{17}$(5) [9], a Prandtl number of 0.146 (6) [9], and a Rayleigh number of $1.92*10^{16}$ (7) [9]. These numbers represented the flow type and diffusion within the water. An average convection coefficient could be determined from the Nusselt number along with the characteristic length and the thermal conductivity of the water (9) [9]. This value was found to be 48 W/m^2*K.

$$Gr = \frac{g * \beta * (T_s - T_\infty) * Length^3}{v^2} \quad (5)$$

$$Pr = \frac{k_f}{\rho * Cp * v} \quad (6)$$

$$Ra = Gr * Pr \quad (7)$$

$$Nu_{vp} = \frac{0.825 + 0.387 * Ra^{\frac{1}{6}^2}}{1 + \frac{0.492}{Pr}^{\frac{9}{16}^{\frac{8}{27}}}} \quad (8)$$

$$h_{avg} = \frac{k_{f*} Nu_{vp}}{Length} \quad (9)$$

Temperature within the formation remained constant at a distance of approximately 20 meters as shown in Figure 2. This value was used as a set boundary condition for the 2-D finite difference model as well as future 3-D simulations.

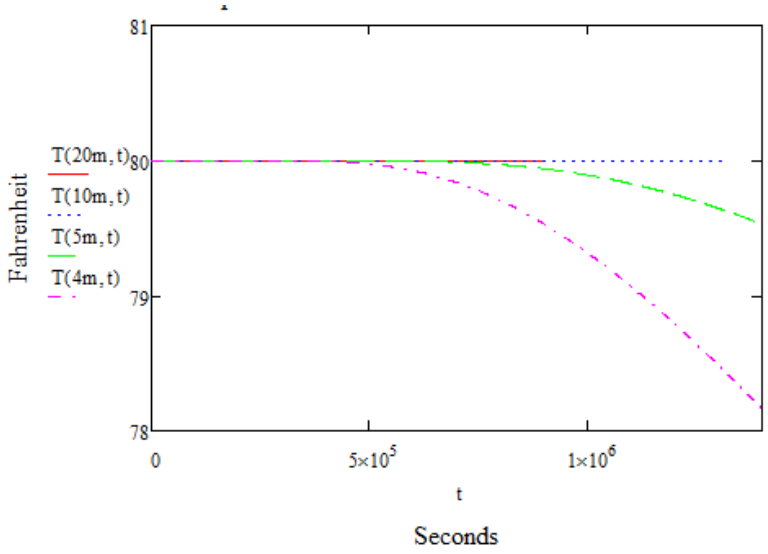

Figure 2: Transient temperature for a semi-infinite solid with surface convection over time

Even when symmetry is involved, the total area of heat transfer is still over 6000-m^2. For further simplification, the total area was cut down to 529-m^2 with the distance of 20 meters remaining. The reduction in area allowed for a smaller linear matrix for calculation. Finite difference modeling of the system was set up on a 2-D grid as seen in Figure 3 below. The partial distance for the X and Y direction were set equal to each other at 3 meters. Each node represents a steady-state temperature for that section.

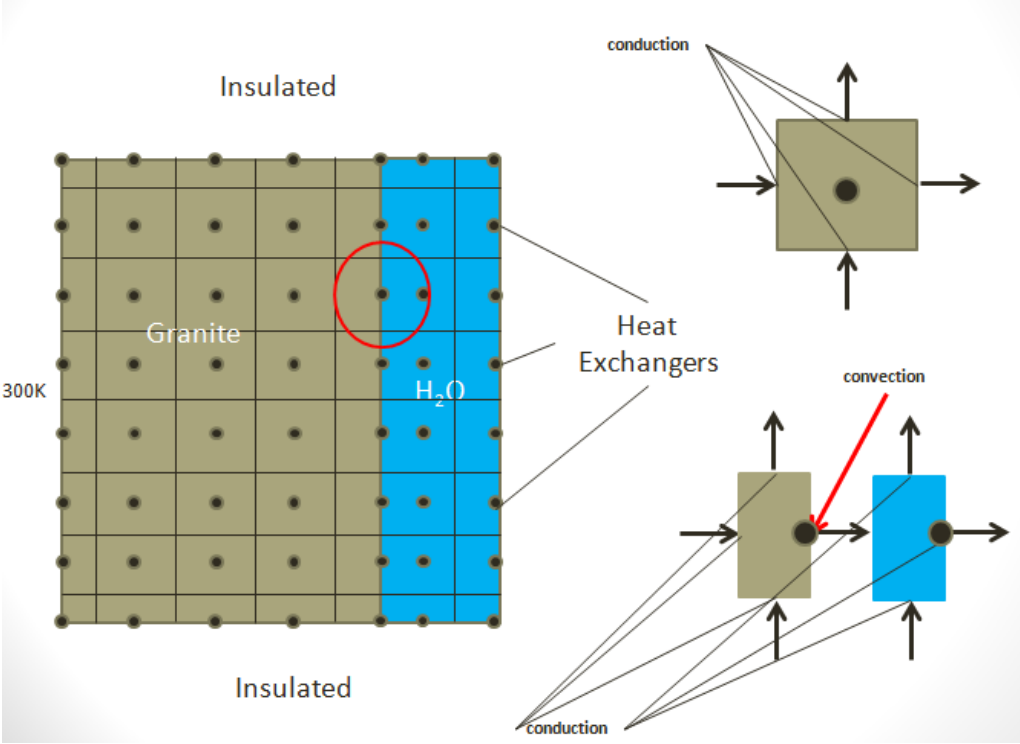

Figure 3: Nodal grid of mine shaft & formation and an energy balance of each node.

For each section of the grid, the energy entering and leaving the section was summed using with the first law of thermodynamics. Conservation of energy within the granite was represented by Fourier's Law meaning that only conduction occurs in the granite, while convection was assumed from the surface of the granite to the water, which was represented by Newton's Law of Cooling (10) [5]. The steady-state heat transfer that occurred within the water

itself was calculated by only Fourier's Law (11) [5]. This is not 3-D and thus is not the most appropriate geometry, but this does provide representative parameters of heat transfer within the system. Once the equations were set, a 42x42 matrix was created using MATLAB [10]. The full code is presented in Appendix 1.

$$\boldsymbol{Convective\ Heat\ Transfer = h_{avg} * A * (T_s - T_\infty)} \quad (10)$$

$$\boldsymbol{Conductive\ Heat\ Transfer = k * A * \frac{\Delta T}{\Delta x}} \quad (11)$$

Once boundary conditions could be quantified within the system, more accurate methods of calculating temperature change could be used. Instability at medium heat extraction values was the major shortcoming of the 2-D finite difference model. Therefore, a 3-D model was built using CAD software, SolidWorks, and CFD software, FloEFD [8]. Prior to building a 3-D model of the system, smaller geometric models were built to validate the software.

A cylinder, 20 feet in diameter and 10 feet deep, was modeled in SolidWorks and boundary conditions were set in FloEFD where the boundary conditions were set and the fluid dynamics was simulated. Both geometric models are shown below in Figure 4. This model was simulated to be filled with water and heated from the bottom surface. A surface heat source was set at 1500 BTU/hr at the bottom of the cylinder while standard atmospheric conditions were set at the top. The outer wall of the cylinder was set to be adiabatic and the working fluid was water. This would confirm if convection would occur within a closed shaft filled with water with energy being transferred.

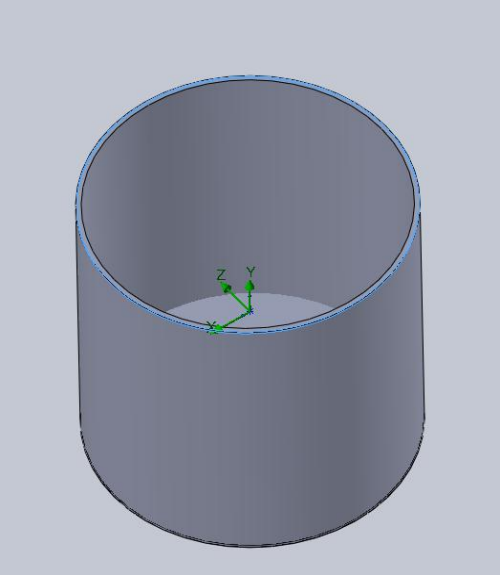

Figure 4: 3-D validation model - "Sauce Pan."

Once convection could be seen through the software, steps to build a small 3-D version of the system in question could be taken. First, a cylinder representing the formation surrounding the shaft was built in SolidWorks. The cylinder was set to a length of 800 feet, a radius of 60 feet with a square shaft voided in the middle having a cross-sectional area of 108 ft^2. The top and bottom of the cylinder representing the formation was left open. The material assigned to the cylinder representing the formation was "granite," a custom material that was made using SolidWorks' "custom material" function. Thermal material properties defined in this section were conductivity, specific heat, and a thermal expansion coefficient. There is a "lid" function in FloEFD that lets the user set boundary conditions and assign material. However, for this particular simulation, two separate geometric models were constructed in SolidWorks to represent the top and bottom of the shaft. The complete geometric model of the system can be seen below in Figure 5.

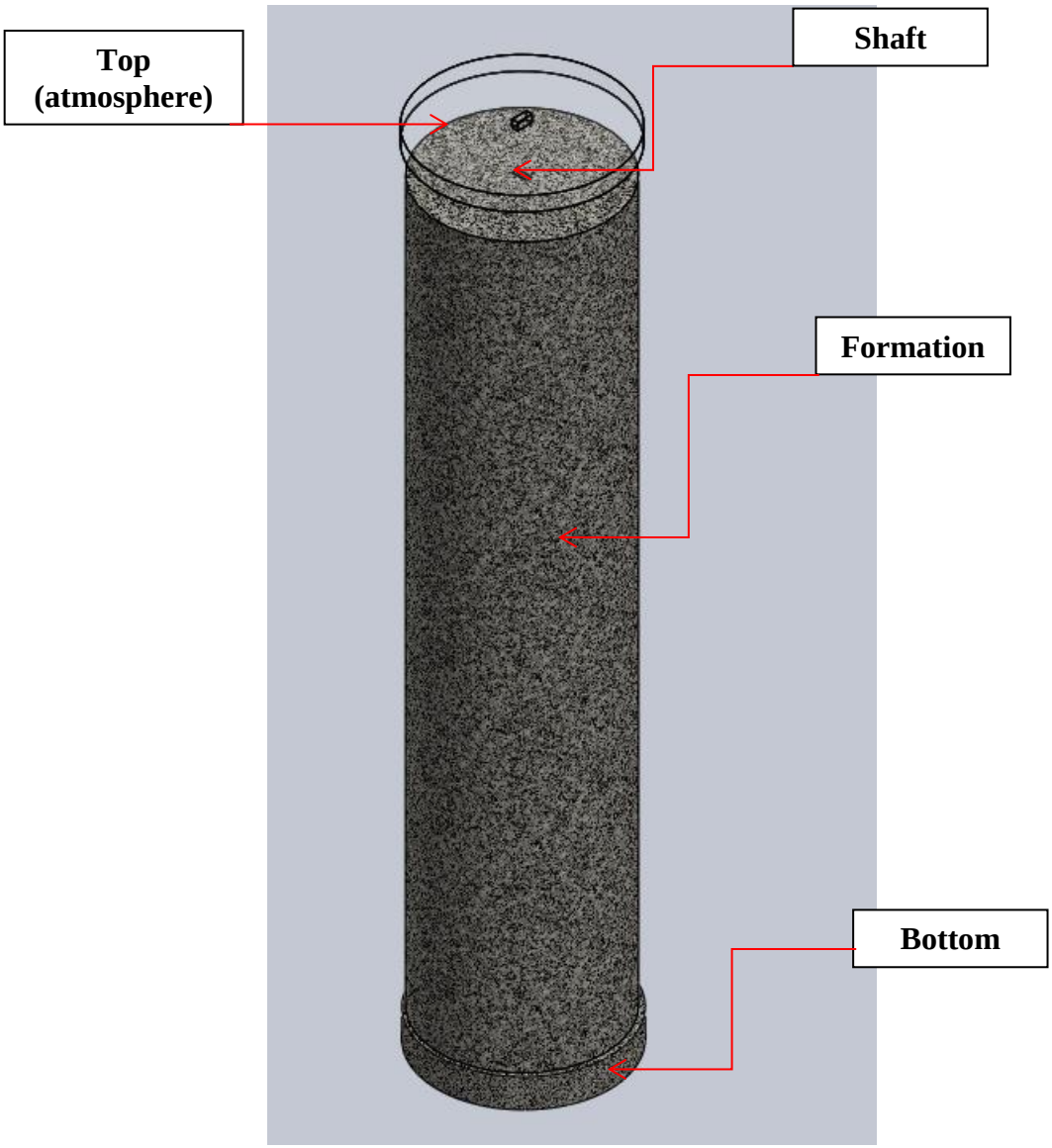

Figure 5: Full-scale geometric model of the Orphan Boy mine shaft and surrounding formation.

The top and bottom were built as 20-ft thick cylinders having the same radius as the formation and structural properties were assigned, as well. The granite section (shaft and bottom) was assigned a conductivity of 2.79 W/m*K [14], a specific heat of 775 J/kg*K [14], and a thermal expansion coefficient of $0.80*10^{-5}$ K^{-1} [14]. The top section was assigned a material of 'air.' This was a set material within SolidWorks, so material properties were already defined with a conductivity of 0.02 W/m*K [8], a specific heat of 1005 J/kg*K [8], and a thermal

expansion coefficient of $3.0*10^{-3}$ K^{-1} [8]. 15 cylinders that represented the DHEs were modeled with a 2-ft diameter and a 2-ft length and were placed in the center of the shaft. Once these parts were assembled, a simulation in FloEFD was conducted, but no results could be quantified.

The time the simulation took to complete its calculation was significant. This was because of the number of elements within the model. The shaft itself is quite small when compared to the rest of the formation. The focus of the study is to determine whether natural convection exists within the shaft, but with this particular model there is so much more rock then there is water that the computer resources available cannot handle the number of iterations this model requires. The model was scaled down to reduce computational time.

The complete model of the Orphan Boy was divided into three 200-ft sections. The thickness of the cylinders representing the formation surrounding the shaft had to be somehow reduced while keeping the boundary condition of a constant 80° F at a point that was 60 feet into the formation. Accomplishing this required defining a pseudo material so that the diameter of the formation could be changed from 120 feet to 12 feet. The thermodynamic properties of granite were scaled down by a factor of ten. The thermal conductivity was changed from 2.79 W/m*K to 0.279 W/m*K and the heat capacity was changed from 775 J/kg*K to 7750 J/kg*K. This scaling reduced the number of elements in the finite element analysis of the CFD software, thus reducing the computational time by a factor of approximately seven. Each section was modeled in SolidWorks as 200-feet long with a diameter of 12 feet. The cross-sectional area of the shaft was once again 108-ft^2. Boundary conditions were set for each section such that they matched between sections. In other words, hydrostatic pressure was set at each section with respect to its depth and each section was forced to match continuity. Unfortunately, the computational time was still too long. Since the thermal properties were fixed and the model divided into three

sections, the only factor that was problematic was the sharp corners on the geometric models. The flow trajectory models showed a larger quantity of mathematical abstracts or areas where the software could not converge on the final iterations. The solution to this was to build a circular shaft instead of a rectangular one and creating spheres instead of cylinders for heat exchangers. The geometric model of the new shaft can be seen in Figure 6.

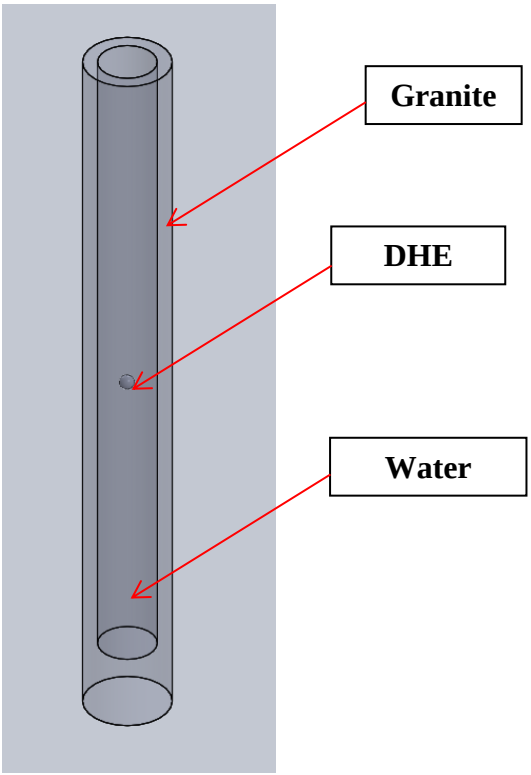

Figure 6: Circular shaft with spherical heat exchanger

Changing the material properties of the model, dividing the model into three sections, and removing the corners reduced the computational time significantly, which gave an opportunity to build an alternative design. Also, the limitations to the system in question could now be visualized. In other words, it was possible to see how much heat could be transferred before the water reached 32° F. This was achieved by running several simulations with a defined heat

extraction at each heat exchanger. Simulations were modeled until a temperature of 32° F was recorded anywhere near a heat exchanger.

The following segments describe the three sections that were modeled with the appropriate boundary conditions.

4.1. Section I: 100 feet to 300 feet

Atmospheric pressure of 14.7 psi and an initial temperature of 75° F represented the boundary conditions at the top of Section I of the model. There is a crosscut that enters just above the atmosphere. However, the water level lies just below it, so it was not built in the geometric model. The outer wall temperature was set to 80° F with conduction only occurring within the solid part of the model. The working fluid was set to water and initial temperature within the entire system was set to 75° F.

4.2. Section II: 300 feet to 500 feet

A hydrostatic pressure of 86.7 psi from the bottom of Section I and an initial temperature of 73° F represented the boundary conditions at the top of the Section II section of the model. Another crosscut entering at the top was modeled again with the same inlet volumetric flow rate of 11.3 gallons/minute. The bottom section was set to have an outlet volumetric flow rate of 35 gallons/minute. The outer wall temperature was set to 80° F with conduction in solids only. The working fluid was once again set to water and the initial temperature was set to 75° F.

4.3. Section III: 500 feet to 700 feet

Hydrostatic pressure of 173.3 psi from the bottom of Section II and an initial temperature of 68° F represented the boundary conditions at the top of Section III. Another crosscut entering at the top was once again modeled with an inlet volumetric flow rate of 11.3 gallons/minute. However, this time an outlet of 35 gallons/minute was modeled towards the bottom with the

actual bottom being set to a surface heat source of 0 BTU/hr, making it adiabatic. The outer wall was set to 80° F with conduction only occurring in solids.

Two scenarios were simulated with this 3-D model of the shaft having the 810,000 BTU/hr load extracted. The first scenario was the preliminary plan designed with 15 heat exchangers evenly spaced 33-ft apart making five in each section. The spheres that represented heat exchangers were set to have a volume heat source of -54 kBTU/hr at each sphere. Figure 7 shows the geometric models of all three sections with the 15 heat exchangers.

a b c

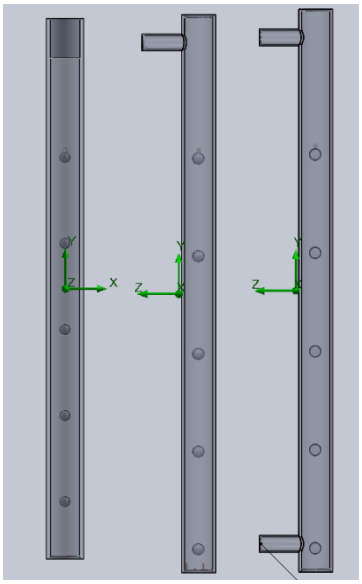

Figure 7: Geometric model of the Orphan Boy with 15 evenly distributed heat exchangers, Section I (a), Section II (b), and Section III (c).

The second design focused on placing 11 heat exchangers where the bulk of convection currents would ideally occur. Three heat exchangers were placed in the Section I section at 60-ft apart. Six were placed in Section II with the beginning sphere placed in close proximity of the crosscut then descending at 30-ft apart, and two were placed in Section III in close proximity of the 500-ft level crosscut at 12-ft apart. This is where the water was believed to be the coolest due

to the slight density difference in the water. The geometric models of the three sections that had 11 heat exchangers can be seen below in Figure 8.

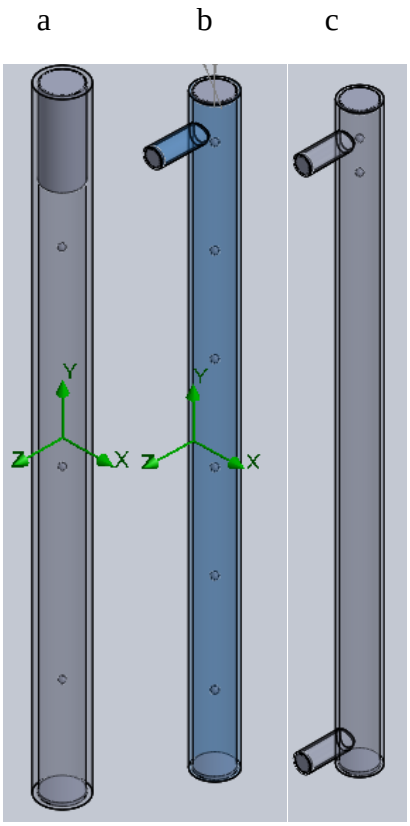

Figure 8- the final geometric models with spherical shape Heat exchangers, Section I (a), Section II (b), and Section III (c)

With the 11 DHE design, there was an energy extraction gradient in each section with 20% of the 810,000 BTU/hr being extracted from the Section I section, 70% being extracted from Section II, and 10% being extracted from Section III. Section I had a descending extraction gradient with the beginning heat exchanger being set at -113,400 BTU/hr, the second being set at -32,400 BTU/hr, and the third being set at -16,200 BTU/hr. Section II also had a descending energy extraction gradient with the first heat exchanger being set at -226,400 BTU/hr. This was set high because of its location being so close to the inlet flow of the crosscut. The second carried a load of -141,750 BTU/hr, the third was set at -85,050 BTU/hr, the fourth was set at

-56,700 BTU/hr, and the bottom two were set at -28,350 BTU/hr. Section III's two heat exchangers were both set at -41,500 BTU/hr.

When both these simulations were completed, Newton's Law of Cooling [5] was used to get the temperature differentials required between the horizontal surface of the heat exchangers and the water. Since an exact solution to our problem is not probable, the employment of dimensionless parameters is needed. That is why it is important to have an exact (or close) replica of the mass that we are trying to model and the forces acting on that model correspond to the ratio of the mass and the prototype [13]. This was done by using an equation for convection between long, horizontal cylinders and a working fluid. The equation consisted of finding dimensionless parameters based on the temperature of the water. A Nusselt number (13) [12] specifically for a horizontal cylinder, but in this case a thin coiled tube, gives an average convection coefficient with the designed coil of 1-inch diameter and 700-ft long (14)[12]. However, a Rayleigh's number(12) [12] needed to be found using the kinematic viscosity of the 78° F water, the thermal diffusivity of the water, and the water's coefficient of thermal expansion.

$$\boldsymbol{Ra} = \frac{\boldsymbol{g} * \boldsymbol{\beta} * (\boldsymbol{T_{H2O}} - \boldsymbol{T_{sc}}) * \boldsymbol{OD^3}}{\boldsymbol{\alpha} * \boldsymbol{\upsilon}} \tag{12}$$

$$\boldsymbol{Nu_{hc}} = \boldsymbol{0.53} * \boldsymbol{Ra^{0.25}} \tag{13}$$

$$\boldsymbol{h_{avg}} = \frac{\boldsymbol{k_{f*}Nu_{hc}}}{\boldsymbol{OD}} \tag{14}$$

With the known temperature of the water, a differential temperature could be determined for the given load on each heat exchanger. This would also mean that the convection coefficient would change along with the different temperatures of the heat exchangers.

5. Results

Validating CFD software was important because without the software it would have been extremely difficult to determine natural convection occurring within the Orphan Boy. The 20-ft diameter cylinder simulation helped confirm that the software could provide a visually-accurate convection model. The 1500 BTU/hr that was defined at the bottom surface of the cylinder heated the water to steady state. Toroid-like flow trajectories can be seen in Figure 9. Even though low velocities were calculated, convection still occurred throughout the system.

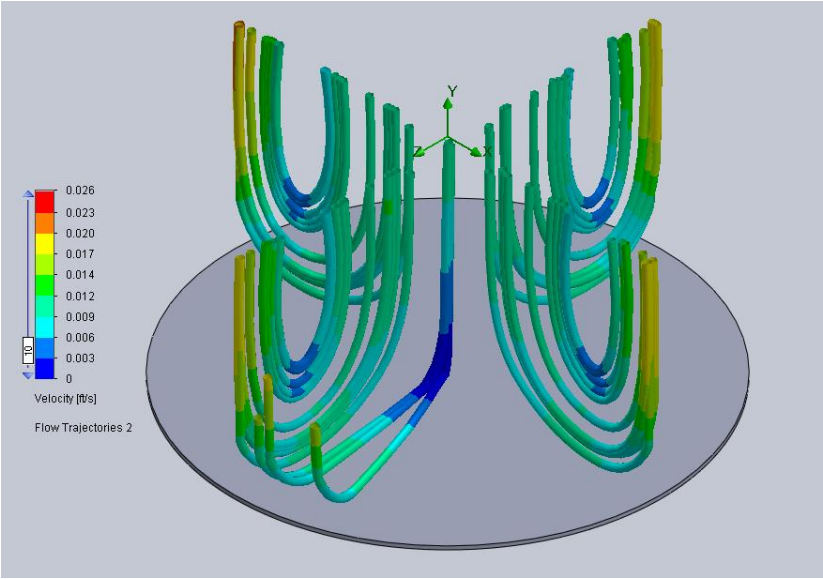

Figure 9: "Sauce pan" simulation with a surface heat rate of 1500 BTU/hr.

When it was determined that the software was capable of accurately simulating natural convection in a cylinder, it was possible to run a simulation with a simple geometric model of the Orphan Boy with only one heat exchanger. The results showed sporadic flow trajectories, but a reasonable temperature profile. With the boundary conditions of 80° F set to the outer wall, atmospheric conditions set at the top, a -200,000 BTU/hr heat extraction, and an adiabatic

bottom produced maximum velocities of 0.312 ft/s and a low temperature of 65° F. The temperature profile and flow trajectories around the heat exchanger can be seen in Figure 10.

a b

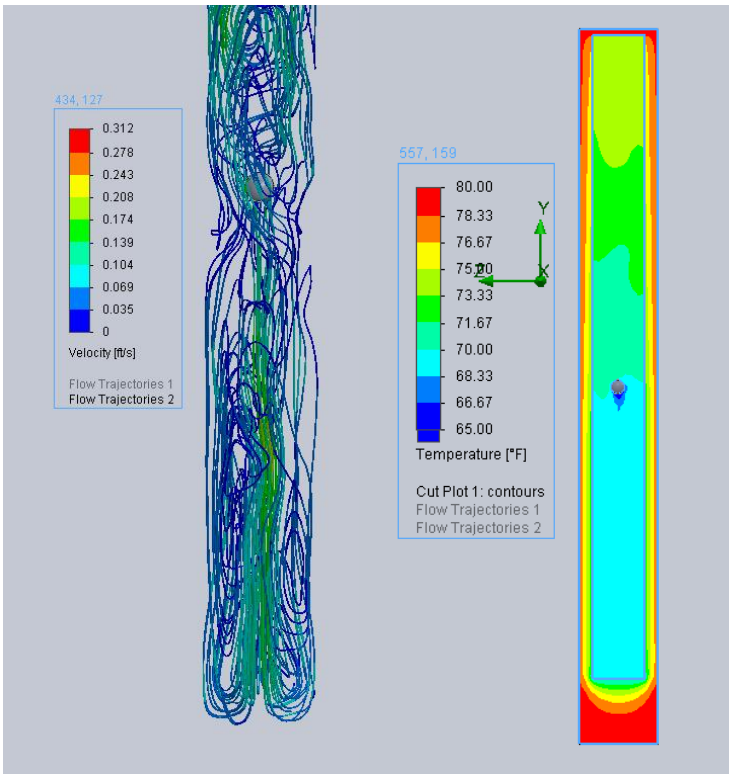

Figure 10: Circular shaft with spherical heat exchanger simulation with flow trajectories (a) and temperature profile (b)

The 15 heat-exchanger design had a limit load of 17.5 million BTU/hr. This was after reaching steady state and setting each heat exchanger to have a heat extraction rate of 1.17 million BTU/hr. This gave a low temperature of 33 °F and velocities reaching a maximum of 0.42 ft/s. This was promising in that the system could easily handle the 810,000 BTU/hr load of the NRB. The visual results were not pertinent to this paper, but they can be seen in Appendix A.

The original plan that called for 15 heat exchangers was simulated in CFD software and showed a temperature range from approximately 65° F to 75° F. The 65° F was found at the

bottom of the simulated mine shaft with the -810,000 BTU/hr evenly distributed throughout the 15n heat exchangers at -54,000 BTU/hr each. The velocities simulated reached a maximum of 0.248 ft/s and occurred within Section II near the heat exchanger located at the entrance of the crosscut. Flow trajectories and temperature profiles of Section I and Section II can be seen in Figures 10 and 11. Visuals for the flow trajectories and the temperature profile of Section III can be seen in Appendix A. Additional models were built and simulated as well. They can also be seen in Appendix A.

a b

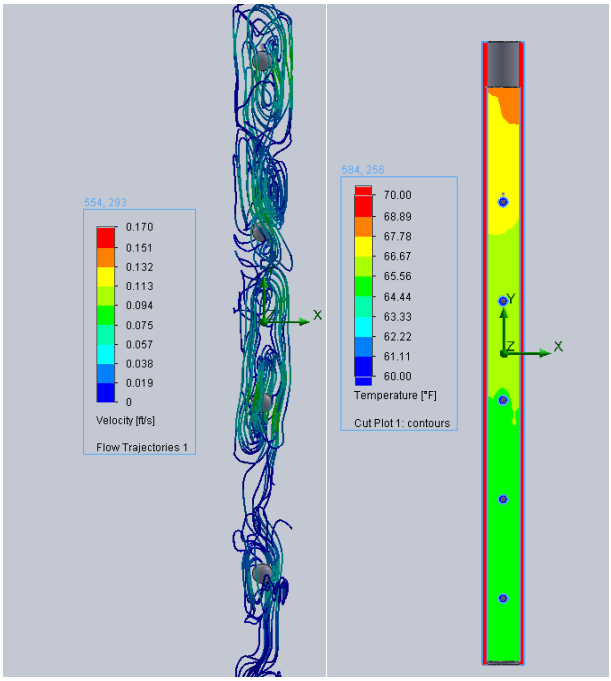

Figure 11: Section I flow trajectories
(a) and temperature profile (b) of the original 15 heat-exchanger design

a b

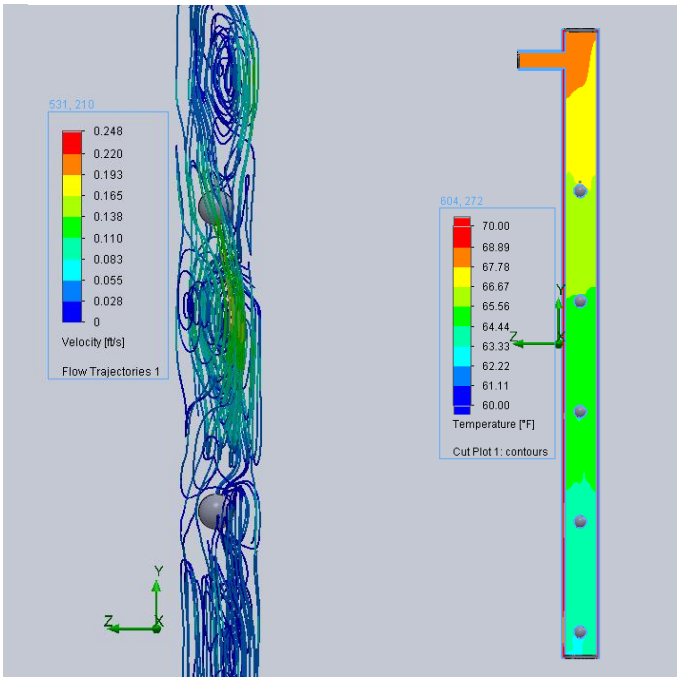

Figure 12: Section II flow trajectories
(a) and temperature profile (b) of the original 15 heat exchanger design

The revised design that focused on the middle section of the mine shaft simulated a temperature range of 68° F to 78° F. The biggest temperature range was measured at the bottom of the middle section of the mine shaft as shown in Figure 15. Even with the largest amount of energy being extracted simulated at the crosscut entrance of the middle section; the low temperature of 68° F was measured at the bottom of the middle section.

Section I, which consisted of the three heat exchangers that carried 20% of the 810,000 BTU/hr load, saw only a one degree change (74° F-75° F) as shown in Figure 14. The velocities that were simulated reached a maximum of 0.30 ft/s. The flow patterns were consistent with natural convection, as seen in Figure 13.

a b

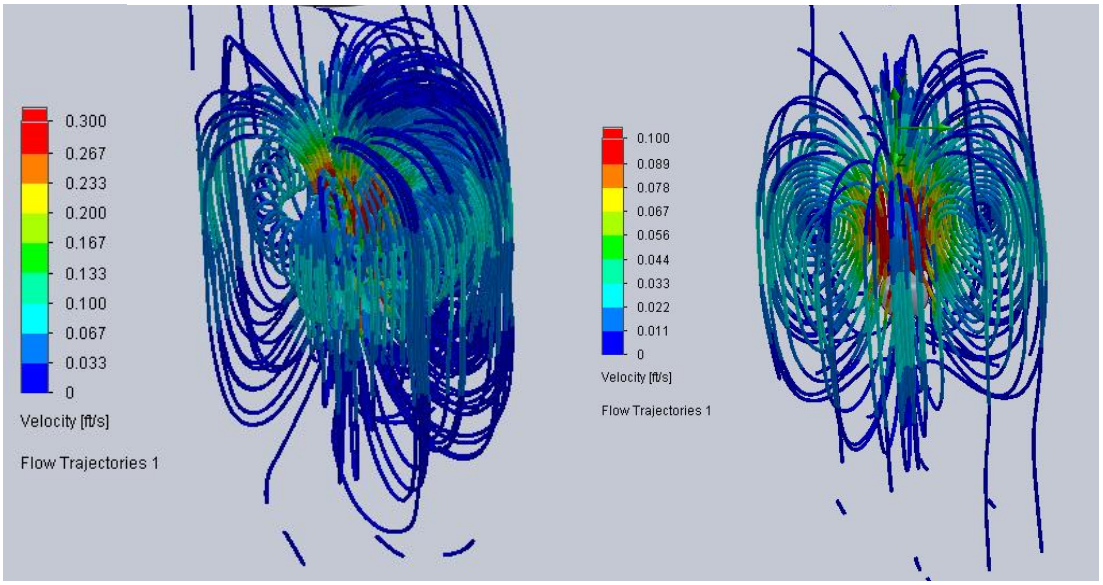

Figure 13: Flow trajectory from DHEs set at 120'(a) and 170'(b) of Section I of the 11-DHE design

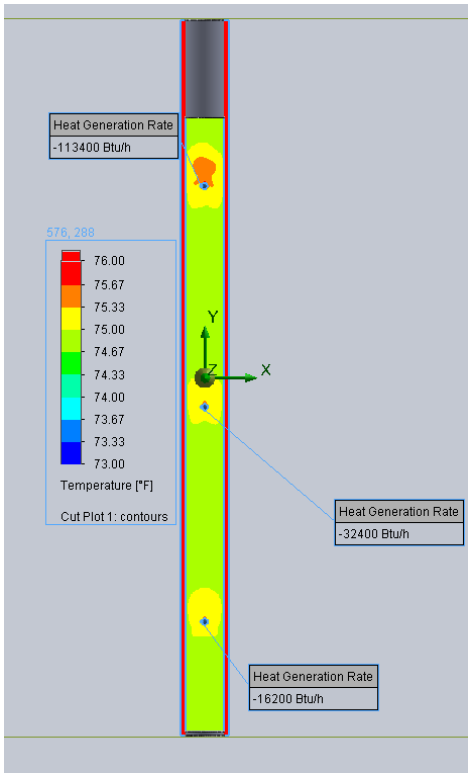

Figure 14-Section I temperature profile the 11-DHE design

Section II had the most heat exchangers placed in the entire model with six DHEs placed 30 feet apart. The velocities reached a maximum of 0.348 ft/s around the heat exchanger located at the 320-ft level near the crosscut. A low temperature of 68° F was calculated at approximately the 500-ft level. The flow trajectories did not reflect ideal flow patterns, but some consistency could be seen near the heat exchanger located near the crosscut. The flow pattern around the 320-ft heat exchanger and the temperature profile of Section II can be seen in Figure 15 and 16. The flow trajectories and temperature profile of Section III can be seen in Appendix A.

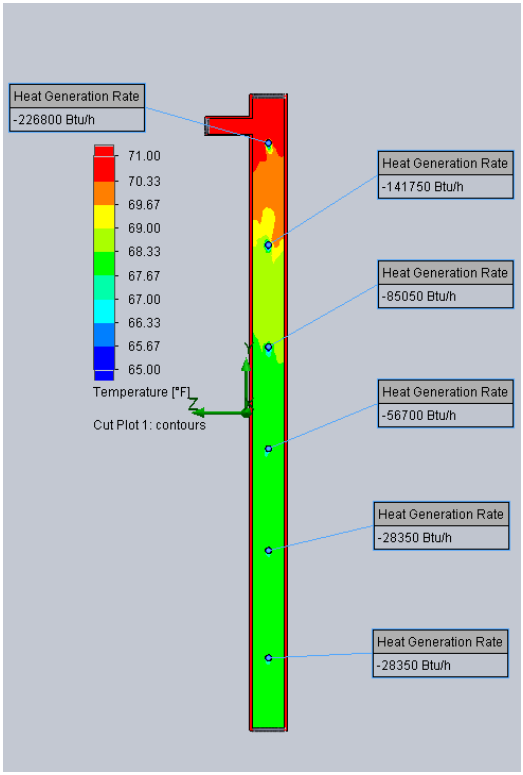

Figure 15-Secton II temperature profile of the 11-DHE design

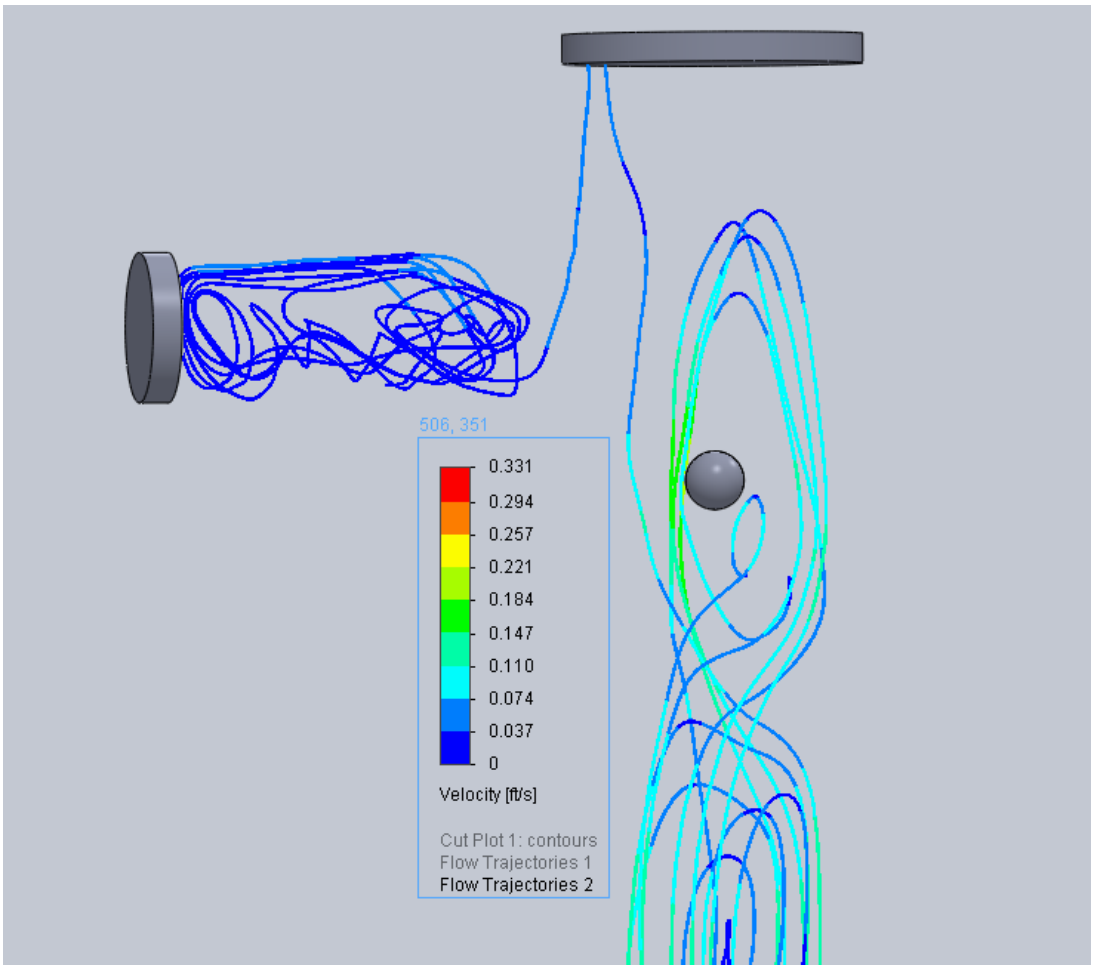

Figure 16: Flow trajectories around the DHE located at the 320' level of Section II of 11-DHE design

Table 1 shows the change in the convective heat transfer coefficients along with the required change in temperature for each load on the heat exchangers. These coefficients were calculated using the temperature surrounding the heat exchangers. With a calculated convection coefficient it was possible to estimate a required temperature difference between the coiled surface of the heat exchangers and the water of the 11-heat exchanger design. The 15 evenly distributed heat exchangers had a temperature difference of 6.8° F between the coiled surface of the heat exchangers and the water for a 54,000 BTU/hr heat transfer.

Table 1- Parameters for new design using Equation 9

h_{avg} (W/m^2*K)	Delta Temp (° F)	Depth (ft)	Load (BTU/hr)
291.0	12.0	120.0	-113400.0
219.0	5.5	180.0	-32400.0
185.0	3.5	230.0	-16200.0
341.0	21.0	320.0	-226000.0
310.0	14.8	350.0	-141750.0
273.0	9.7	380.0	-85050.0
249.0	7.0	410.0	-56700.0
213.0	4.1	440.0	-28350.0
213.0	4.1	470.0	-28350.0
232.0	5.5	520.0	-41500.0
232.0	5.5	530.0	-41500.0

6. Discussion

From viewing the footage from the camera that was placed down-hole in the Orphan Girl, it was safe to conclude that primary heat transfer to the heat exchangers was from natural convection. The ink that was injected showed particles slowly drifting to the top. From this, a measured velocity of 0.1-ft/sec was found. This was consistent with values the CFD simulations produced without the heat exchangers. Once the heat exchangers were included, velocities increased to approximately 0.33-ft/sec as shown in Figure 16.

The results show that natural convection is the primary mechanism of heat transfer from the water. Since the temperature has reached steady state, the surrounding formation rock could be supplying the heat to the water. The measured flow rates from the Green Springs seep and the footage from the down-hole camera in the Orphan Girl indicates that there is no forced convection. This leaves only natural convection to be the primary means of heat transfer from the water.

There is very small movement of the water currently. From the simulations that were modeled there is a significant increase in the velocity of water once the heat exchangers are

turned on. From the simulated temperature changes there is enough energy within the system to heat the building via natural convection.

This project found that 11 heat exchangers was the optimum number to be placed in the three sections of the model. The lowest temperature surrounding a heat exchanger was modeled to be 67° F. The original design had 15 heat exchangers and modeled a low temperature of 65° F. There is a small change in temperature between the two designs, but having to install only 11 heat exchangers as opposed to 15 would save time and money.

Section II of the 11-DHE design with six heat exchangers simulated the most water movement around the heat exchangers. This indicates that with the current boundary conditions set at that section, natural convection would most likely occur there. What could be ascertained from the simulated model is that the highest density of heat exchangers should be placed in Section II. However, further investigation is needed to be certain.

Placement of the heat exchangers is critical in the installation. This is because the Orphan Boy is a vertical mine shaft and the location of the crosscut that feeds the water is in middle section. The crosscut in the bottom section located at approximately the 500-ft level would carry water having a significant lower temperature than the upper or middle section simply because of buoyancy. This would have its greatest effect when the heat exchangers are operational.

124 billion BTU is a significant amount of energy to have available. The velocities that are occurring within the shaft without any heat exchangers indicate that there is little exchange between the stope and the shaft. When the heat exchangers are installed the movement within the shaft would cause an exchange distributing the water throughout the system. This would grant sufficient exchange between the stope and the shaft assuring good heat transfer.

7. References Cited (or Bibliography)

1. Fickes, M, “Below the Surface”,College Planning & ManagementVolume 15, Issue 4 (2012) Michael Fickes

2. Watzlaf G.R., Ackman T.E. Underground Mine Water for Heating and Cooling using Geothermal Heat Pump Systems (2006) George R. Watzlaf and Terry E. Ackman

3. U.S. Department of Interior, U.S. Geological Survey, Integrated Investigations of Environmental Effects of Historical Mining in the Basin and Boulder Mining Districts, Boulder River Watershed, Jefferson County, Montana, Chapter D1, “Geologic Framework”

4. Wallace M, “Montana Tech Heat Pump, Design Guides for Second Phase” (2010) Mack Wallace

5. NCEES, “FE fundamentals of engineering, Supplied Reference Hanbook” 8th edition, 2nd revision (2010)

6. Culver G., Lund J.W., “Downhole Heat Exchangers”, (1999) Gene Culver, John W. Lund, Geo-Heat Center

7. Nydeck Schenck H., Heat Transfer Engineering, Chapter 3 ppg 60-75 “Heat Transfer by Natural Convection” (1959) Prentice Hall – Hilbert van Nydeck Schenck

8. FloEFD 11 for SolidWorks Mentor Graphics 2011

9. Hellums J.V., Churchill S.W., “Transient and Steady State, Free and Natural Convection, Numerical Solutions”: “The Isothermal Vertical Plate”-University of Michigan, Ann Arbor, Michigan (1962) J.V. Hellums, S.W. Churchill

10. Fausett L.V., “Applied Numerical Analysis Using MATLAB” ppg 29-35 (1999) Laurene V. Fausett

11. Guerrieri, S.A., “A Study of Heat Transfer to Organic Liquids in Single-tube, Natural-circulation, Vertical-tube Boilers” (Jan, 1956) American Institute of Chemical Engineers,

12. Gebhart B., “Heat Transfer” “Ch.8 Convection with Body Forces” ppg 370-380 (1961) Benjamin Gebhart

13. Robertson, A., Crowe C. T., Engineering Fluid Mechanics, 6th Edition, Chapter 8 ppg 270-297 “Dimensional Analysis and Similitude” (1997) A. Robertson, Clayton T. Crowe

14. Incropera F.P., Dewitt D.P., Bergman T.L., Lavine A.S., Introduction to Heat Transfer 5th Edition, Chapter 1 ppg 4-10 “Physical Origins and Rate Equations” (2007) Frank P. Incropera, David P. Dewitt, Theodore L. Bergman, Adrienne S. Lavine

Appendix A: Simulated Models

This appendix includes a small portion of the simulation models that were considered failures, but paved the way to the final model that gave the best results

Figure A1 shows the square shaft geometric model and its simulation results. It is noticeable in Figure A1b that natural convection is occurring within the shaft below the DHE. There is a distinct density difference in the water with no other force involved. However, it is apparent that very little movement is occurring above the DHE. The cut-plot shows promise in that water does not fall below 62° F at a transfer rate of -40kBTU/hr. This model also took an exceptionally long time to run a simulation with only one DHE and modeled at a depth of only 50-ft. This may have been due to the fact that mesh resolution was raised and the element size was lowered for accuracy. However, this was considered too long just for one heat exchanger.

a b c

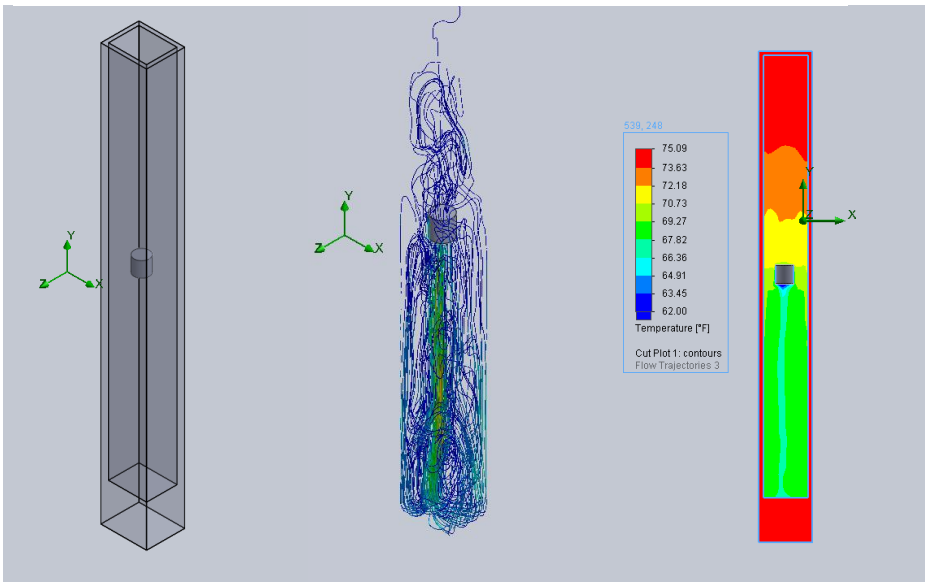

Figure A1: Squared-shaft geometric model (a), flow trajectory model inside shaft (b), steady-state temperature cut-plot (c)

Figure A2 shows the squared shaft geometric model, but including the surrounding formation. This time the mesh resolution and element size were kept at default settings. Figure A2a shows a geometric model of the system in question with two cylinders as heat exchangers with a 2-ft diameter and a length of 2 feet set at the 140-ft and 175-ft level of the system. This shaft was considered to be one compartment of the system, so its cross-sectional area was a third of the total cross-sectional area of the Orphan Boy. The surrounding shaft was changed from the 120-ft diameter that represented the formation to 12-ft as was the thermal properties of granite to reduce the computational time. The flow patterns around the bottom heat exchanger can be seen in Figure A2b. Velocities were simulated to be as high as 0.40 ft/s at the location of the bottom heat exchanger, but there was virtually no movement simulated at the top heat exchanger. This is confirmed in Figure A2c. The temperature drop from the initial temperature at the bottom heat exchanger is nearly 10° F. However, there is only a 2° F temperature drop in a small area on the temperature profile near the top heat exchanger.

a b c

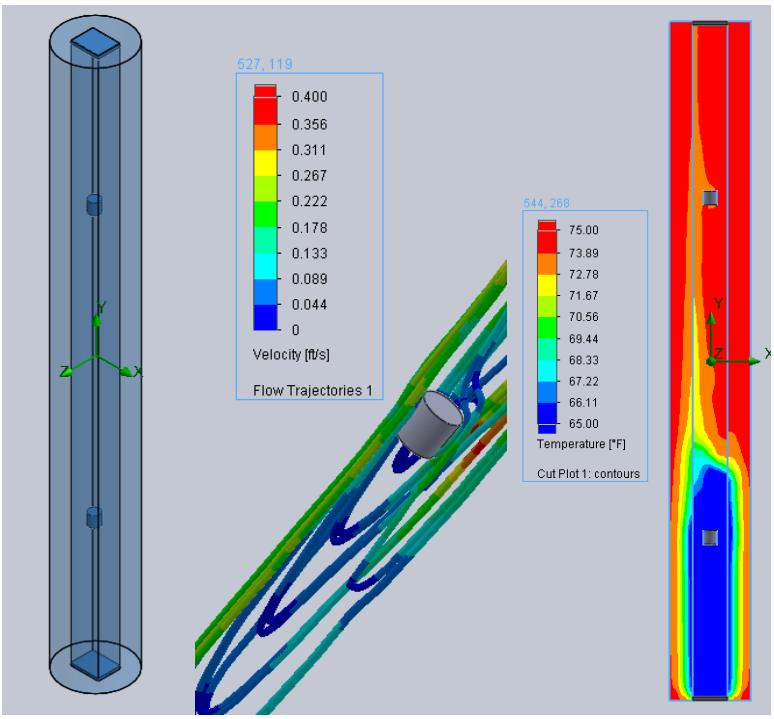

Figure A2: Geometric model of squared-shaft with surrounding formation (a), flow trajectory and velocity measure around cylindrical DHE (b), steady-state temperature profile of the system (c)

Figure A3 shows a circular-shaft geometric model and its results. The model included two cylindrical heat exchangers set at depths of 140 feet and 175 feet as seen in Figure A3a. The flow trajectory model, as shown in Figure A3b, shows sporadic movement with low velocity. This was believed to be because the cylindrical shape of the heat exchangers and the software having difficulty calculating the elements around them. Figure A3c shows a cut-plot that was very promising in that the lowest temperature calculated was approximately 72° F. However, the calculation time was simply too long with given resources.

a b c

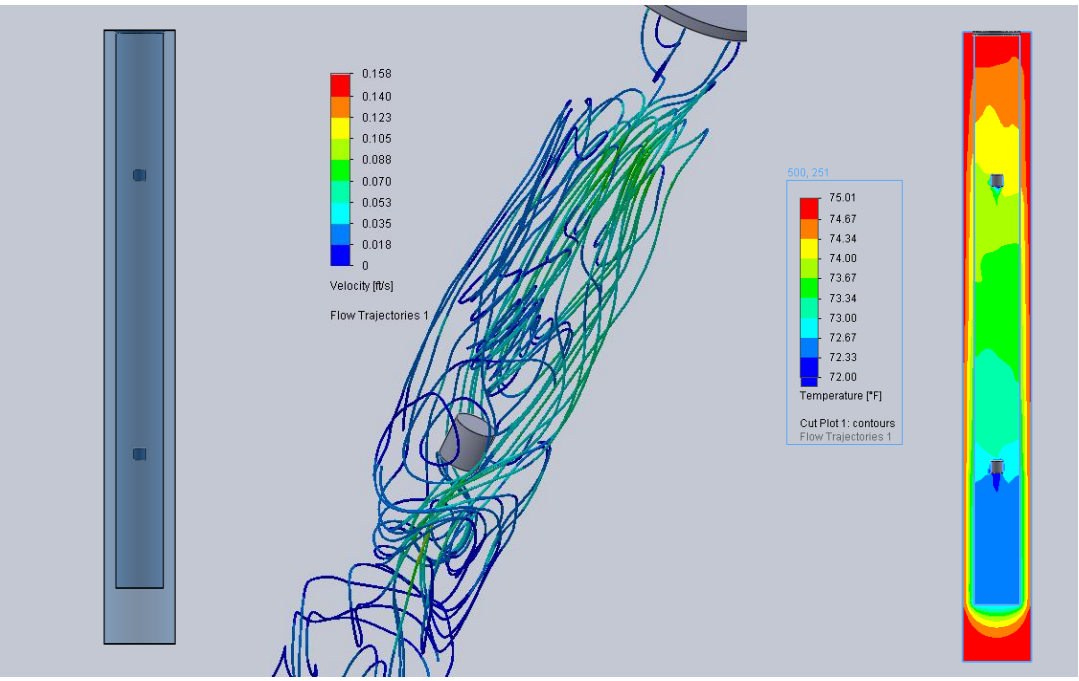

Figure A3: Geometric model of shaft with circular cross-section (a), flow trajectory model inside shaft (b), steady-state temperature cut-plot (c)

17.5 million BTU/hr was the system's limit on a heat transfer from between the heat exchangers and the water in the system with given boundary conditions. Figure A4a shows the flow trajectories around the heat exchangers. It should be noted that even with a significantly higher heat transfer rate than the required load of the NRB, only a maximum velocity of 0.391 ft/s was simulated. This was also an indication that an optimum number of heat exchangers as well as heat extraction gradient.

Figure A4b shows the steady-state temperature profile of Section II having 5.17 million BTU/hr extracted. Ice would most likely form on the bottom heat exchangers before the top simply due to density differences. This is regardless of the extraction rate of any heat exchanger. From this it was possible to conclude that the least amount of heat exchangers should be placed in Section III and the most should be placed in Section II.

a b

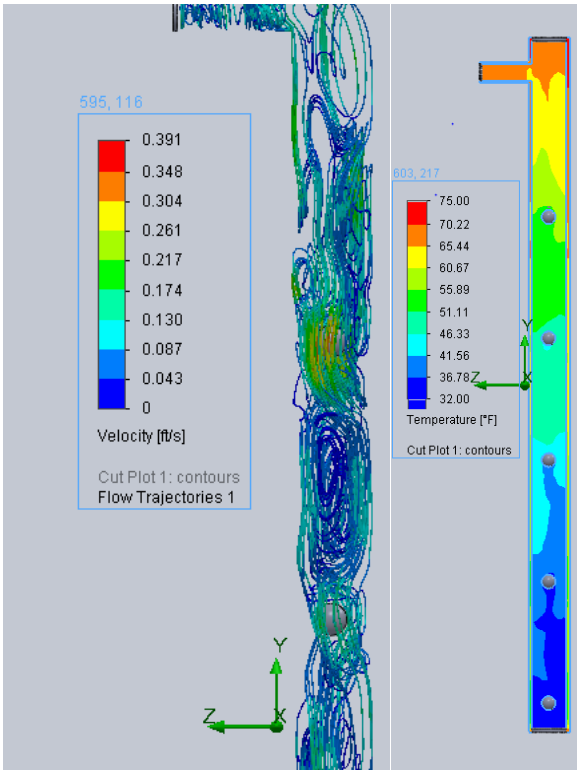

Figure A4: Flow trajectories around the DHE of the limitation model in the Section II (a), steady-state temperature profile showing a low temp of 32° F (b)

Section III of the 15 heat exchanger design was not shown in the main section of this paper because of its inability to produce convectional current. This may be due to the hydrostatic pressure or simply the colder water migrating to the bottom and staying there. Therefore, it is impertinent to put Section II's results with Section I and Section II's results. It can be seen in Figure A5a that the maximum velocity simulated was only 0.218 ft/s, and had very little occurrence through the entire section. This was a small difference from Section II's velocity of 0.248 ft/s, but this did indicate that placing five heat exchangers in Section III would be a waste.

Figure A5b shows the steady-state temperature profile of Section III. There is good temperature distribution throughout the section with the 810,000 BTU/hr being extracted from the system. As previously mentioned, the low temperature simulated was 62° F at the very

bottom of Section III. This was slightly lower than the 11 heat exchanger design's low temperature of 67° F. This was a confirmation that five heat exchangers was an excessive amount to install below the 500-ft level of the Orphan Boy.

a b

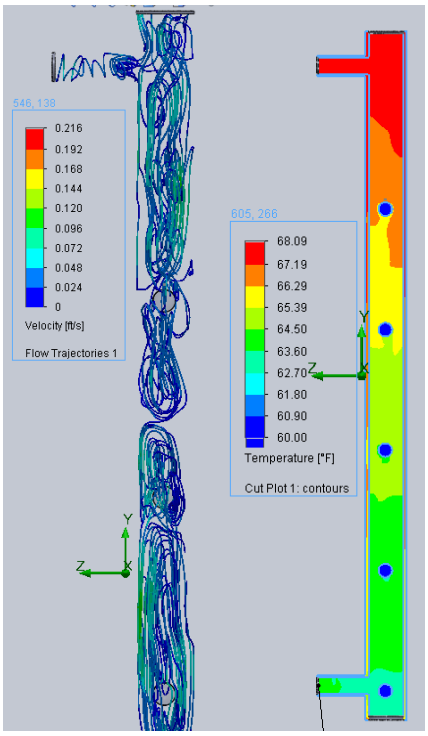

Figure A5: Flow trajectories of Section III of the 15 DHE design with an 810,000 BTU/hr load (a), steady-state temperature profile of said configuration

Section III of the 11-DHE design had low velocities simulated around the heat exchangers. The heat exchangers were both spaced 10 feet apart in the 200-ft section and placed near the crosscut at the 520-ft level. The crosscut at the 520-ft level was set to have an inlet flow rate of 35 gallons/min, while the crosscut at the 700-ft level had an outlet flow rate of the same amount. The flow trajectories around the two heat exchangers can be seen in Figure A6. It can be seen that the maximum velocity does not even occur around the heat exchangers, but as the heavier water is sinking to the bottom. The velocity around the heat exchangers were simulated

at approximately 0.20 ft/s to 0.50ft/s. Each heat exchanger had an extraction rate of 41,500 BTU/hr.

The temperature profile of Section III was promising given the boundary conditions that were set. The low temperature was 67° F and simulated in a small area around each heat exchanger. The rest of the water had a constant temperature of 67.5° F.

a b

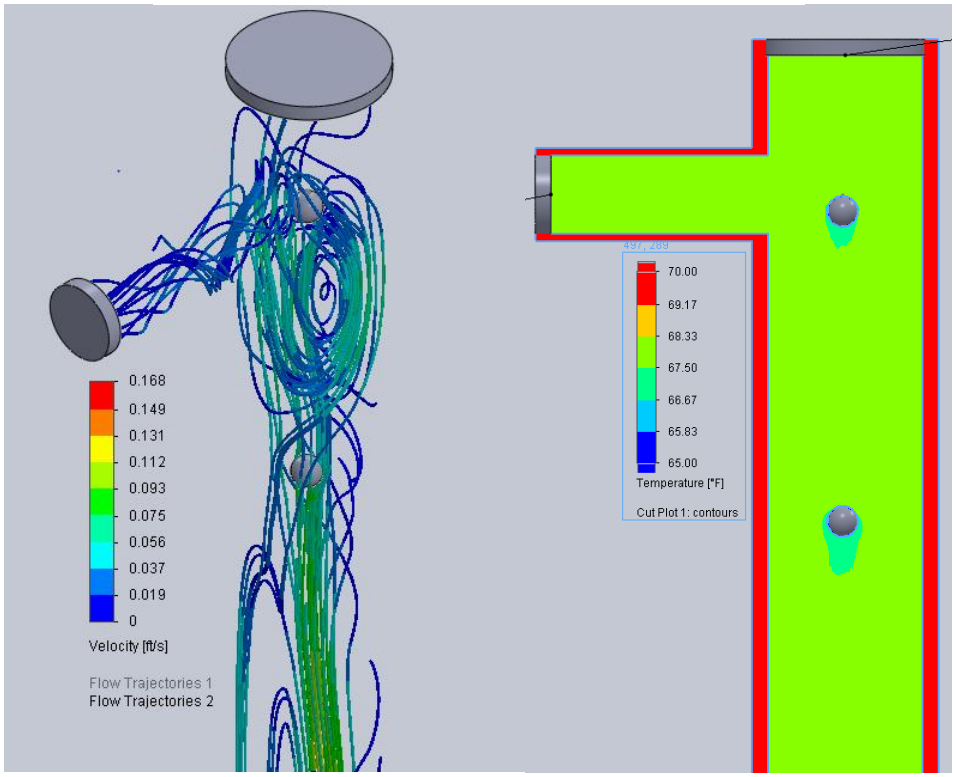

Figure A6: Flow trajectories surrounding the two heat exchangers in Section III of the 11 DHE design (a), steady-state temperature profile around the two heat exchangers of the 11 DHE design

Appendix B: MATLAB Code

The following code was made in respect to the Orphan Boy mine shaft's characteristics. This code solves a 42x42 matrix and gives the product in temperature Kelvin for each node. The code produced a description of how the heat migrates towards the placement of the heat exchangers. However, the code becomes unstable when a large heat extraction is assigned to the heat exchangers. The code would calculate temperatures that are improbable (e.g. -113° K), but the isothermal graph would still show steady temperature migration.

```
%Rory's Steady State Finite Difference Heat Transfer
%11/16/2011

clear all
close all
clc

%% Input Parameters

% Ti=input('Please input the initial temperature in Kelvin:');
% q=input('Please input qdot in Watts/m^3:');
% k=input('Please input k value for granite in Watts/(m*K):');
% kw=input('Please input kw value for water in Watts/(m*K):');
% h=input('Please input the convection coefficient h in Watts/(m^2*K):');
% dy=input('Please input the delta y in meters:');

Ti=300;
q=-2;
kg=2.79;
kw=0.6;
h=48;
dy=3;
dx=dy;
% Coefficient Matrix A

C1=h*dy/kg;
C2=h*dy/kw;


R1=[-2 .5 0 0 0 0 1 0 0 0 0 0 0 0 0 0 0 0 0 0 0 0 0 0 0 0 0 0 0 0 0 0 0 0 0 0 0 0 0 0];
R2=[.5 -2 .5 0 0 0 0 1 0 0 0 0 0 0 0 0 0 0 0 0 0 0 0 0 0 0 0 0 0 0 0 0 0 0 0 0 0 0 0 0];
R3=[0 .5 -2 .5 0 0 0 0 1 0 0 0 0 0 0 0 0 0 0 0 0 0 0 0 0 0 0 0 0 0 0 0 0 0 0 0 0 0 0 0];
```

```
R4=[0 0 .5 (-1-C1/2) C1/2 0 0 0 0 .5 0 0 0 0 0 0 0 0 0 0 0 0 0 0 0 0 0 0 0 0
0 0 0 0 0 0 0 0 0 0 0 0];
R5=[0 0 0 C2/2 (-C2/2-1.5) .5 0 0 0 0 1 0 0 0 0 0 0 0 0 0 0 0 0 0 0 0 0 0 0 0
0 0 0 0 0 0 0 0 0 0 0 0];
R6=[0 0 0 0 .5 -1 0 0 0 0 0 .5 0 0 0 0 0 0 0 0 0 0 0 0 0 0 0 0 0 0 0 0 0 0 0
0 0 0 0 0 0 0];
R7=[1 0 0 0 0 0 -4 1 0 0 0 0 1 0 0 0 0 0 0 0 0 0 0 0 0 0 0 0 0 0 0 0 0 0 0 0
0 0 0 0 0 0];
R8=[0 1 0 0 0 0 1 -4 1 0 0 0 0 1 0 0 0 0 0 0 0 0 0 0 0 0 0 0 0 0 0 0 0 0 0 0
0 0 0 0 0 0];
R9=[0 0 1 0 0 0 0 1 -4 1 0 0 0 0 1 0 0 0 0 0 0 0 0 0 0 0 0 0 0 0 0 0 0 0 0 0
0 0 0 0 0 0];
R10=[0 0 0 .5 0 0 0 0 1 (-2-C1) C1 0 0 0 0 .5 0 0 0 0 0 0 0 0 0 0 0 0 0 0 0 0
0 0 0 0 0 0 0 0 0 0];
R11=[0 0 0 0 1 0 0 0 0 C2 (-C2-3) 1 0 0 0 0 1 0 0 0 0 0 0 0 0 0 0 0 0 0 0 0 0
0 0 0 0 0 0 0 0 0];
R12=[0 0 0 0 0 .5 0 0 0 0 1 -2 0 0 0 0 0 .5 0 0 0 0 0 0 0 0 0 0 0 0 0 0 0 0 0
0 0 0 0 0 0 0];
R13=[0 0 0 0 0 0 1 0 0 0 0 0 -4 1 0 0 0 0 1 0 0 0 0 0 0 0 0 0 0 0 0 0 0 0 0 0
0 0 0 0 0 0];
R14=[0 0 0 0 0 0 0 1 0 0 0 0 1 -4 1 0 0 0 0 1 0 0 0 0 0 0 0 0 0 0 0 0 0 0 0 0
0 0 0 0 0 0];
R15=[0 0 0 0 0 0 0 0 1 0 0 0 0 1 -4 1 0 0 0 0 1 0 0 0 0 0 0 0 0 0 0 0 0 0 0 0
0 0 0 0 0 0];
R16=[0 0 0 0 0 0 0 0 0 .5 0 0 0 0 1 (-2-C1) C1 0 0 0 0 .5 0 0 0 0 0 0 0 0 0 0
0 0 0 0 0 0 0 0 0 0];
R17=[0 0 0 0 0 0 0 0 0 0 1 0 0 0 0 C2 (-C2-3) 1 0 0 0 0 1 0 0 0 0 0 0 0 0 0 0
0 0 0 0 0 0 0 0 0];
R18=[0 0 0 0 0 0 0 0 0 0 0 .5 0 0 0 0 1 -2 0 0 0 0 0 .5 0 0 0 0 0 0 0 0 0 0 0
0 0 0 0 0 0 0];
R19=[0 0 0 0 0 0 0 0 0 0 0 0 1 0 0 0 0 0 -4 1 0 0 0 0 1 0 0 0 0 0 0 0 0 0 0 0
0 0 0 0 0 0];
R20=[0 0 0 0 0 0 0 0 0 0 0 0 0 1 0 0 0 0 1 -4 1 0 0 0 0 1 0 0 0 0 0 0 0 0 0 0
0 0 0 0 0 0];
R21=[0 0 0 0 0 0 0 0 0 0 0 0 0 0 1 0 0 0 0 1 -4 1 0 0 0 0 1 0 0 0 0 0 0 0 0 0
0 0 0 0 0 0];
R22=[0 0 0 0 0 0 0 0 0 0 0 0 0 0 0 .5 0 0 0 0 1 (-2-C1) C1 0 0 0 0 .5 0 0 0 0
0 0 0 0 0 0 0 0 0 0];
R23=[0 0 0 0 0 0 0 0 0 0 0 0 0 0 0 0 1 0 0 0 0 C2 (-C2-3) 1 0 0 0 0 1 0 0 0 0
0 0 0 0 0 0 0 0 0];
R24=[0 0 0 0 0 0 0 0 0 0 0 0 0 0 0 0 0 .5 0 0 0 0 1 -2 0 0 0 0 0 .5 0 0 0 0 0
0 0 0 0 0 0 0];
R25=[0 0 0 0 0 0 0 0 0 0 0 0 0 0 0 0 0 0 1 0 0 0 0 0 -4 1 0 0 0 0 1 0 0 0 0 0
0 0 0 0 0 0];
R26=[0 0 0 0 0 0 0 0 0 0 0 0 0 0 0 0 0 0 0 1 0 0 0 0 1 -4 1 0 0 0 0 1 0 0 0 0
0 0 0 0 0 0];
R27=[0 0 0 0 0 0 0 0 0 0 0 0 0 0 0 0 0 0 0 0 1 0 0 0 0 1 -4 1 0 0 0 0 1 0 0 0
0 0 0 0 0 0];
R28=[0 0 0 0 0 0 0 0 0 0 0 0 0 0 0 0 0 0 0 0 0 .5 0 0 0 0 1 (-2-C1) C1 0 0 0
0 .5 0 0 0 0 0 0 0 0];
R29=[0 0 0 0 0 0 0 0 0 0 0 0 0 0 0 0 0 0 0 0 0 0 1 0 0 0 0 C2 (-C2-3) 1 0 0 0
0 1 0 0 0 0 0 0 0];
R30=[0 0 0 0 0 0 0 0 0 0 0 0 0 0 0 0 0 0 0 0 0 0 0 .5 0 0 0 0 1 -2 0 0 0 0 0
.5 0 0 0 0 0 0];
R31=[0 0 0 0 0 0 0 0 0 0 0 0 0 0 0 0 0 0 0 0 0 0 0 0 1 0 0 0 0 0 -4 1 0 0 0 0
1 0 0 0 0 0];
```

```
R32=[0 0 0 0 0 0 0 0 0 0 0 0 0 0 0 0 0 0 0 0 0 0 0 0 0 1 0 0 0 0 1 -4 1 0 0 0
0 1 0 0 0 0];
R33=[0 0 0 0 0 0 0 0 0 0 0 0 0 0 0 0 0 0 0 0 0 0 0 0 0 0 1 0 0 0 0 1 -4 1 0 0
0 0 1 0 0 0];
R34=[0 0 0 0 0 0 0 0 0 0 0 0 0 0 0 0 0 0 0 0 0 0 0 0 0 0 0 0 .5 0 0 0 0 1 (-2-
C1) C1 0 0 0 0 .5 0 0];
R35=[0 0 0 0 0 0 0 0 0 0 0 0 0 0 0 0 0 0 0 0 0 0 0 0 0 0 0 0 1 0 0 0 0 C2 (-
C2-3) 1 0 0 0 0 1 0];
R36=[0 0 0 0 0 0 0 0 0 0 0 0 0 0 0 0 0 0 0 0 0 0 0 0 0 0 0 0 0 .5 0 0 0 0 1 -
2 0 0 0 0 0 .5];
R37=[0 0 0 0 0 0 0 0 0 0 0 0 0 0 0 0 0 0 0 0 0 0 0 0 0 0 0 0 0 0 1 0 0 0 0 0
-2 .5 0 0 0 0];
R38=[0 0 0 0 0 0 0 0 0 0 0 0 0 0 0 0 0 0 0 0 0 0 0 0 0 0 0 0 0 0 0 1 0 0 0 0
.5 -2 .5 0 0 0];
R39=[0 0 0 0 0 0 0 0 0 0 0 0 0 0 0 0 0 0 0 0 0 0 0 0 0 0 0 0 0 0 0 0 1 0 0 0
0 .5 -2 .5 0 0];
R40=[0 0 0 0 0 0 0 0 0 0 0 0 0 0 0 0 0 0 0 0 0 0 0 0 0 0 0 0 0 0 0 0 0 .5 0 0
0 0 .5 (-1-C1/2) C1/2 0];
R41=[0 0 0 0 0 0 0 0 0 0 0 0 0 0 0 0 0 0 0 0 0 0 0 0 0 0 0 0 0 0 0 0 0 0 1 0
0 0 0 C2/2 (-1.5-C2/2) .5];
R42=[0 0 0 0 0 0 0 0 0 0 0 0 0 0 0 0 0 0 0 0 0 0 0 0 0 0 0 0 0 0 0 0 0 0 0 .5
0 0 0 0 .5 -1];
A=[R1;R2;R3;R4;R5;R6;R7;R8;R9;R10;R11;R12;R13;R14;R15;R16;R17;R18;R19;R20;R21
;R22;R23;R24;R25;R26;R27;R28;R29;R30;R31;R32;R33;R34;R35;R36;R37;R38;R39;R40;
R41;R42];
Ainv=A^-1;
%% C MATRIX
C=[-Ti/2;0;0;0;0;-q*dx*dy/(4*kw);-Ti;0;0;0;0;0;-Ti;0;0;0;0;-q*dx*dy/(2*kw);-
Ti;0;0;0;0;0;-Ti;0;0;0;0;-q*dx*dy/(2*kw);-Ti;0;0;0;0;0;-Ti/2;0;0;0;0;-
q*dx*dy/(4*kw)];
%% SOLUTION

T=A^-1*C;

Tgrid=[T(1),T(2),T(3),T(4),T(5),T(6);
       T(7),T(8),T(9),T(10),T(11),T(12);
       T(13),T(14),T(15),T(16),T(17),T(18);
       T(19),T(20),T(21),T(22),T(23),T(24);
       T(25),T(26),T(27),T(28),T(29),T(30);
       T(31),T(32),T(33),T(34),T(35),T(36);
       T(37),T(38),T(39),T(40),T(41),T(42)];


contour(Tgrid(1:7,1:6),'DisplayName','Tgrid(1:7,1:6)');figure(gcf)
xlabel('Node Position')
ylabel('Node Position')
title('Isothermal Contour Plot')
```

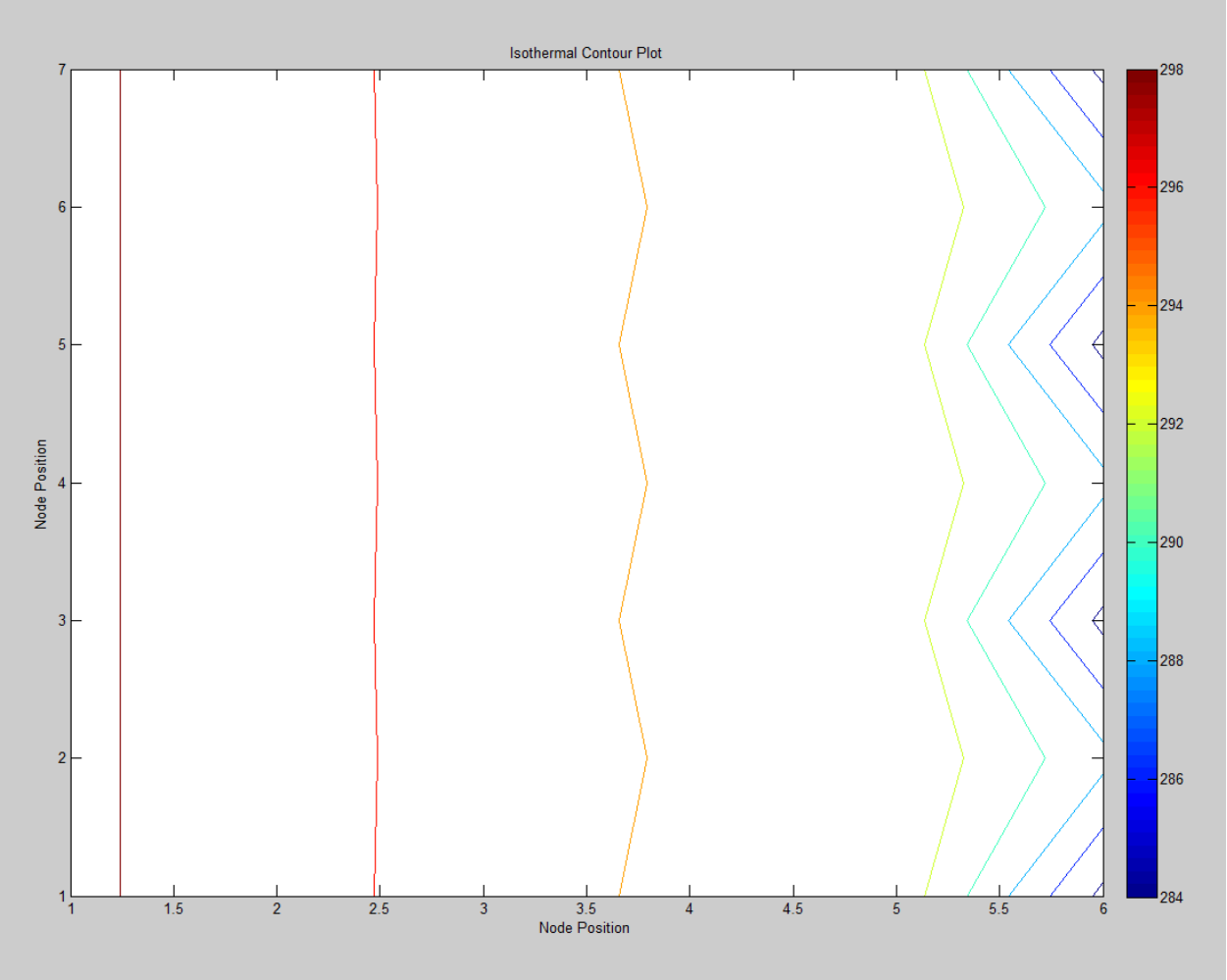

Figure A1.1: Isothermal plot showing temperature profile with the DHE at the far right of the grid

SIGNATURE PAGE

This is to certify that the thesis prepared by Rory Thornton entitled "Convection Mechanisms for Geothermal Heat Exchangers in a Vertical Mine Shaft" has been examined and approved for acceptance by the Department of General Engineering, Montana Tech of The University of Montana, on this 1st day of October, 2012.

Neil Wahl, PhD, Professor
Department of General Engineering
Chair, Examination Committee

Don Blackketter, PhD, Chancellor
Montana Tech of The University of Montana
Member, Examination Committee

David Bunnell, PhD, Assistant Professor
Department of General Engineering
Member, Examination Committee